Fibroblast growth factor 10 and mesenchymal lineage commitment in the mouse lung during development and disease

Inaugural Dissertation

submitted to the

Faculty of Medicine

in partial fulfillment of the requirements

for the PhD-Degree

of the Faculties of Veterinary Medicine and Medicine

of the Justus Liebig University Giessen

by

El Agha, Elie

of

Saida, Lebanon

Giessen 2014

From the Department of Internal Medicine II

Director / Chairman: Prof. Dr. Werner Seeger

of the Faculty of Medicine of the Justus Liebig University Giessen

First Supervisor and Committee Member: Prof. Dr. Saverio Bellusci

Second Supervisor: Dr. Mohammad Hajihosseini

Committee Member (Chair): Prof. Dr. Norbert Weissmann

Committee Member: Prof. Dr. Martin Witzenrath

Committee Member: Prof. Dr. Stefan Arnhold

Date of Doctoral Defense: 03/04/2014

Declaration

"I declare that I have completed this dissertation single-handedly without the unauthorized help of a second party and only with the assistance acknowledged therein. I have appropriately acknowledged and referenced all text passages that are derived literally from or are based on the content of published or unpublished work of others, and all information that relates to verbal communications. I have abided by the principles of good scientific conduct laid down in the charter of the Justus Liebig University of Giessen in carrying out the investigations described in the dissertation."

Elie El Agha

Table of Contents

List of Tables

List of Figures

Abbreviations and Acronyms

ADRP	Adipose differentiation-related protein (Adipophilin or ADFP)
AEC I	Type I alveolar epithelial cells
AEC II	Type II alveolar epithelial cells
ALI	Acute lung injury
Alv.	Alveolus
APC	Allophycocyanin
AQP5	Aquaporin-5
BAC	Bacterial artificial chromosome
BADJ	Bronchoalveolar duct junction
BALF	Bronchoalveolar lavage fluid
BASC	Bronchoalveolar stem cell
BF	Bright field
BLM	Bleomycin
BMP-4	Bone morphogenetic protein 4
BMPR	Bone morphogenetic protein receptor
bp	Base pairs
BPD	Bronchopulmonary dysplasia
Br.	Bronchus
Brl.	Bronchiole
BSA	Bovine serum albumin

C/EBPα	CCAAT/enhancer binding protein alpha
C/EBPβ	CCAAT/enhancer binding protein beta
CCSP	Clara cell secretory protein
cDNA	Complementary DNA
Ce	Cecum
CGRP	Calcitonin gene-related peptide
c-Kit	Mast/stem cell growth factor receptor Kit
Co	Colon
COPD	Chronic obstructive pulmonary disease
Cre-ERT2	Fusion protein between Cyclization recombinase and triple mutated human estrogen receptor ligand binding domain
Cy7	Cyanine 7
CYP2F2	Cytochrome P450, family 2, subfamily f, polypeptide 2
DAPI	4′,6-diamidino-2-phenylindole, dihydrochloride
ddH_2O	Double distilled water
DMEM	Dulbecco's Modified Eagle's Medium
DNA	Deoxyribonucleic acid
dNTP	Deoxyribonucleotide triphosphate
DTA	Diphtheria Toxin A
E. coli	Escherichia coli
ECM	Extracellular matrix

ECRs	Evolutionary conserved regions
EGF	Epidermal growth factor
eGFP	Enhanced GFP
EGFR	Epidermal growth factor receptor
EpCAM	Epithelial cell adhesion molecule
Epi.	Epithelium
ERK	Extracellular signal-regulated kinases
ES cells	Embryonic stem cells
eYFP	Enhanced yellow fluorescent protein
FACS	Fluorescence-activated cell sorting
FBS	Fetal bovine serum
FCS	Fetal calf serum
FGF	Fibroblast growth factor
FGFR	Fibroblast growth factor receptor
FITC	Fluorescein isothiocyanate
FLK-1	Fetal liver kinase 1 (or VEGFR2)
Flp	Flippase enzyme
GAPDH	Glyceraldehyde 3-phosphate dehydrogenase
GFP	Green fluorescent protein
H/E	Hematoxylin/Eosin
H3K4me3	Histone H3 trimethylated at Lysine 4

HBSS	Hank's balanced salt solution
HPRT	Hypoxanthine-guanine phosphoribosyltransferase
iCre	Inducible Cre
IP	Intraperitoneal
IPF	Idiopathic pulmonary fibrosis
IRES	Internal ribosome entry site
IT	Intratracheal
KGF	Keratinocyte growth factor
KRT14	Cytokeratin-14
KRT5	Cytokeratin-5
LacZ	Bacterial β-galactosidase gene
LECs	Lymphatic endothelial cells
LIF	Lipofibroblasts
MAPK	Mitogen-activated protein kinases
Mes.	Mesenchyme
Meso.	Mesothelium
MMP14	Matrix metalloproteinase 14
MSC	Mesenchymal stromal (stem) cell
MYF	Myofibroblasts
NCCs	Neural crest-derived cells
NE	Neuroendocrine cell

NEB	Neuroepithelial body
Neo	Neomycin-resistance gene
NO_2	Nitrogen dioxide
PAH	Pulmonary arterial hypertension
PBGD	Porphobilinogen deaminase
PBS	Phosphate buffered saline
PBSMC	Parabronchial smooth muscle cell
PCR	Polymerase chain reaction
PDGF-A	Platelet-derived growth factor A
PDGFRα	Platelet-derived growth factor receptor alpha
PDGFRβ	Platelet-derived growth factor receptor beta
PE	Phycoerythrin
PECAM-1	Platelet/endothelial cell adhesion molecule 1
PEEP	Positive end-expiratory pressure
P-ERK	Phospho-ERK
PFA	Paraformaldehyde
pGK	Phosphoglycerate kinase promoter
PPARγ	Peroxisome proliferator-activated receptor gamma
PROX1	Prospero homeobox protein 1
PTC	Patched (SHH receptor)
PTHrP	Parathyroid hormone-related protein

PVDF	Polyvinylidene fluoride
qPCR	Quantitative real-time PCR
RAS	Rat sarcoma
RET	Receptor tyrosine kinase
RFP	Red fluorescent protein
rhFGF10	Recombinant human FGF10
RIPA	Radioimmunoprecipitation assay
RNA	Ribonucleic acid
RT	Room temperature
RT-PCR	Reverse transcription PCR
S.E.M.	Standard error of mean
SAL	Saline
SCA-1	Stem cell antigen 1
SCGB1A1	Secretoglobin, family 1A, member 1
SEM	Sub-epithelial mesenchyme
SFTPA	Surfactant protein A
SFTPC	Surfactant protein C
SHH	Sonic Hedgehog
SMGs	Submucosal glands
SMM	Sub-mesothelial mesenchyme
SO_2	Sulfur dioxide

SOPF	Specific and opportunist pathogen free
SP	Side population
SPF	Specific pathogen free
Tam	Tamoxifen
TBS	Tris buffered saline
TBST	Tris buffered saline + 0.1% Tween20
TGF-β	Transforming growth factor beta
THY-1	Thymocyte antigen 1
Tr.	Trachea
TTF-1	Thyroid transcription factor 1 or NKX2.1
UTR	Untranslated region
VAF	Virus antibody free
VCAM-1	Vascular cell adhesion molecule 1
VEGF-A	Vascular endothelial growth factor A
VEGFR2	Vascular endothelial growth factor receptor 2
VSMC	Vascular smooth muscle cell
WT1	Wilm's tumor protein 1
X-Gal	5-Bromo-4-chloro-indolyl-β-D-galactopyranoside
XLMR	X-chromosome-linked mental retardation
ZFP423	Zinc finger protein 423
αSMA	Alpha Smooth muscle actin

1. Introduction

1.1. Progenitor/stem cells in the adult mouse lung

The adult mouse lung consists of at least 40-60 different types of cells that are organized in a highly sophisticated 3D structure inside the thoracic cavity (Crapo et al., 1982; McQualter and Bertoncello, 2012). This complexity is necessary in order to carry out gas exchange between the blood stream and the external environment and thus maintain body homeostasis. These cell types can be broadly classified into epithelial cells (populating the airways) and mesenchymal cells (populating the surrounding extracellular matrix).

From an anatomical point of view, the mouse lung can be divided into a proximal and distal region (Fig. 1). The proximal region consists of the trachea and mainstem bronchi and is distinguished by its pseudostratified epithelium and the presence of cartilageous rings. This region is populated by basal cells, goblet cells, neuroendocrine cells, ciliated cells and non-ciliated secretory cells (or Clara cells). On the other hand, the distal region is characterized by its columnar epithelium and the absence of basal cells or cartilageous tissue. This region contains few goblet cells and in addition to ciliated and secretory cells, type I and type II alveolar epithelial cells (AEC I/II). AEC I are squamous epithelial cells that occupy around 95% of the alveolar space and are responsible for gas exchange. AEC II are cuboidal epithelial cells and they produce surfactants that maintain a low surface tension in the alveolar space and prevent the alveoli from collapsing [Reviewed in (Rawlins and Hogan, 2006; Rock et al., 2010; Rock and Hogan, 2011; McQualter and Bertoncello, 2012)].

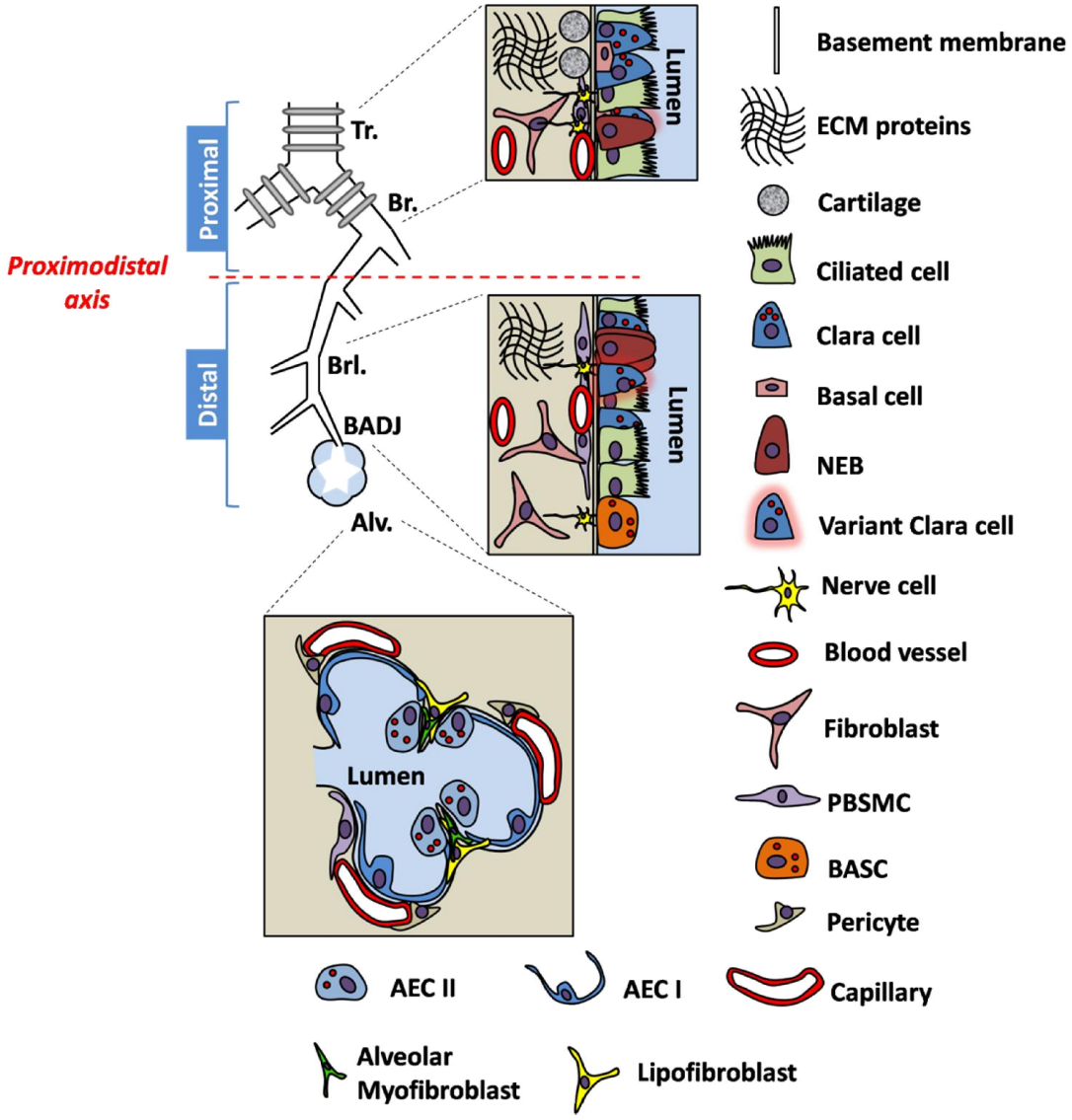

Figure 1. Schematic representation of the postnatal mouse lung showing the different cell types along the proximodistal axis.

Note that cartilage rings do not extend beyond mainstem bronchi in mice while in humans, they are found deep within the lung. Abbreviations: AEC I: Type I alveolar epithelial cell; AEC II: Type II alveolar epithelial cell; Alv: Alveolus; BADJ: Bronchoalveolar duct junction; BASC: Bronchoalveolar stem cell; Br: Bronchus; Brl: Bronchiole; ECM: Extracellular matrix; NEB: Neuroepithelial body (containing neuroendocrine cells); PBSMC: Parabronchial smooth muscle cell; Tr: Trachea. *Adopted and modified from* (Rawlins and Hogan, 2006; Rock et al., 2010; Rock and Hogan, 2011; Garcia et al., 2012; McQualter and Bertoncello, 2012).

Along the proximodistal axis, the mouse lung is rich with stem/progenitor cells that are capable of self-renewal, multipotent differentiation and pollutant resistance. In this section, the different types of lung progenitor/stem cells will be reviewed.

1.1.1. Epithelial stem cells and their niches in the adult mouse lung

The adult lung epithelium has a remarkably low cell-turnover rate (Rawlins and Hogan, 2008). However, many injury models have been devised to selectively target various cell types in the lung epithelium. Upon injury, progenitor/stem cells located in certain microenvironments (niches) undergo rounds of proliferation and differentiation to ensure epithelial regeneration.

Most of our knowledge regarding the lineage tree of epithelial cells derives from *ex vivo* studies (eg. rat tracheal xenograft model) (Shimizu et al., 1992), *in vitro* cell cultures and epithelial regeneration after injury. The latter includes the naphthalene injury model (to study regeneration of Clara cells), injury by inhalation of oxidants such as NO_2/Ozone and Oxygen (to study regeneration of ciliated and AEC I respectively) and injury by inhalation of SO_2 (to study regeneration of multiple epithelial lineages). These experimental approaches are reviewed in (Rawlins and Hogan, 2006).

Using the aforementioned approaches, it has been shown that in the upper (or proximal) airways, there are at least three distinct populations of epithelial progenitors. These include basal cells ($Krt5^+$; $Krt14^+$) (Hong et al., 2004; Schoch et al., 2004; Rock et al., 2009) and variant Clara cells ($Scgb1a1^+$; $Cyp2f2^-$) within neuroepithelial bodies (as progenitors for ciliated and secretory cells) (Stripp et al., 1995) as well as Submuscosal gland (SMG) duct cells ($Krt5^+$; $Krt14^+$) (as progenitors for the tracheal epithelium) (Borthwick et al., 2001). As for the lower (or distal) airways, variant Clara cells at the Bronchoalveolar duct junctions (BADJs) ($Scgb1a1^+$; $Sftpc^+$; $Cyp2f2^-$) have been suggested as stem cells (termed BASCs for Bronchoalveolar stem cells) as they are capable of regenerating bronchiolar Clara cells as well as alveolar cells (Giangreco et al., 2002; Kim et al., 2005). Moreover, AEC II ($Sftpc^+$) have been shown to be progenitors for AEC I ($Aqp5^+$) (Adamson and Bowden,

1974; Evans et al., 1975; Rock et al., 2011). These findings are summarized in Table 1.

Table 1. Epithelial progenitors in the adult mouse lung.
Distinct types of epithelial progenitors populate the adult mouse lung along the proximodistal axis. SMG duct cells, basal cells and variant Clara cells within NEBs populate the upper airways whereas variant Clara cells at BADJs and AEC II populate the distal airways. Abbreviations: Cyp2f2: Cytochrome P4502F2; Krt5: Cytokeratin-5; Krt14: Cytokeratin-14; Scgb1a1: Secretoglobin, family 1A, member 1; Sftpc: Surfactant protein C; SMGs: Submucosal glands. *Reviewed in* (Garcia et al., 2012).

Progenitor / stem cells	Markers	Progeny	Experimental model
		Proximal airways	
SMG duct cells of the upper trachea	$Krt5^+$; $Krt14^+$	Tracheal epithelium	Rat tracheal xenograft
Basal cells in trachea and main bronchi	$Krt5^+$; $Krt14^+$	Ciliated and secretory cells	Rat tracheal xenograft/SO_2 inhalation/Naphthalene injury
Variant Clara cells within NEBs	$Scgb1a1^+$; $Cyp2f2^-$	Ciliated and secretory cells	Naphthalene injury
		Distal airways	
Variant Clara cells at BADJs (putative BASCs)	$Scgb1a1^+$; $Sftpc^+$; $Cyp2f2^-$	Bronchiolar and alveolar cells	Naphthalene injury/Bleomycin injury
AEC II	$Sftpc^+$	AEC I	O_2/NO_2/Bleomycin

In a similar context, Kim et al. have identified BASCs as $CD45^-$ $CD31^-$ $Sca\text{-}1^+$ $CD34^+$ cells. These cells showed resistance to bronchiolar and alveolar damage and proliferated during epithelial regeneration following injury. These cells represent 0.008-0.064% of the total F1 129/SvJ/C57BL/6 adult lung (Kim et al., 2005). On the other hand, McQualter et al. were able to define lung epithelial stem/progenitor cells as $EpCam^{hi}$ $CD49f^+$ $CD104^+$ $CD24^{low}$. Their study was based on the ability of this cell population to form colonies in the presence of mesenchymal support, giving rise to airway, alveolar and mixed epithelial lineages. These epithelial stem/progenitor cells constitute less than 0.02% of the total C57BL/6 adult lung (McQualter et al., 2010). This work was complemented by Chapman et al. who used the bleomycin injury model to demonstrate that $Sftpc^-$ $CD49f^+$ $CD104^+$ cells constitute a stable progenitor population that replenishes AEC II during lung repair (Chapman et al., 2011). The various cluster of differentiation (CD) molecules used to define progenitor/stem cell populations are summarized in Supplementary Table S1.

1.1.2. Mesenchymal stromal (stem) cells (MSCs) in the adult mouse lung

Contrary to the lung epithelium, the lineage tree of the lung mesenchyme is poorly understood. This part of the lung consists of a wide array of cell types such as smooth muscle cells, endothelial cells, chondrocytes, nerve cells, lipofibroblasts, myofibroblasts, lymphatic cells and others. Whereas epithelial progenitors have been identified using the aforementioned epithelial injury models, very little success has been made in understanding the hierarchy, if any, of mesenchymal progenitors in the adult mouse lung. Models of fibroblast hyper-proliferative diseases such as asthma, pulmonary arterial hypertension (PAH) and lung fibrosis have been routinely used and many hypotheses have been suggested regarding the origin of over-proliferating fibroblasts. For instance, the origin of collagen-secreting, *αSma*-positive activated myofibroblasts in lung fibrosis is still unknown. It is believed that they originate from resident fibroblasts (Phan, 2002; Hoyles et al., 2011), bone marrow-derived circulating fibrocytes (Phillips et al., 2004; Lama and Phan, 2006) or AEC II via epithelial-to-mesenchymal transition (EMT) (Grunert et al., 2003; Kim et al., 2006). However, due to the lack of cell-specific markers, these

hypotheses remain controversial. Rock et al. have recently demonstrated that stromal cells, in bleomycin-induced pulmonary fibrosis in mice, exhibit heterogeneity and that pericyte-like cells undergo proliferation but fail to express high levels of the myofibroblast marker (*αSma*). The authors also used a *Sftpc*$^{Cre\text{-}ERT2}$ knock-in line to demonstrate the absence of EMT by AEC II (Rock et al., 2011).

Despite our poor knowledge regarding mesenchymal hierarchy in the lung, many studies have reported the presence of mesenchymal stromal (stem) cells (MSCs) in adult mouse lungs as well as fetal human lungs (Pittenger et al., 2000; Sabatini et al., 2005; Summer et al., 2007). These cells have the ability to commit to multiple fates including chondrogenic, adipogenic and myogenic lineages. Isolation and characterization of murine lung stem cells is based on their ability to efflux Hoechst 33342 dye and expression of *Stem cell antigen 1* (*Sca-1*) and *Mast/stem cell growth factor receptor Kit (c-Kit)*. Cells that have the preference to efflux Hoechst 33342 dye are referred to as Side population (SP) cells and they can be further categorized as having hematopoietic ($CD45^+$) or non-hematopoietic ($CD45^-$) origins (Goodell et al., 1996; Giangreco et al., 2004). $CD45^-$ $CD31^-$ $Sca\text{-}1^+$ $CD34^+$ SP cells were found to highly express stem cell markers such as *Sca-1* as well as markers specific to mesenchymal lineages such as *Thymocyte antigen 1 (Thy-1)* and *Platelet-derived growth factor receptor alpha (Pdgfrα)*. This population of cells is referred to as resident MSCs and accounts for approximately 1% of the total C57BL/6 adult lung (McQualter et al., 2009) (Fig. 2).

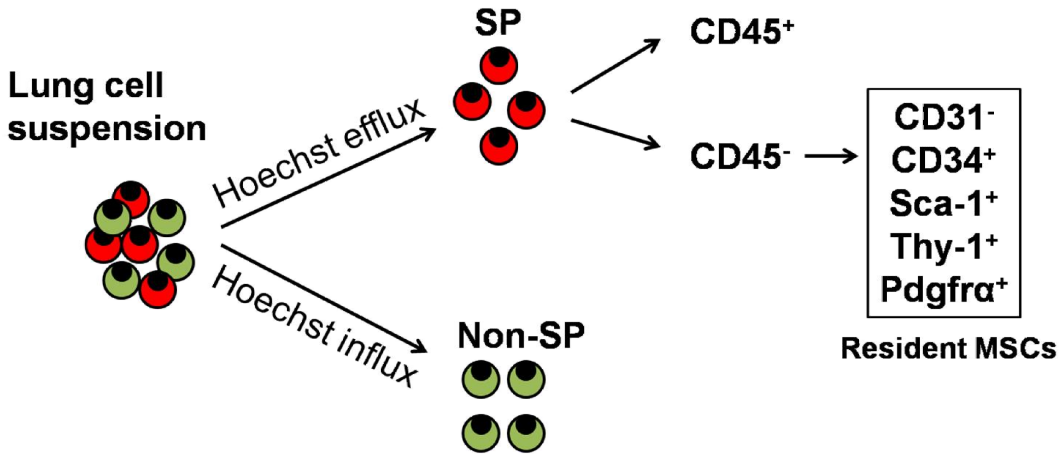

Figure 2. Scheme for the isolation strategy of resident MSCs from the adult mouse lung.
Cell suspensions from adult mouse lungs can be divided into SP and non-SP based on their ability to retain Hoechst dye. McQualter et al. have demonstrated that $CD45^-$ $CD31^-$ $Sca\text{-}1^+$ $CD34^+$ SP cells represent a population of resident progenitor cells and express mesenchymal-specific markers such as *Thy-1* and *Pdgfrα*. Abbreviations: MSCs: Mesenchymal stromal (stem) cells; SP: Side population.

In a similar context, Volckaert et al. have demonstrated that parabronchial smooth muscle cells (PBSMCs) represent a mesenchymal stem cell niche that is critical for epithelial regeneration following naphthalene injury. Their data suggest that *Fgf10* expression by PBSMCs is required for epithelial repair by variant Clara cells (Volckaert et al., 2011).

1.2. Overview of lung development: Progenitor cells are enriched in the embryonic lung

During murine embryonic development, the respiratory tract starts to form at embryonic day 9.5 (E9.5) as a budding of the ventral foregut endoderm. This respiratory domain is marked by *Thyroid transcription factor 1 (Ttf-1 or Nkx2.1)* expression. Around one day later (E10.5), the two lung buds are formed. At this stage, the splanchnic mesoderm sends instructive signals to the endoderm-derived epithelium to undergo branching morphogenesis (Spooner and Wessells, 1970). This developmental stage, termed

'Pseudoglandular stage', lasts until E16.5 (Fig. 3). The currently accepted branching model for the embryonic mouse lung consists of domain branching, planar bifurcation and orthogonal bifurcation (Metzger et al., 2008). In the meantime, many of the cell types that will populate the lung later on start to emerge. These include basal, neuroendocrine, ciliated and secretory cells. The lung then undergoes a short canalicular stage (E16.5 to E17.5) that is characterized by the formation of blood capillaries. During this stage, AEC I and II start to appear. In mice, functional alveoli start to form postnatally (from postnatal day 5 up to one month of age) whereas in humans, this process starts during late gestation and lasts up to two years. The alveolar stage is characterized by secondary septa formation and microvascular maturation (Burri, 2006). Reviews on lung development include (Cardoso, 2000; Warburton et al., 2000; Affolter et al., 2003; Cardoso and Lu, 2006; Morrisey and Hogan, 2010).

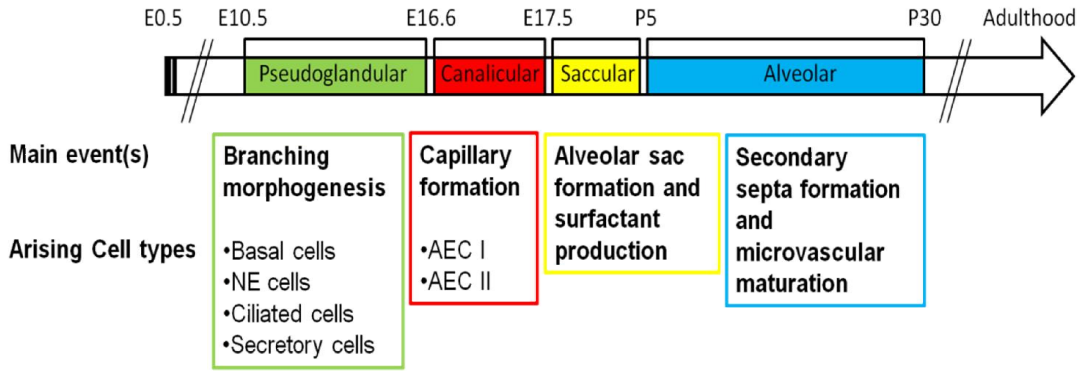

Figure 3. Overview of murine lung development showing the main events and arising cell types according to their chronological order.
NE: Neuroendocrine.

During the time course of lung development, proximal-distal patterning arises from a complex network of signaling pathways that control the proliferation, migration and differentiation of progenitor cells. In this section, epithelial and mesenchymal progenitors will be reviewed, with special emphasis on the role of paracrine interactions in specifying cell fate in the embryonic lung.

1.2.1. Epithelial progenitors are located at the distal tips in the embryonic lung

One of the early attempts to establish an epithelial progenitor cell hierarchy in the embryonic lung was done by Wuenschell et al. who used an immunohistochemical approach to demonstrate the spatio-temporal expression of epithelial markers during development (Wuenschell et al., 1996). The authors used Calcitonin gene-related peptide (*Cgrp*), Clara cell secretory protein (*Ccsp or Scgb1a1*) and Surfactant protein-A (*Sftpa*) as markers of differentiated neuroendocrine cells, Clara cells and AEC II respectively. The authors concluded that all three markers are co-expressed in the distal epithelium between E13 and E15, after which they are restricted to specific cell lineages. The data suggest that most epithelial lineages are derived from common progenitors from the pseudoglandular stage.

On the other hand, Perl et al. used transgenic mice carrying (rat) *Ccsp-rtTA* or (human) *SFTPC-rtTA; Tet(O)-Cre* constructs combined with Alkaline phosphatase or GFP reporters to demonstrate that ciliated and non-ciliated cells, but not neuroendocrine cells, derive from common Scgb1a1^{+} Sftpc^{+} progenitors (Perl et al., 2005).

More recently, Rawlins et al. used an *Inhibitor of differentiation 2* knock-in mouse line *(Id2$^{Cre-ERT2}$)* to target epithelial progenitors during the pseudoglandular and canalicular stages of lung development (Rawlins et al., 2009). Their data show that *Id2*-positive progenitor cells, located in the distal tips of the lung epithelium, give rise to ciliated, non-ciliated and neuroendocrine cells when labeled at the pseudoglandular stage. In contrast, these cells only contribute to alveolar cells when labeled at the canalicular stage. Lastly, the *Id2*-positive progenitor cell population is not retained after birth.

In this context, Notch signaling pathway has been proposed to be critical for establishing a balance between ciliated and non-ciliated cell fates in the developing lung. Conditional inactivation of Notch signaling in the endoderm using *Shh^{Cre}* leads to the enrichment of ciliated cells at the expense of non-

ciliated secretory cells (Tsao et al., 2009). Moreover, members of the Forkhead box protein family have also been proposed to be involved in specifying cell fate and controlling proliferation rates of epithelial progenitors. Recently, it has been shown that FOXP1 and 4 transcription factors act during development to repress the Goblet cell program in epithelial progenitors (Li et al., 2012).

Wnt signaling has been shown to play an important role in proximal-distal patterning of the developing lung epithelium. Loss of function of *β-Catenin* using *SFTPC-rtTA; Tet(O)-Cre* system leads to the inhibition of distal airways and enlargement of the proximal airways (Mucenski et al., 2003). An opposite phenotype was reported with gain of function of *β-Catenin* using *Ccsp-rtTA; Tet(O)-Cre* system (Mucenski et al., 2005).

To sum up, distal epithelial progenitors, having a high proliferation index and expressing *Sox9* and *Id2*, give rise to most of the epithelial cell types during the pseudoglandular stage. As these cells lose *Sox9* and *Id2* expression and start expressing the proximal lung marker *Sox2*, their lineage commitment becomes restricted to specific cell types. Notch, Wnt, BMP and FGF signaling pathways are believed to be involved in fate determination of epithelial progenitors during lung development [Reviewed in (Rock and Hogan, 2011)].

1.2.2. Mesenchymal progenitor cells in the developing mouse lung

The lung mesenchyme consists of a widely heterogeneous population of cells that play crucial roles during development and homeostasis after birth. Some of these cell types derive from a common multipotent mesenchymal progenitor whereas others derive from a unique progenitor population. A number of mesenchymal progenitors have been identified using transgenic and knock-in mouse lines that allow fate mapping of mesenchymal cells during lung development. For example, our research group has previously used *Fibroblast growth factor 10 (Fgf10)-LacZ* transgenic line (originally reported as *Mlcv1v-nLacZ-24*) to demonstrate that *Fgf10*-expressing cells are progenitors for PBSMCs in the distal lung during early embryonic development (Mailleux et al., 2005). Shan et al., on the other hand, have

identified a population of mesenchymal cells, initially located near the lung hilum, as progenitors for airway smooth muscle cells (Shan et al., 2008). Using *Wilm's tumor protein 1 (Wt1)-Cre* transgenic line, Que et al. have suggested that the mesothelium is a source of vascular – but not airway – smooth muscle cells (Que et al., 2008). On the contrary, Greif et al. have shown that vascular smooth muscle cells arise from *Pdgfrβ*-positive mesenchymal cells rather than *Wt1*-positive mesothelial cells (Greif et al., 2012). *Fetal liver kinase 1* (*Flk-1*), another term for *Vascular endothelial growth factor receptor 2* (*Vegfr2*), has been identified as the earliest marker for endothelial progenitors (angioblasts). These cells respond to epithelial as well as mesenchymal VEGF-A, and give rise to the capillary plexus surrounding the airways. *Flk-1*-positive endothelial progenitors were identified using *Flk-1-LacZ* transgenic mice (Yamaguchi et al., 1993; Kappel et al., 1999; Del Moral et al., 2006). Hematopoietic cells were shown to also derive from *Flk-1*-positive cells in the lung (Lugus et al., 2009). Using *Prospero homeobox protein 1 (Prox1)*$^{Cre\text{-}ERT2}$ knock-in line, Srinivasan et al. have shown that lympthatic cells arise from *Prox1*-positive progenitor cells (Srinivasan et al., 2007). On the hand, Langsdorf et al. have shown that nerve cells originate from the neural crest. The authors used *Receptor tyrosine kinase (Ret)*^{eGFP} knock-in line to transiently trace neuronal progenitors during embryonic development (Langsdorf et al., 2011). Table 2 shows some of the different mesenchymal cell types and their progenitors as well as the developmental stage at which they start to appear in the lung.

Table 2. Mesenchymal cell types, the stage at which they start to emerge and their corresponding progenitors in the embryonic and postnatal mouse lung. Abbreviations: Flk-1: Fetal liver kinase 1 (or Vegfr2); LECs: Lymphatic endothelial cells; NCCs: Neural crest-derived cells; Pdgfrα/β: Platelet-derived growth factor receptor alpha/beta; Prox1: Prospero homeobox protein 1; Ret: Receptor tyrosine kinase; Wt1: Wilm's tumor protein 1.

Mesenchymal cell type	Time of onset	Progenitor cells	Reference(s)
Endothelial cells	E9.5	Flk-1$^+$ cells	(Yamaguchi et al., 1993; Kappel et al., 1999)
Hematopoietic cells	E9.5	Flk-1$^+$ cells	(Lugus et al., 2009)
Lymphatic cells	E9.5	Prox1$^+$ LECs	(Srinivasan et al., 2007)
Nerve cells	E11.5	Ret$^+$ NCCs	(Langsdorf et al., 2011)
Parabronchial smooth muscle cells	E11.5	Fgf10$^+$ cells	(Mailleux et al., 2005) and (El Agha et al., in revision)
Vascular smooth muscle cells	E11.5	Wt1$^+$ cells	(Que et al., 2008)
		Pdgfrβ$^+$ cells	(Greif et al., 2012)
		Fgf10$^+$ cells	(El Agha et al., in revision)
Cartilage	E13.5-E15.5	Unknown	(Miller et al., 2004)
Lipofibroblasts	E15.5	Fgf10$^+$ cells	(El Agha et al., in revision)
Alveolar myofibroblasts	P4	Pdgfrα$^+$ cells	(Boström et al., 1996; Lindahl et al., 1997)

Most of the aforementioned mesenchymal lineages start to emerge during early stages of lung development (Table 2). In mice, the last stage of lung development occurs postnatally and is characterized by the transition from primitive alveoli (sacs) to mature alveoli (Fig. 3). This stage is characterized by the prevalence of two mesenchymal lineages: Alveolar myofibroblasts and lipofibroblasts. Alveolar myofibroblasts represent a population of *αSma*-positive interstitial fibroblasts that populate the lung during postnatal alveolarization. These cells deposit ECM proteins that are critical for secondary septa formation (Vaccaro and Brody, 1978; Noguchi et al., 1989; Yamada et al., 2005) and are believed to derive from *Pdgfrα*-positive cells. *Platelet-derived growth factor a* (*Pdgfa)*-null newborns suffer from arrest in alveologenesis due to the absence of alveolar myofibroblasts (Boström et al., 1996; Lindahl et al., 1997).

On the other hand, the origin of lipofibroblasts is poorly understood. Lipofibroblasts are adipocyte-like interstitial fibroblasts that reside in the late fetal and postnatal lung parenchyma in the vicinity of AEC II (O'Hare and Sheridan, 1970; Vaccaro and Brody, 1978). AEC II signal to lipofibroblasts via Parathyroid hormone-related protein (PTHrP) to activate the Peroxisome proliferator-activated receptor gamma (PPARγ) pathway. This signaling pathway has shown to be critical for the induction and maintenance of the lipofibroblast phenotype. *In vivo* inactivation of the PTHrP pathway leads to abnormal alveolarization with defective surfactant synthesis (Rubin et al., 2004; Torday and Rehan, 2007; Rehan and Torday, 2012). In response to PPARγ activation, lipofibroblasts express *Adipose differentiation-related protein* (*Adrp*) that is critical for trafficking of lipid substrates and subsequently providing AEC II with triglycerides for surfactant production (Schultz et al., 2002). Lipofibroblasts also secrete leptin that stimulates surfactant production by AEC II (Torday et al., 2002) (Fig. 4). In addition to triglycerides, lipofibroblasts also store retinoic acids which are essential for alveolar septation (Simon and Mariani, 2007).

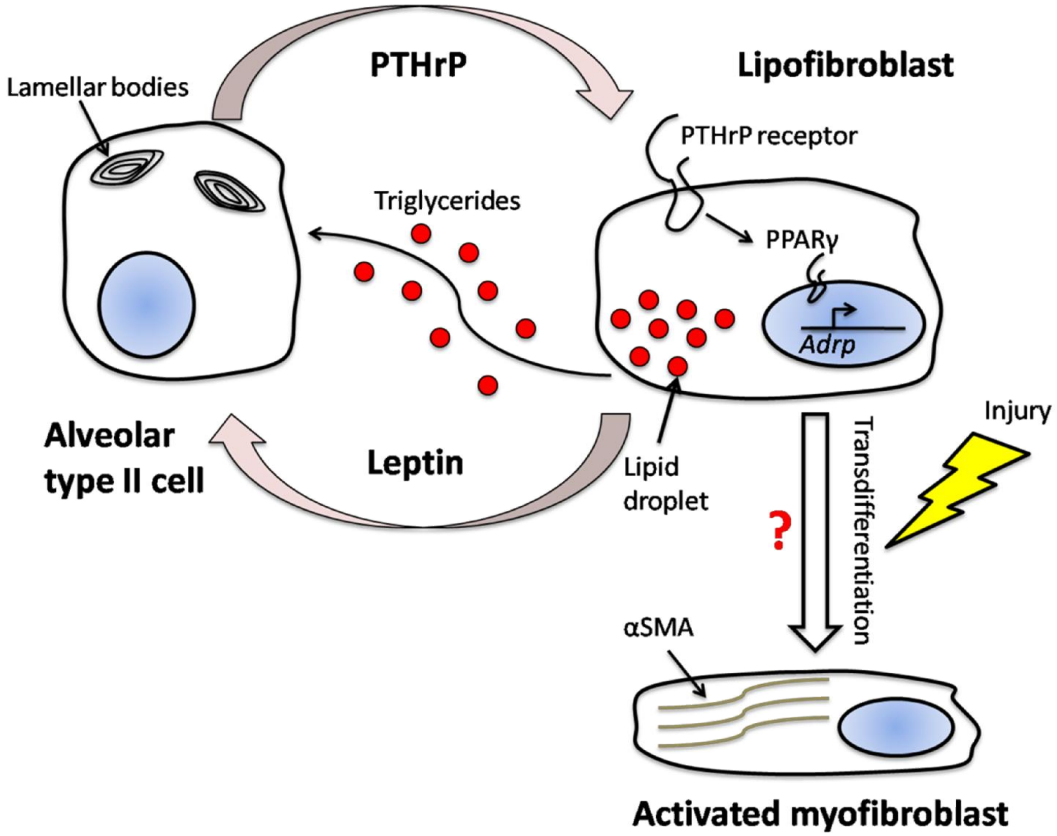

Figure 4. Schematic representation of lipofibroblast-AEC II interactions.
AEC II signal to lipofibroblast progenitors via PTHrP to induce and maintain the lipofibroblast phenotype and prevent their transdifferentiation to activated myofibroblasts. In response to PTHrP, PPARγ pathway is activated, resulting in *Adrp* and *Leptin* expression. Lipofibroblasts provide AEC II with triglycerides for surfactant production. It has been proposed that injury to AEC II leads to downregulation of *PTHrP* leading to lipofibroblast-to-myofibroblast transdifferentiation. Abbreviations: Adrp: Adipose differentiation-related protein; PPARγ: Peroxisome proliferator-activated receptor gamma; PTHrP: Parathyroid hormone-related protein.

In summary, lipofibroblasts are believed to be critical not only for surfactant production but also for alveolar septation. It has been demonstrated that injury to AEC II, caused by prematurity, barotrauma, hyperoxia, nicotine or infections, disrupts paracrine PTHrP signaling leading to lipofibroblast-to-myofibroblast transdifferentiation (Torday et al., 2003) (Fig. 4). This scenario is likely to occur in idiopathic pulmonary fibrosis (IPF) especially that it has

been shown that lipofibroblasts exist in adult human lungs (Rehan et al., 2006). In this dissertation, we provide evidence that *Fgf10*-expressing cells are progenitors for lipofibroblasts in the embryonic as well as postnatal lung.

The simplest developmental stage that allows studying of paracrine signaling pathways in the embryonic lung is the mid-pseudoglandular stage (around E13.5). At this stage, it is easy to distinguish the three layers that constitute the lung: the mesothelium that constitutes the outer-most layer, the mesenchyme that constitutes the ECM and the epithelium which is the inner-most layer. The mesenchyme can be further divided into two compartments, each of which is populated by distinct mesenchymal progenitors: the dense circumferentially-oriented sub-epithelial mesenchyme (SEM) and the rather loose non-oriented sub-mesothelial mesenchyme (SMM) (White et al., 2006) (Fig. 5A). It is widely accepted that the interaction between these multiple cellular domains is critical for amplification of progenitors as well as cell-fate determination. Tissue interactions and their role in lineage commitment of mesenchymal cells will be discussed in the following section.

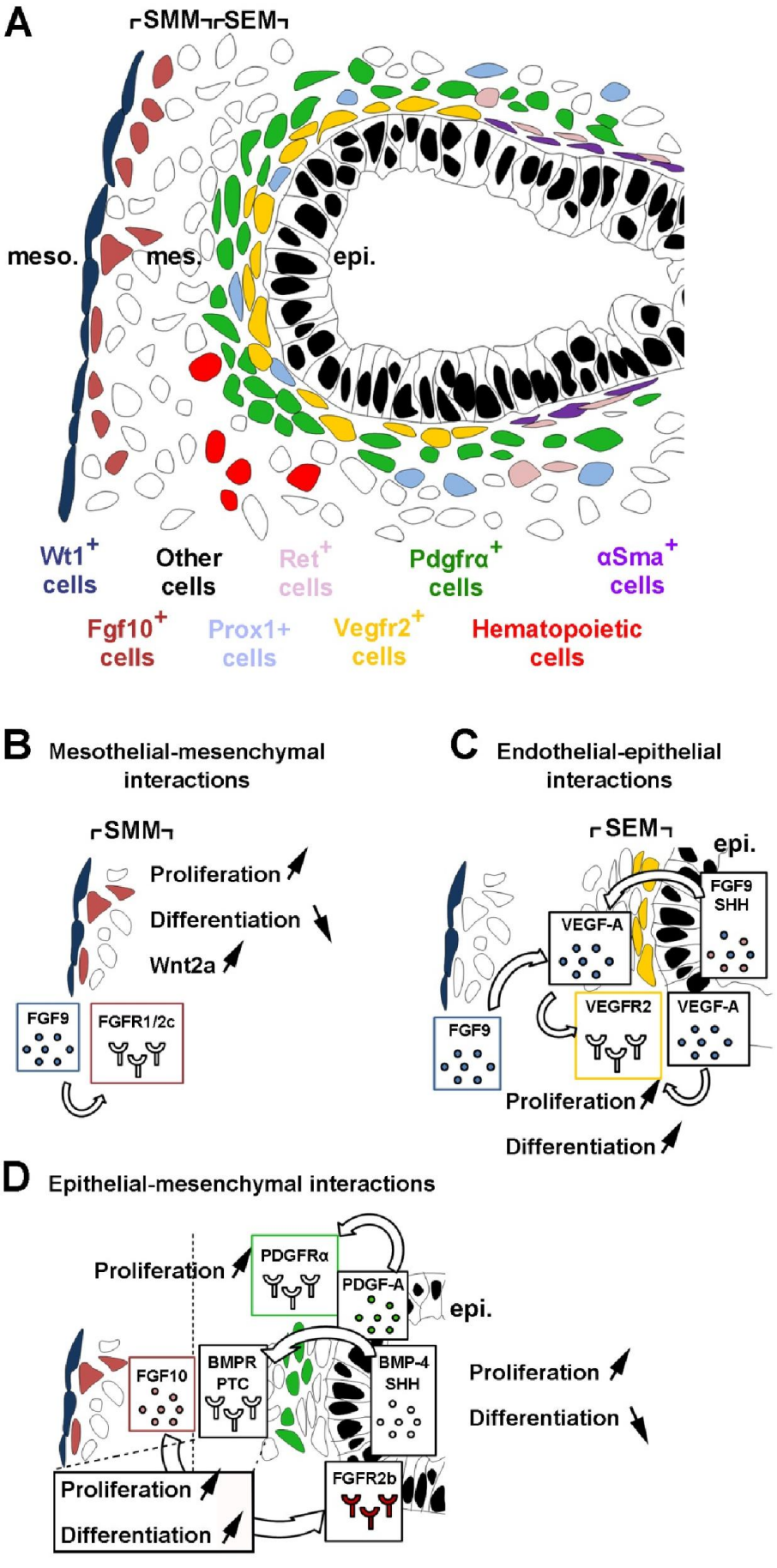
A
⌐SMM¬⌐SEM¬
meso.
mes.
epi.
Wt1+ cells
Other cells
Ret+ cells
Pdgfrα+ cells
αSma+ cells
Fgf10+ cells
Prox1+ cells
Vegfr2+ cells
Hematopoietic cells
B Mesothelial-mesenchymal interactions
⌐SMM¬
Proliferation
Differentiation
Wnt2a
FGF9
FGFR1/2c
C Endothelial-epithelial interactions
⌐SEM¬
epi.
FGF9 SHH
VEGF-A
VEGFR2
VEGF-A
FGF9
Proliferation
Differentiation
D Epithelial-mesenchymal interactions
Proliferation
PDGFRα
PDGF-A
epi.
FGF10
BMPR PTC
BMP-4 SHH
Proliferation
Differentiation
FGFR2b
Proliferation
Differentiation

Figure 5. Tissue interactions and mesenchymal cell-fate determination in the embryonic lung.
(**A**) Schematic representation showing the different cellular layers as well as mesenchymal and mesothelial progenitor cells in the embryonic mouse lung at E13.5. The lung epithelium is lined by PBSMCs (violet) from the proximal side. The smooth muscle cell layer is innervated by neural crest-derived *Ret*-positive cells (pink). The latter cells exist in the form of neuronal fibers (surrounding the PBSMC layer) or cell bodies in the mesenchyme. *Vegfr2*-positive cells (yellow), *Pdgfrα*-positive cells (green) and *Prox1*-positive cells (light blue) lie within the SEM. *Fgf10*-positive cells (dark red) reside in the SMM whereas *Wt1*-positive cells (dark blue) reside in the mesothelium. Note the presence of hematopoietic cells (red) in the lung mesenchyme. (**B**) FGF9, secreted by the mesothelium, induces proliferation and inhibits differentiation of *Fgf10*-positive cells via Wnt2a-mediated Wnt signaling. (**C**) VEGF-A, secreted by the epithelium and the mesenchyme, induces amplification and differentiation of *Vegfr2*-positive progenitor cells residing in the SEM. These cells give rise to the capillary plexus surrounding the epithelium. (**D**) FGF10, secreted by the SMM, acts via its epithelial receptor FGFR2b to induce branching morphogenesis as well as maintenance of epithelial progenitors. On the other hand, SHH and BMP-4, secreted by the epithelium, act as negative regulators of *Fgf10* but induce mesenchymal proliferation and differentiation through PTC and BMPR respectively. *Pdgfrα*-positive cells in the SEM respond to epithelial PDGF-A and undergo proliferation. These cells eventually give rise to alveolar myofibroblasts during alveologenesis. Abbreviations: BMP-4: Bone morphogenetic protein 4; BMPR: Bone morphogenetic protein receptor; Epi: Epithelium; Mes: Mesenchyme; Meso: Mesothelium; PTC: Patched; SEM: Sub-epithelial mesenchyme; SHH: Sonic hedgehog; SMM: Sub-mesothelial mesenchyme; VEGF-A: Vascular endothelial growth factor A; αSma: Alpha Smooth muscle actin. *Adopted and modified from an H/E stained E13.5 lung section from* (White et al., 2006).

1.2.2.1. Mesothelial-mesenchymal interactions: The SMM is under the effect of FGF9 signaling via the Wnt pathway

Both being of mesodermal origin, the lung mesothelium and the adjacent mesenchyme undergo paracrine signaling that is critical for proper lung development. FGF9, secreted by the mesothelium, acts through the

mesenchymal splice variant (c) of Fibroblast growth factor receptor 1 and 2 (FGFR1/2c) to induce proliferation of mesenchymal cells in the SMM, including *Fgf10*-positive cells (Colvin et al., 2001) (Fig. 5B). FGF9 maintains these cells in a progenitor-like state by preventing their differentiation to smooth muscle cells. Loss of function of *β-Catenin* in the lung mesenchyme using *Dermo1^{Cre}; β-Catenin^{flox}* system has shown that FGF9 effect on mesenchymal cells is mediated by Wnt signaling. Wnt2a seems to provide a permissive signal for FGF9 signaling, allowing the activation of β-Catenin signaling that leads to proliferation of mesenchymal cells in the SMM (White et al., 2006; De Langhe et al., 2008; Yin et al., 2008, 2011). Furthermore, Del Moral et al. have shown that FGF9 acts not only on the mesenchyme, but also on the epithelium to induce proliferation, but not differentiation, via Wnt signaling (Del Moral et al., 2006).

1.2.2.2. Endothelial-epithelial interactions: VEGF-A/VEGFR2 signaling is critical for the formation of the capillary network

The lung vasculature starts to develop as soon as the primary lung buds are formed (Gebb and Shannon, 2000). deMello et al. proposed a model in which central vessels (proximal) are formed by angiogenesis (branching of pre-existing vessels) and peripheral vessels (distal) by vasculogenesis (*in situ* differentiation of endothelial progenitors). The two components fuse to form a continuous vascular lumen via a lytic process around E13/14 and the pulmonary circulation would be established (deMello et al., 1997).

The earliest marker of endothelial cells in the developing lung is *Flk-1* or *Vegfr2* (Yamaguchi et al., 1993; Kappel et al., 1999). VEGF-A, an endothelial cell mitogen and angiogenic factor, is secreted by the developing epithelium as well as mesenchyme and it acts on *Vegfr2*-positive progenitor cells residing in the SEM (Bhatt et al., 2000; Del Moral et al., 2006) (Fig. 5C). These mesenchymal cells eventually give rise to the capillary plexus that surrounds the epithelium. Interestingly, Lugus et al. have reported that *Vegfr2*-positive cells also give rise to primitive and definitive blood cells. The authors used *Flk-1$^{Cre/+}$; Rosa26R^{LacZ}* and *Flk-1$^{Cre/+}$; Rosa26R^{eYFP}* systems to demonstrate that hematopoietic cells residing in the lung mesenchyme derive

from resident *Vegfr2*-positive cells (Lugus et al., 2009). White et al. have shown that SHH (epithelial derived) and FGF9 (epithelial and mesothelial-derived) upregulate the expression of *Vegf-a* in the lung mesenchyme (Fig. 5C) (White et al., 2007). On the other hand, VEGF-A has also been shown to act indirectly on the lung epithelium. Del Moral et al. have shown that exogenous VEGF-A promotes branching morphogenesis in the epithelium and increases the proliferation index in both the epithelium and mesenchyme of E11 lung explants. VEGF-A upregulates *Bmp-4* and *Sftpc* and induces proliferation of *Vegfr2*-positive cells (Del Moral et al., 2006).

Endothelial-epithelial interactions have been shown to be critical for lung regeneration after pneumonectomy. Ding et al. have demonstrated that VEGFR2 and FGFR1 activation in pulmonary capillary endothelial cells is required for inducing MMP14 secretion. MMP14 unmasks EGFR ecto-domains in the lung epithelium and thus increases the bioavailability of EGFR ligands. This mechanism induces the expansion of epithelial progenitors during compensatory lung growth (Ding et al., 2011).

1.2.2.3. Epithelial-mesenchymal interactions: Paracrine signaling controls cell proliferation and differentiation in the epithelium and mesenchyme

Epithelial-mesenchymal interactions are critical for proper lung development. Sonic hedgehog (SHH), Bone morphogenetic protein-4 (BMP-4), FGFs and Wnt ligands are diffusible molecules that mediate epithelial-mesenchymal interactions in the developing lung [Reviewed in (Shannon and Hyatt, 2004)]. SHH, secreted by the epithelium, acts through its mesenchymal receptor Patched (PTC) to induce mesenchymal cell proliferation and differentiation (Fig. 5D). Treatment of E11.5 lung explants with recombinant SHH has shown to upregulate mesenchymal markers including its own receptor (*Ptc)*, *Noggin*, *Sma* and *Myosin* (Bellusci, Furuta, et al., 1997; Weaver et al., 2003). On the other hand, *Bmp-4* has a dynamic expression pattern in the distal endoderm as well as the mesenchyme during early pseudoglandular stage (E11.5). Its expression is rather restricted to the epithelium beyond E13.5 (Fig. 5D). BMP-

4 mediates epithelial-interactions and is critical for PBSMC formation (Weaver et al., 1999, 2003).

One of the main features of SHH and BMP-4 signaling is inhibition of *Fgf10* expression. FGF10 is one of the key growth factors secreted by stromal cells in the distal mesenchyme (Bellusci, Grindley, et al., 1997). It acts in a paracrine fashion on the opposite epithelium expressing the epithelial isoform (b) of FGFR2-III (FGFR2-IIIb or simply FGFR2b) (Fig. 5D). FGF10/FGFR2b signaling is critical for proper lung development and disruption of this pathway by genetic manipulation leads to detrimental consequences that range from branching simplification to agenesis of the lung (Peters et al., 1994; Sekine et al., 1999; De Moerlooze et al., 2000; Perl and Gale, 2009). FGF10 promotes epithelial survival and branching and its dosage is crucial for the amplification of epithelial progenitors (Ramasamy et al., 2007).

In the following section, the FGF superfamily will be introduced and the role of FGF10 during development and postnatal life will be reviewed.

1.3. The FGF superfamily: From development to postnatal life

Fibroblast growth factors (FGFs) constitute a family of polypeptides that are involved in diverse organogenetic programs during development as well as homeostatic balance during postnatal life. The FGF ‘story’ dates back to the mid-70s when Hugo A. Armelin observed that pituitary extracts have a proliferative effects on NIH3T3 fibroblasts growing *in vitro* (Armelin, 1973). The first FGFs (FGF1/2/3) were later purified from bovine brain and pituitary gland (Gospodarowicz, 1975; Gospodarowicz et al., 1978). To date, the *FGF* gene family has shown to consist of 22 members (*FGF1-23*). *FGF15* has not been identified in humans whereas *Fgf19* has not been identified in mouse and rat [Reviewed in (Itoh and Ornitz, 2011)].

According to their mode of action, FGFs can be classified into intracrine, endocrine and paracrine FGFs (Table 3). As the name suggests, intracrine FGFs (FGF11-14) are not secreted extracellularly and they do not require the FGF receptor (FGFR) to function. Rather, they are retained inside the cell

where they interact with other intracellular signaling pathways. Intracrine FGFs are believed to control the excitability of nerve cells (Goldfarb et al., 2007; Shakkottai et al., 2009). Recently, it has been shown that *Fgf13* knockout mice suffer from impaired neuronal polarization and migration, in addition to weakened learning and memory. This phenotype mimics X-chromosome-linked mental retardation (XLMR) in humans (Wu et al., 2012).

Endocrine FGFs (FGF15/19, 21 and 23) are hormone-like FGFs and they are involved in multiple metabolic pathways, especially lipid metabolism. They have low affinities to FGFRs and heparin/heparan sulphate which enables them to function in a hormone-like fashion. Endocrine FGFs are believed to function in a common signal transduction pathway with the transmembrane protein Klotho, mediating lipid, bile acid, phosphate and vitamin D metabolisms (Shimada et al., 2004; Urakawa et al., 2006; Kurosu et al., 2007; Hotta et al., 2009).

Table 3. Subfamilies of human *FGF* genes and the corresponding phenotypes of *Fgf*$^{-/-}$ mice.

* *FGF19* is the human ortholog of mouse *Fgf15*. ND: Not determined. *Reviewed in* (Ornitz and Itoh, 2001; Itoh and Ornitz, 2004, 2008, 2011; Itoh, 2007; Beenken and Mohammadi, 2009).

	Human gene	Corresponding murine *Fgf*$^{-/-}$ phenotype	Phenotype description
Paracrine			***FGF1* subfamily**
	FGF1	Viable	ND
	FGF2	Viable	Cardiovascular, neuronal and skeletal defects
			***FGF4* subfamily**
	FGF4	Lethal E4-5	Blastocyst formation defect
	FGF5	Viable	Hair development defect
	FGF6	Viable	Impaired muscle regeneration

	***FGF7* subfamily**		
	FGF3	Viable	Inner ear, tail and CNS defects
	FGF7	Viable	Impaired hair and kidney development
	FGF10	Lethal P0	Impaired multi-organ development
	FGF22	Viable	Impaired synapse differentiation and delayed weight gain
	***FGF9* subfamily**		
	FGF9	Lethal P0	Lung, heart, vascular, GI tract and testis developmental defects
	FGF16	Viable	Impaired cardiac and facial development
	FGF20	Viable	Impaired inner ear development
	***FGF8* subfamily**		
	FGF8	Lethal E8	Defects in gastrulation; brain, eye, ear and limb development
	FGF17	Viable	Impaired hind brain development
	FGF18	Lethal P0	Impaired multi-organ development
Intracrine	***FGF11* subfamily**		
	FGF11	ND	ND
	FGF12	Viable	ND
	FGF13	Viable	Impaired neuronal polarization and migration
	FGF14	Viable	Ataxia; Paroxysmal hyperkinetic movement disorder
Endocrine	***FGF19* subfamily**		
	FGF19*	Lethal E13.5-P7	Impaired cardiac outflow tract morphogenesis and bile acid metabolism
	FGF21	Viable	Impaired lipid metabolism
	FGF23	Lethal wk4-13	Impaired phosphate and vitamin D metabolism

On the other hand, paracrine FGFs (FGF1, 4, 7, 9 and 8 subfamilies) bind with high affinities to heparin/heparan sulphate and strictly function via FGFRs. These FGFs are involved in multiple organogenetic programs such as heart, lung, brain, muscle, kidney, hair, ear, limb and craniofacial development. Depending on ligand-receptor specificity, these FGFs bind and activate epithelial (b) or mesenchymal (c) isoforms of FGFRs. Table 4 summarizes the different FGFR isoforms and their corresponding FGF ligands.

Table 4. Ligand-receptor specificity of human FGFRs.
Demonstrated and reviewed in (Ornitz et al., 1996; Itoh and Ornitz, 2004; Zhang et al., 2006).

Human Gene	Protein	Ligands
FGFR1	FGFR1b	FGF1, 2, 3, 10 and 22
	FGFR1c	FGF1, 2, 4, 5 and 6
FGFR2	FGFR2b	FGF1, 3, 7, 10 and 22
	FGFR2c	FGF1, 2, 4, 6 and 9
FGFR3	FGFR3b	FGF1 and 9
	FGFR3c	FGF1, 2, 4, 8 and 9
FGFR4	FGFR4	FGF1, 2, 4, 6, 8 and 9

To demonstrate the receptor-ligand specificity of FGF signaling, we carried out an experiment where embryonic lungs (E11.5) were isolated and allowed to grow in an air-liquid interphase in the presence of recombinant human FGF7, 9 or 10 (Fig. 6). Having FGFR2b as their main receptor, FGF7 and FGF10 act on the epithelium to induce proliferation/dilation (Fig. 6D-F) or migration/branching (Fig. 6J-L) respectively. On the other hand, FGF9 signals through epithelial as well as mesenchymal isoforms of FGFRs and induces epithelial dilation and mesenchymal thickening (Fig. 6G-I).

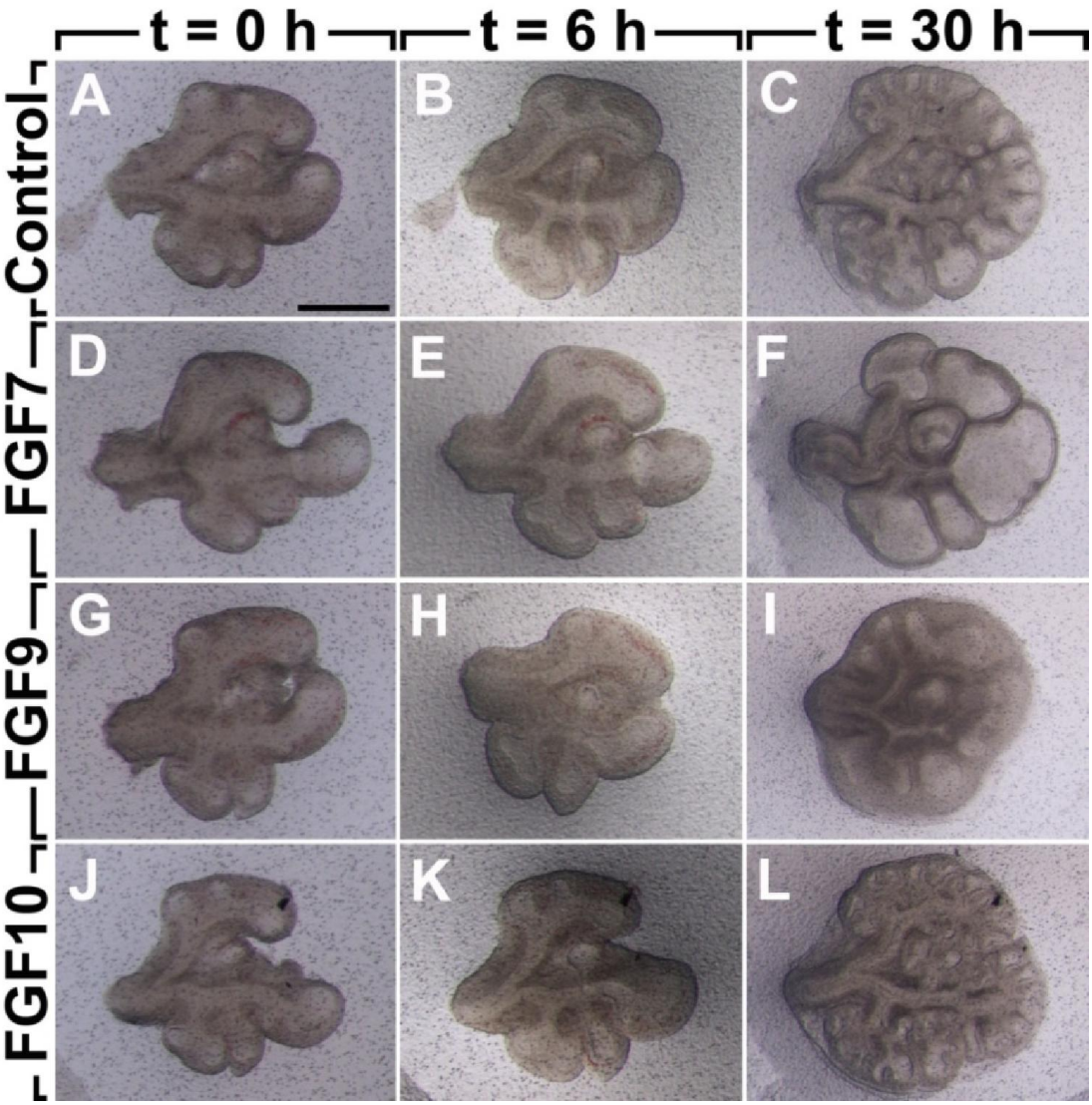

Figure 6. Recombinant FGFs confer unique effects on organotypic cultures *in vitro*.

E11.5 lungs were cultured in an air-liquid interphase for 30 h. (**A-C**) Lung growing in the absence of exogenous recombinant growth factors. The epithelium undergoes branching morphogenesis and the mesenchyme becomes thinner over time. (**D-F**) In the presence of recombinant FGF7 (100 ng/mL), the epithelium is dilated at the expense of the mesenchyme. (**G-I**) Recombinant FGF9 (200 ng/mL) induces dilation of the epithelium as well as thickening of the mesenchyme. (**J-L**) Addition of recombinant FGF10 (250 ng/mL) enhances epithelial branching. Scale bar: 500 µm.

Since FGF10 is central in the reported project, we will discuss its role in embryogenesis and homeostasis in a more detailed manner in the following section.

1.3.1. FGF10 is a key regulator of organogenesis, maintenance of epithelial progenitors and controls the formation of mesenchymal lineages during embryonic development

Fgf10 was first reported in 1996 by Yamasaki et al. who used homology PCR to identify and isolate a novel *Fgf* cDNA from rat embryos. Being the 10th reported FGF at that time, it was named FGF10 (Yamasaki et al., 1996). One year later, the expression pattern of *Fgf10* was described in the rat brain (Hattori et al., 1997) and its roles in chick limb bud outgrowth (Ohuchi et al., 1997) and murine lung endoderm branching (Bellusci, Grindley, et al., 1997) were reported. FGF10 was proposed to have a chemotactic effect on the opposite endoderm expressing *Fgfr2b* (Bellusci, Grindley, et al., 1997; Park et al., 1998; Ohuchi et al., 2000). The role of FGF10 in lung and limb development was demonstrated by *Fgf10*- and *Fgfr2b*-null embryos that suffer from lung and limb agenesis (Sekine et al., 1999; De Moerlooze et al., 2000). FGF10 was also shown to be critical for the development of diverse organs and tissues including the prostate (Thomson and Cunha, 1999), white adipose tissue (Yamasaki et al., 1999; Sakaue et al., 2002), lacrimal glands (Makarenkova et al., 2000), thyroid (Ohuchi et al., 2000), pituitary gland (Ohuchi et al., 2000; Rosenfeld et al., 2000), kidney (Ohuchi et al., 2000), inner ear (Ohuchi et al., 2000; Pirvola et al., 2000), thymus (Ohuchi et al., 2000; Revest et al., 2001), pancreas (Ohuchi et al., 2000; Bhushan et al., 2001), mammary glands (Mailleux et al., 2002), incisors (Ohuchi et al., 2000; Harada et al., 2002), whiskers (Ohuchi et al., 2003), hair follicle (Ohuchi et al., 2000; Petiot et al., 2003), cecum (Burns et al., 2004; Fairbanks, Kanard, et al., 2004), anorectum (Fairbanks, De Langhe, et al., 2004), palate (Rice et al., 2004), external genitalia (Satoh et al., 2004), duodenum (Kanard et al., 2005), colon (Fairbanks et al., 2005), urethra (Petiot et al., 2005), eyelids (Tao et al., 2005), submandibular salivary glands (Ohuchi et al., 2000; Jaskoll et al., 2005), stomach (Ohuchi et al., 2000; Nyeng et al., 2007) and liver (Berg et al.,

2007).

Early transcriptional targets of FGF10 during lung bud morphogenesis were studied by Lu et al. The authors used microarray analysis on mesenchyme-free lung epithelial explants and *in situ* hybridization on intact embryonic lungs to show that FGF10 induces genes that are involved in cell rearrangement and migration, inflammatory processes, lipid metabolism and tumor invasion. No proliferative effect on the lung epithelium was observed (Lu et al., 2005).

The currently accepted mode of action for FGF10 on the lung epithelium during development is divided into two parts: Chemotaxis and maintenance of epithelial progenitors. The chemotactic function of FGF10, related to its dynamic expression pattern, is demonstrated by the perturbed branching pattern in *Fgf10*-overexpressing lungs (Clark et al., 2001). More recently, it has been suggested that FGF10 controls the mitotic spindle orientation in the developing epithelium via RAS-regulated ERK1/2 signaling pathway, thus determining lung tube shape (Tang et al., 2011). On the other hand, FGF10 is critical for the maintenance of epithelial cells in a progenitor-like state. While *Fgf10*-null embryos suffer from arrested growth in the pancreas and stomach (Bhushan et al., 2001; Nyeng et al., 2007), *Fgf10* overexpression leads to the expansion of epithelial progenitors and attenuation of epithelial differentiation in these organs (Norgaard et al., 2003). A similar effect is also seen in the lung where gain of function of *Fgf10* during development leads to progenitor state arrest and distalization of the lung (Nyeng et al., 2008). Finally, *Fgf10* inactivation reveals a decrease in epithelial progenitors in the colon (Sala et al., 2006).

During murine lung development, FGF10 functions in a dose-dependent manner as hypomorphic *Fgf10* lungs reveal branching simplification as well as vascular abnormalities (demonstrated by the simplification of the vascular tree and the presence of large hemorrhagic areas). Decreased *Fgf10* expression in *Fgf10-LacZ/-* lungs is coupled with a decrease in the number of *Ttf-1* and *Sp-B*-expressing cells, indicating that *Fgf10* dosage is critical for the amplification of epithelial progenitors. Mesenchymal lineages such as the endothelium and smooth muscle are also affected in *Fgf10-LacZ/-* lungs.

These lungs have decreased numbers of *Pecam* and *αSma*-positive cells (Ramasamy et al., 2007).

The role of FGF10 in the formation of smooth muscle during early lung development was demonstrated by Mailleux et al. The authors used the *Fgf10-LacZ* line to show that *LacZ*-expressing cells, originally located in the distal mesenchyme, migrate proximally and relocate around the epithelium giving rise to PBSMCs (Mailleux et al., 2005). As a follow up on this finding, De Langhe et al. have shown that β-Catenin signaling in the mesenchyme, mediated by the PITX family of transcription factors, is critical for the amplification but not the differentiation of *Fgf10*-expressing progenitor cells (De Langhe et al., 2008).

Taken together, the aforementioned data demonstrate that during lung development, *Fgf10* orchestrates epithelial branching and maintains epithelial progenitors. In the mesenchyme, *Fgf10*-expressing cells are progenitors for PBSMCs and *Fgf10* dosage is critical for the formation of multiple mesenchymal lineages.

1.3.2. Role of FGF0 in homeostasis and wound healing during postnatal life

After birth, *Fgf10* transcripts are detected at considerable levels in the lung during the alveolar stage (P5-P30) as well as during adulthood (Fig. 7).This implies that the role of this growth factor is not limited to embryonic life but rather extends to postnatal life. However, the role of FGF10 in lung homeostasis during postnatal life is poorly understood.

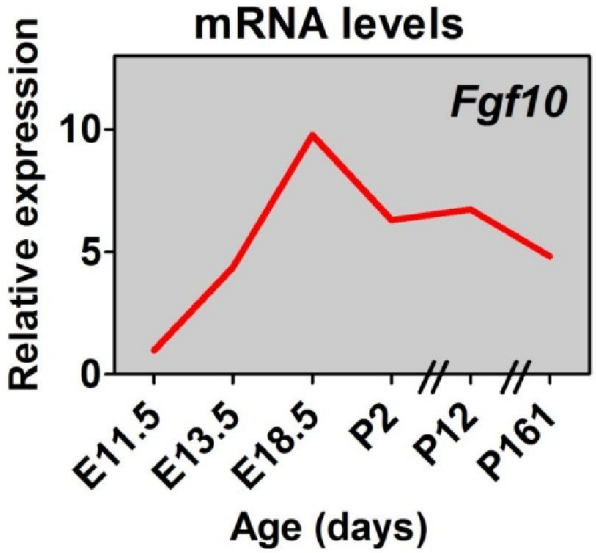

Figure 7. *Fgf10* expression levels increase throughout development and are maintained postnatally.
Relative expression levels of *Fgf10* during embryonic development and postnatally as determined by quantitative real-time PCR (qPCR) on $Fgf10^{iCre/+}$ background. *Fgf10* expression levels increase throughout development and then decrease after birth. *Fgf10* expression is sustained during adulthood. Reference gene: *β-actin.*

Ramasamy et al. have shown that lungs that are hypomorphic for *Fgf10* have impaired septation/alveolarization postnatally (Ramasamy et al., 2007). Moreover, inactivation of FGFR2b signaling prenatally – but not postnatally – leads to emphysema (Hokuto et al., 2003). Yet, it has been suggested that FGFR2b ligands are not needed for normal lung homeostasis; rather they are required for repair and restoring homeostasis after hyperoxia (Hokuto et al., 2004) and naphthalene injury (Volckaert et al., 2011). In the latter study, it was demonstrated that *Fgf10* expression is induced in PBSMCs and that FGF10/FGFR2b signaling between PBSMCs and surviving variant Clara cells is critical for epithelial regeneration.

On the other hand, FGF10/FGFR2b signaling is critical for normal homeostasis of other organs and tissues such as the incisors, mammary glands and osteoblasts. It has been shown that FGF10/FGFR2b signaling controls the regenerative capacity of the adult mouse incisors. Attenuation of

FGFR2b signaling using a dominant negative approach leads to decreased amplification of the transient-amplifying cells that are progenitors of the enamel-producing cells in the mouse incisors (Parsa et al., 2010). Similarly, attenuating FGFR2b signaling postnatally yields a rudimentary mammary epithelial tree and the absence of terminal end buds (Parsa et al., 2008). Lastly, FGFR2 attenuation throughout development and postnatally has shown to regulate osteoblast function and bone growth (Yu et al., 2003).

In the lung, *Fgf10* overexpression postnatally has shown to produce reversible adenomas in addition to enriching the lung with *Sftpc*-positive cells (Clark et al., 2001). This is consistent with the role of FGF10 during lung development in inducing epithelial cell migration/invasion (Lu et al., 2005) and maintaining distal epithelial progenitors (Nyeng et al., 2008). However, FGF10 has shown to have anti-fibrotic properties as *Fgf10* overexpression is preventive and therapeutic against bleomycin-induced pulmonary fibrosis in mice (Gupte et al., 2009). We speculate that FGF10 is a vital survival factor for AEC II and it antagonizes the detrimental effect of TGF-β signaling during fibrosis.

Studying the function of FGF10 postnatally is clinically relevant because many human disorders related to *FGF10* mutations have been reported. Mutations in the human *FGF10* gene are associated with autosomal dominant Aplasia of lacrimal and salivary glands (ALSG) (Entesarian et al., 2005, 2007). These individuals suffer from irritable eyes and dryness of the mouth. Another autosomal dominant anomaly caused by *FGF10* mutations is the Lacrimo-auriculo-dento-digital (LADD) syndrome. This syndrome is characterized by aplasia, atresia or hypoplasia of the lacrimal and salivary glands, cup-shaped ears, hearing loss and dental and digital abnormalities (Milunsky et al., 2006). Moreover, recent evidence suggests that *FGF10* mutations are associated with Autism spectrum disorder (ASD) (Casey et al., 2012). ASD patients suffer from social and communicative difficulties. Furthermore, FGF10 haploinsufficiency has been shown to be associated with chronic obstructive pulmonary disease (COPD). Lung function parameters from these patients indicate COPD and the modest response to treatment confirms irreversibility of the disease (Klar et al., 2011).

2. Objectives

The lineage tree of the lung epithelium has been thoroughly studied. Lineage tracing experiments during embryonic development, postnatal homeostasis and repair after injury have shown that basal cells can regenerate both ciliated and secretory cells and are thus on top of the hierarchy of epithelial lineages (Hong et al., 2004; Rock et al., 2009). These cells, in addition to variant Clara cells in NEBs and BADJs, have the ability to regenerate the adult lung epithelium (Stripp et al., 1995; Giangreco et al., 2002). On the other hand, the mesenchyme holds as the 'black box' of the lung. This compartment of the lung is populated by multiple cell types belonging to myogenic, adipogenic, chondrogenic and other lineages. Yet, no clear hierarchy for these lineages has been established.

Over the past few years, *Fgf10*-expressing cells have emerged as progenitors for PBSMCs during early lung development (Mailleux et al., 2005). Induced *Fgf10* expression in PBSMCs during postnatal life has shown to be critical for the initiation of epithelial repair in the context of naphthalene-induced epithelial injury (Volckaert et al., 2011). Moreover, FGF10 has shown to counteract the fibrotic effect of bleomycin administration (Gupte et al., 2009). Finally, FGF10 is required for the growth of epithelial stem cells *in vitro* (McQualter et al., 2010).

The work presented in this dissertation is intended to explore the status of *Fgf10*-positive cells in the lineage hierarchy of the lung mesenchyme. In the first part of the Results section, we show the validation aspect of a novel *Fgf10 inducible Cre* (*Fgf10*^{iCre}) knock-in mouse line that allows specific labeling of *Fgf10*-expressing cells, which can be lineage-traced temporally and spatially (El Agha et al., 2012). In the second part, we show the main findings from the lineage tracing work that was carried out using this line [(El Agha et al., *Fgf10*-positive cells represent a progenitor cell population during lung development and postnatally; in revision) and (Al Alam, El Agha et al., *Fgf10* identifies lipofibroblast progenitors and controls their lineage commitment during lung development; in progress)]. We used time-lapse

fluorescence imaging on intact embryonic lungs to study the behavior of these cells during *ex vivo* lung growth. We also performed histological analysis on lung tissues as well as FACS analysis on disaggregated lungs to identify the progeny of *Fgf10*-expressing cells and explore surface markers that help to position these cells in the lineage tree of the lung mesenchyme. Lineage tracing was carried out during embryonic development, neonatally (during the alveolar stage of lung development) and postnatally (in the context of lung fibrosis). We also investigated the role of FGF10 in the formation of the adipogenic lineage in the lung (lipofibroblasts) using primary cultures of embryonic lung mesenchyme as well as embryonic human lung fibroblast cell line (WI-38) as models to study FGF10-mediated adipogenesis *in vitro*.

The aims of the reported work are summarized as the following:

1. Validation of a novel *Fgf10*^{iCre} knock-in mouse line that allows inducible genetic labeling and manipulation of *Fgf10*-expressing cells *in vivo*

2. Studying the behavior and identifying the progeny of *Fgf10*-positive cells at multiple embryonic stages as well as postnatally

3. Identifying surface markers that allow better characterization of these cells

4. Studying the role of these cells in the context of lung fibrosis

5. Investigating the role of FGF10 in the formation of the adipogenic lineage in the lung (lipofibroblasts) *in vivo* and *in vitro.*

3. Materials and Methods

3.1. Targeting strategy of the endogenous *Fgf10* locus to generate *C57BL/6-Fgf10Cre-ERT2-eYFP/J* knock-in mice

5' and 3' homology regions (10.3 kb) for *Fgf10* were amplified by PCR using DNA from an *Fgf10*-specific BAC clone derived from a BAC library of 129Sv/AB2.2 mouse strain (Wellcome Trust Sanger Institute, Cambridge, UK). The isolated sequences were used to design the targeting construct. The linearized targeting construct was transfected into TVB2 mouse ES cells (following the electroporation procedure: 5 x 10^6 ES cells in presence of 40 µg of linearized plasmid, 260 Volt, 500 µF). Positive selection was started 48 h after electroporation by addition of 200 µg/mL of G418. G418-resistant colonies were selected based on cell growth and morphology. One electroporation session was performed and a total of 209 clones were isolated and amplified in 96-well plates. Duplicates of 96-well-plates were made; one copy was frozen down and the other copy was amplified on gelatine to be used for genomic DNA preparation. Clones were screened by PCR for homologous recombination and verified by Southern blotting. Altogether, PCR, sequencing and Southern blot screening allowed the characterization of ten recombined clones, seven of which were suitable for blastocyst injection. Recipient blastocysts were isolated from pregnant C57BL/6J females (Health status VAF – Virus antibody free). Based on screening results and morphological criteria, ES cell clones were injected into C57BL/6J blastocysts. Injected blastocysts were then re-implanted into OF1 pseudo-pregnant females and allowed to develop to term. Four of the highly chimeric males generated were selected to breed with C57BL/6J Flp-deleter mice (health status SOPF – Specific and opportunist pathogen free) to allow germline excision of the neomycin selection cassette.

3.2. Genotyping of *C57BL/6-Fgf10Cre-ERT2-eYFP/J* knock-in mice

Two primer pairs were used to genotype *Fgf10^{iCre}* knock-in mice. Primers P1 (5'-AGCAGGTCTTACCCTTCCAGTATGTTCC-3') and P2 (5'-CTCCTTGGAGGTGATTGTAGCTCCG-3') were used to detect the wild-type allele (297 bp band) whereas primers P3 (5'-CAAACCCCAAAAGAACAGCTTTGTGTAC-3') and P4 (5'-GACATTTGAGTTGCTTGCTTGGCACT-3') were used to detect the knock-in allele (271 bp band). The PCR program consists of a denaturation step at 94°C for 2 min, followed by 35 cycles of denaturation (94°C for 30 s), annealing (65°C for 30 s) and extension steps (68°C for 300 s). The program ends with a completion step at 68°C for 480 s. Each PCR tube contains 2.6 U of Expand Long Template Polymerase in 5 µL of Reaction buffer 3 (Roche Applied Science, Mannheim, Germany), 15 pmol of each primer, 0.5 mM dNTPs and 10 ng of genomic DNA in a final volume of 50 µL.

3.3. Mice and tamoxifen administration

Tomato$^{flox/flox}$ reporter mice (B6;129S6-*Gt(ROSA)26Sor$^{tm9(CAG-tdTomato)Hze}$*/J) were purchased from Jackson lab (stock number 007905) and *Fgf10$^{flox/flox}$* mice were a kind gift from Professor Suzanne L. Mansour (University of Utah, USA). Embryonic day 0.5 (E0.5) was assigned to the day when a vaginal plug was detected. Mice were housed in a Specific pathogen free (SPF) environment. Harvesting organs and tissues from wild type and transgenic mice was approved by Justus Liebig University Giessen (Approval numbers 405_M and 437_M). Animal experiments were approved by the Regierungspräsidium Giessen. Tamoxifen injections were approved in (GI 20/10 Nr. 38/2011 and 117/2012) and bleomycin treatment was approved in the amendment to (GI 20/10 Nr. 73-2012).

Tamoxifen stock solution was prepared by dissolving tamoxifen powder (T5648, Sigma, Schnelldorf, Germany) in corn oil at a concentration of 20 mg/mL at room temperature (RT). Pregnant females carrying *Fgf10$^{iCre/+}$; Tomato$^{flox/+}$* embryos received a single intraperitoneal (IP) injection of 0.1 mg

of tamoxifen per gram of body weight. For continuous tamoxifen exposure, pregnant females were fed tamoxifen-containing food (0.4 g of tamoxifen per kg of food) (Altromin, Lage, Germany). Dissected embryos and lungs were examined using Leica M205 FA fluorescence stereoscope (Leica, Wetzlar, Germany) and images were acquired using Leica DFC360 FX camera. Cecum lengths were measured using Leica's LAS AF software and digit peripheries were measured using Image J software (NIH, Bethesda, MD, USA).

3.4. Organ culture and time-lapse microscopy

Embryonic lungs were harvested in Dulbecco's Modified Eagle's Medium (DMEM) and cultured on Whatman Nuclepore membrane filters (GE Healthcare, Solingen, Germany) placed on 500 µL of DMEM with 10% Fetal Bovine Serum (FBS) and 1% Penicillin/Streptomycin. Culture dishes with embryonic lungs were then transferred into the culture chamber (37°C; 5% CO_2) of Leica DMI6000 B live imaging microscope and time-lapse imaging was performed. RFP signal intensity was measured using Image J software.

3.5. X-Gal staining

X-Gal staining was performed as previously described (Al Alam et al., 2011). Briefly, *Fgf10-LacZ* lungs were dissected in Hank's Balanced Salt Solution (HBSS) (Invitrogen, Darmstadt, Germany) from E18.5 embryos, shortly fixed in 4% Paraformaldehyde (PFA), washed in PBS and incubated with *LacZ* buffer solution for 10 min. Then, they were incubated with *LacZ* buffer solution containing 40 mg/mL X-Gal (Sigma) at 37°C overnight.

3.6. Quantitative real-time PCR and RT-PCR

Freshly harvested embryos, lungs or cells were lysed and RNA was purified using RNeasy or miRNeasy kit (Qiagen, Hilden, Germany). E11.5 and E13.5 embryos as well as harvested cells were homogenized using QiaShredder columns (Qiagen) whereas lungs from older tissues were homogenized using Bullet Blender Blue (Next Advance, Averill park, NY, USA). 1 µg of RNA was

used for cDNA synthesis using Quantitect Reverse Transcription kit (Qiagen). Primers and probes were designed using Universal ProbeLibrary Assay Design center (Roche Applied Science, available online at https://www.roche-applied-science.com/sis/rtpcr/upl/index.jsp?id=UP030000). More details about the used primers and probes can be found in Supplementary Table S2. Quantitative real-time PCR (qPCR) was performed using LightCycler 480 real-time PCR machine (Roche Applied Science). Samples were run in triplicates using mouse *β-actin* (for TaqMan® assays), mouse *Hprt* or human *PBGD* (for SYBR® Green assays) as reference genes and the ΔΔCT method was used for relative quantification.

3.7. Bleomycin administration and lung function measurement

Female mice were anesthetized with a mixture of Ketamine (0.6 µL/g) (Bela-pharm, Vechta, Germany) and Domitor® (0.3 µL/g) (Janssen animal health, Neuss, Germany) mixed in saline solution. The corneas were protected by Bepanthen® ointment (Bayer, Leverkusen, Germany). Once the animals were anesthetized, they were intubated oro-tracheally under a dissecting microscope. Bleomycin injections (Hexal, Holzkirchen, Germany) were given intratracheally with a 20G plastic catheter and microsprayer (3.5 U of bleomycin per kilogram of body weight in 50 µL of saline). Control groups were injected with saline instead of bleomycin.

Fourteen days after treatment, mice were deeply anesthetized with Ketamine (1.2 µL/g), Domitor® (0.6 µL/g) and 1:4 parts of Heparin (Ratiopharm, Ulm, Germany) mixed in saline solution. 2% Xylocaine analgesic (Astra Zeneca, Wedel, Germany) was applied to the surgical area. The animals were then tracheotomized and intubated with a 20G cathether connected to a FlexiVent™ plesythmograph (Scireq, Montreal, QC, Canada). Lungs were mechanically ventilated at a rate of 150 breaths/min with a positive end-expiratory pressure (PEEP) of 1-3 cmH_2O. PEEP was calculated automatically by FlexiVent 7 software and according to the weight of each animal. After stabile ventilation was achieved, a 3 s tidal volume of 10 µL/g of body weight was initiated every 15-20 s and the single compartment model of lung mechanics (snapshot perturbations) was used to measure lung function

parameters (compliance, elastance and resistance). After plesythmography, animals were euthanized by cervical dislocation and lungs were isolated for further processing.

3.8. Tissue processing and immunostaining

Freshly isolated lungs were washed in PBS and then fixed in 4% PFA/PBS according to standard procedures. Then, tissues were embedded in paraffin and sectioned at 5 µm thickness. Slides were deparaffinized and then blocked with 3% BSA and 0.4% Triton-X (in TBS) at RT for 1 h. Then, they were incubated with primary antibodies at RT for 1 h or at 4°C overnight. Primary and secondary antibodies are summarized in Table 5. After incubation with antibodies, slides were washed three times in TBST (TBS buffer + 0.1% Tween20) for 5 min. Slides were mounted with Prolong® Gold Anti-fade Reagent with DAPI (Invitrogen). The endogenous Tomato signal was detected using the RFP channel. Fluorescent images were acquired using Leica DM5500 B fluorescence microscope and Leica DFC360 FX camera.

Table 5. Antibodies used for immunofluorescence.

Antibodies	Host / Isotype	Supplier	Dilution
Primary Antibodies			
Monoclonal FITC αSMA antibody	Mouse / IgG2a	Sigma	1:100
Polyclonal purified ADFP antibody	Rabbit / IgG	Abcam	1:50
Monoclonal Neuron-specific beta-III Tubulin antibody	Mouse / IgG2a (clone Tuj-1)	R&D	1:50
FITC anti-mouse CD45 Antibody	Rat / IgG2b, κ	Biolegend	1:100
FITC anti-mouse CD31 Antibody	Rat / IgG2a, κ	Biolegend	1:100
Secondary Antibodies			
Alexa Fluor®-488 anti-rabbit	Goat	Invitrogen	1:1000
Alexa Fluor®-488 anti-mouse	Donkey	Invitrogen	1:1000

3.9. FACS analysis

Lungs were dissected, washed with HBSS and kept on ice. Then, they were cut into fine pieces using a sharp blade before being digested with 0.5% Collagenase Type IV/HBSS (Life Technologies, Invitrogen) at 37°C for 45 min. Single cell suspensions were obtained by passing lung homogenates through 18, 21 and 24G syringes before being passed through 70 and 40 µm cell strainers (BD Biosciences, Heidelberg, Germany). Cell count was determined using a Neubauer hemocytometer (Labor Optik, Friedrichshof, Germany) and Trypan Blue was used to distinguish between live and dead cells. Cells were then resuspended in cold staining solution (0.1% Sodium Azide/5% FCS/0.05% Triton-X in 1x PBS) and antibodies were added according to Table 6. Cells were incubated with antibodies (Biolegend, Fell, Germany) for at least 30 min on ice in the dark and then washed with 0.1% Sodium Azide in PBS. The endogenous Tomato signal was detected using the PE channel. FACS measurements were carried out using FACSAria III cell sorter (BD Biosciences). Tomato-positive cells from unstained lung suspensions were sorted and grown in the presence (250 ng/mL) or absence of recombinant human FGF10 (rhFGF10) (R&D Systems, Wiesbaden, Germany) and were then stained for ADRP (Abcam, Cambridge, UK) and P-ERK (New England Biolabs, Frankfurt, Germany) or harvested for RT-PCR.

Table 6. Antibodies used for FACS analysis.

Antibodies	Host / Isotype	Supplier	Dilution
FITC anti-mouse CD45	Rat / IgG2b, κ	Biolegend	1:100
FITC anti-mouse CD31	Rat / IgG2a, κ	Biolegend	1:100
APC-Cy7 anti-mouse EpCAM	Rat / IgG2a, κ	Biolegend	1:50
Pacific Blue anti-mouse Sca-1	Rat / IgG2a, κ	Biolegend	1:100
APC anti-mouse CD140a	Rat / IgG2a, κ	Biolegend	1:100
PE-Cy7 anti-mouse CD117	Rat / IgG2b, κ	Biolegend	1:50

3.10. Primary culture of lung mesenchyme

Single cell suspensions were obtained as described in **Part 3.9.** Instead of immunostaining, cells were plated for 45 min in DMEM with 10% FBS and 1% Penicillin/Streptomycin for differential adhesion (Lebeche et al., 1999). Culture flasks were then washed with sterile PBS, the medium was refreshed and cells were allowed to grow overnight in a humidified cell culture incubator at 37°C and 5% CO_2. Cell were then treated with rhFGF10 and stained for P-ERK, or harvested for Western blotting or RNA extraction.

3.11. WI-38 cell line

Human embryonic lung fibroblast cell line WI-38 (ATCC® number CCL-75) was cultured according to manufacturer's instructions. Cells were grown in the presence or absence of different concentrations of rhFGF10 (0; 1; 10; 100; 250 ng/mL) and were harvested for Western blotting or RNA extraction.

3.12. Western blotting

Cultured lung primary mesenchymal cells and cell lines were disrupted immediately in RIPA buffer (Sigma) containing protease inhibitors. Equal amounts of total lung protein from each assayed sample were used for chemiluminescent Western analysis on Immuno-Blot PVDF membrane (Bio-Rad, Hercules, CA, USA). Immunoblotting was performed using antibodies against PTHrP receptor (1:200), PPARγ (1:200), Leptin (1:200), C/EBPα (1:200) and GAPDH (1:10000) (Santa Cruz Biotechnology, Dallas, TX, USA).

3.13. Statistical analyses and figure assembly

Quantitative data were assembled using GraphPad Prism software (GraphPad Software, La Jolla, CA, USA) and presented as average values ± S.E.M. Statistical analyses were performed using Student's t-test (for comparing two groups) or One-way ANOVA (for comparing three or more groups). Data were considered significant if $P < 0.05$. Figures were assembled using Adobe Photoshop CS5.

4. Results

This section will be divided into three parts**: Part 4.1.** Characterization of a novel *Fgf10* knock-in mouse line to target mesenchymal progenitors during embryonic development, **Part 4.2.** *Fgf10*-positive cells constitute a progenitor cell population during lung development and represent a subpopulation of resident mesenchymal stem cells during postnatal life, and **Part 4.3.** Role of FGF10 in lipofibroblast formation *in vivo* and *in vitro*.

4.1. Characterization of a novel *Fgf10* knock-in mouse line to target mesenchymal progenitors during embryonic development

4.1.1. Generation of *Fgf10^{iCre} (C57BL/6-Fgf10Cre-ERT2-eYFP/J)* driver line

129Sv ES cells were electroporated with a targeting vector containing the 5' end of exon 1 of *Fgf10* open reading frame (Fig. 8A, B). Immediately downstream of the start codon is the coding sequence of a tamoxifen-inducible form of Cre recombinase (Cre-ERT2), followed by IRES sequence, eYFP and Neomycin-resistance gene (*Neo*) respectively. Resistant ES cell clones were selected, screened by PCR and then verified by Southern blotting. Selected ES clones were injected into C57BL/6J blastocysts to generate chimeric pups (Fig. 8C). Chimeras were then crossed with C57BL/6J mice ubiquitously expressing Flp recombinase to generate heterozygous *Fgf10^{iCre}* knock-in mice where the Neo cassette was totally excised (Fig. 8D).

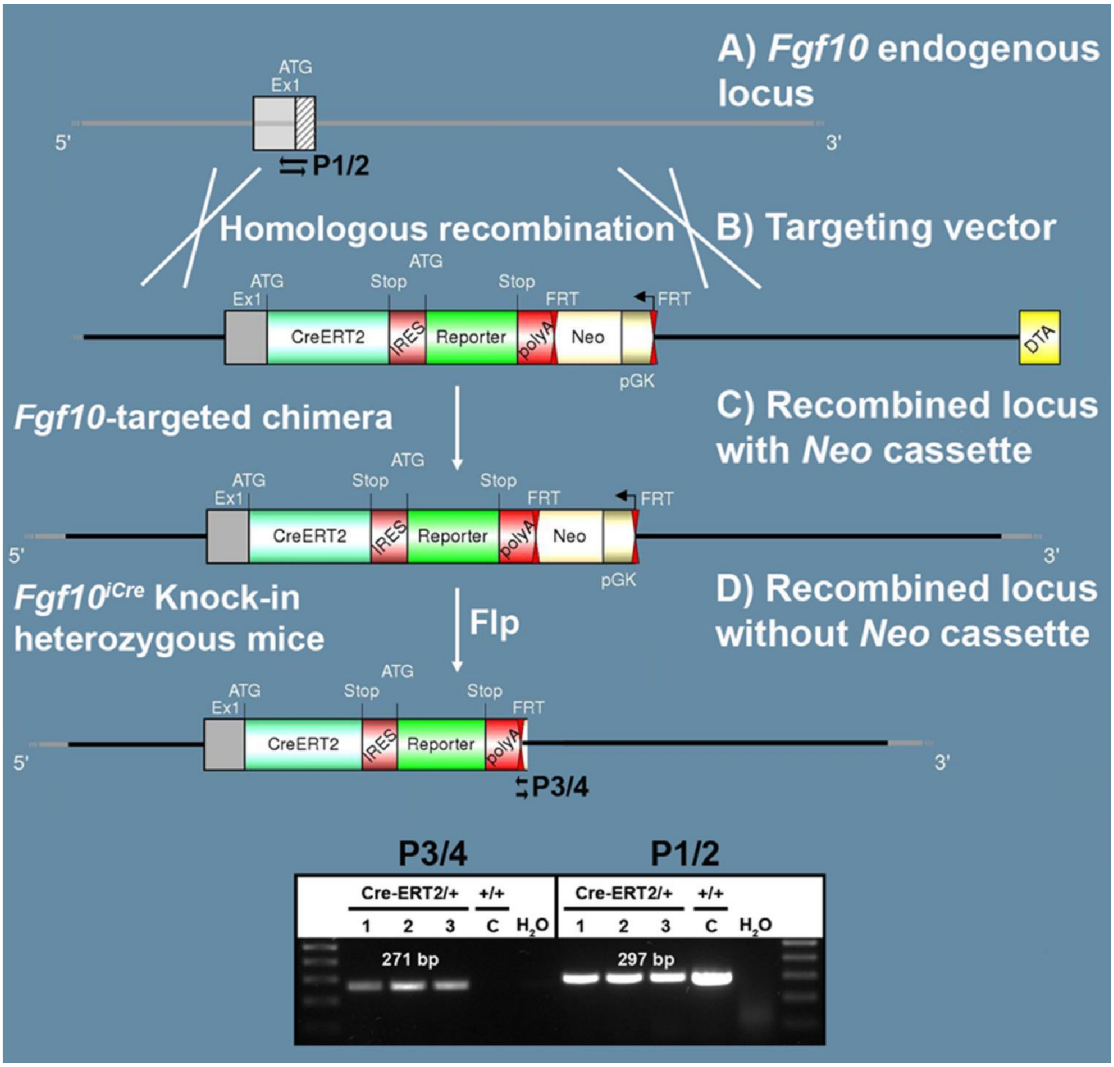

Figure 8. Generation of recombinant *Fgf10*^{iCre} locus.

(**A, B**) *Cre-ERT2-IRES-eYFP-Neo* construct was introduced in frame with ATG of exon 1 by homologous recombination. Genes coding for Neomycin resistance and Diphtheria Toxin A were used for positive and negative selection respectively. (**C**) Chimeras carrying the *Neo* cassette were crossed with C57BL/6J mice ubiquitously expressing Flp recombinase to generate heterozygous knock-in mice lacking the *Neo* cassette (**D**). Primers used for genotyping are shown as black arrows. Note that primers P1 and P2 detect the wild-type locus (297 bp band) whereas primers P3 and P4 detect the recombined locus (271 bp band). Abbreviations: C: Control; DTA: Diphtheria Toxin A; eYFP: Enhanced yellow fluorescent protein; IRES: Internal ribosome entry site; Neo: Neomycin-resistance gene; pGK: Phosphoglycerate kinase promoter.

4.1.2. Insertion of the Cre-ERT2 cassette in exon 1 results in *Fgf10* loss of function

To determine whether the insertion of Cre-ERT2 in the endogenous *Fgf10* locus led to loss of function of *Fgf10*, $Fgf10^{iCre}$ heterozygous animals were crossed and embryos were harvested at E12.5. $Fgf10^{iCre}$ homozygous embryos suffered from lung and limb agenesis in addition to cecal and colonic atresia, consistent with complete loss of function of *Fgf10* (Fig. 9A-C; *n* = *4*; penetrance = 100%). $Fgf10^{iCre/+}$ embryos were used as controls. qPCR revealed minimal expression levels for *Fgf10* in $Fgf10^{iCre/iCre}$ embryos (Fig. 9D; *n* = *4*) compared to $Fgf10^{iCre/+}$ (Fig. 9D; *n* = *5*; *P* < 0.001) and $Fgf10^{+/+}$ embryos (Fig. 9D; *n* = *5*; *P* < 0.001).

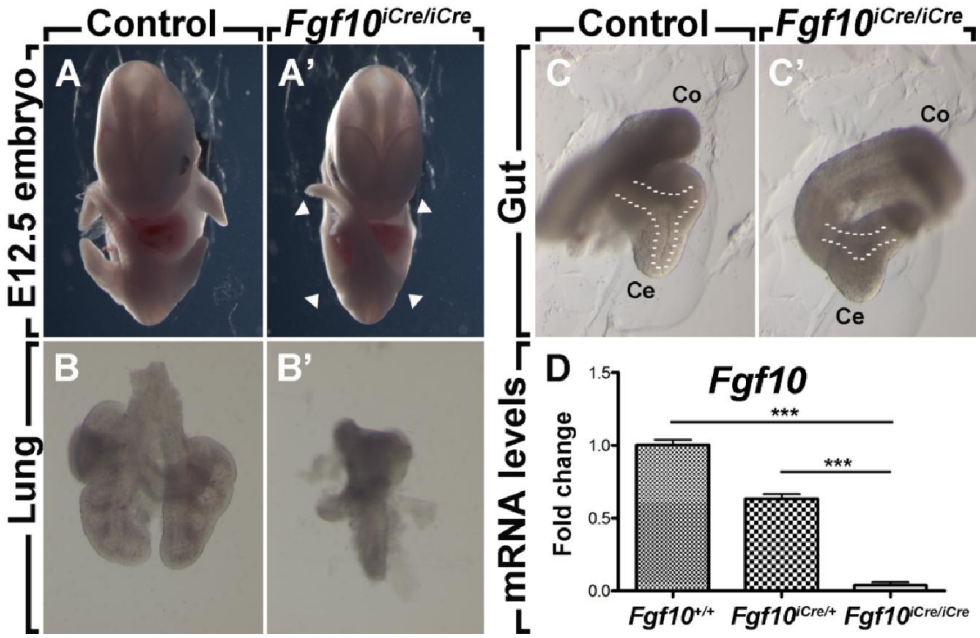

Figure 9. $Fgf10^{iCre}$ is a null allele for *Fgf10*.
E12.5 $Fgf10^{iCre/iCre}$ embryos show agenesis of the limbs (**A, A'**) and lung (**B, B'**) as well as cecal and colonic atresia (**C, C'**). Arrowheads indicate sites of limb agenesis and dashed lines mark the epithelium in the cecum. $Fgf10^{iCre/+}$ embryos were used as controls. (**D**) *Fgf10* relative mRNA levels as quantified by qPCR. $Fgf10^{iCre/iCre}$ embryos (*n* = *4*) express minimal *Fgf10* levels compared to $Fgf10^{iCre/+}$ (*n* = *5*) and $Fgf10^{+/+}$ embryos (*n* = *5*). Data are shown as average values ± S.E.M. * *P* < 0.05; *** *P* < 0.001. Reference gene: *β-actin*. Abbreviations: Ce: cecum; Co: colon.

4.1.3. Labeling of *Fgf10*-positive cells

In order to test the recombinase activity of Cre-ERT2, *Fgf10*^{iCre} heterozygous mice were crossed with *Tomato*$^{flox/flox}$ reporter mice. Pregnant females received a single IP injection of tamoxifen or corn oil at E15.5 and embryos were harvested at E18.5. No recombination was observed in *Fgf10*$^{+/+}$; *Tomato*$^{flox/+}$ embryos (Fig. 10A-D; *n = 4*). Recombination was observed in the ears (Fig. 10A', A''), skin (Fig. 10B', B''), limbs (Fig. 10C', C''), ceca (Fig. 10D', D'') and lungs (Fig. 11A'-C') of *Fgf10*$^{iCre/+}$; *Tomato*$^{flox/+}$ embryos (*n = 3*; penetrance = 100%). Labeled cells in the skin were arranged in discrete spots (Fig. 10B', B''). In the limbs, labeled cells were abundant at the tips of the digits as well as more proximal regions (Fig. 10C', C''). In the cecum, however, elongated cells were labeled (Fig. 10D', D'').

When examining the lungs from *Fgf10*$^{iCre/+}$; *Tomato*$^{flox/+}$ embryos, Tomato-positive cells were detected throughout the mesenchyme (Fig. 11A'; *n = 3*). Interestingly, the signal was intense in interlobular septa (Fig. 11B'). In the trachea, Tomato-positive cells were arranged in ring-like structures (Fig. 11C'). X-Gal staining of *Fgf10-LacZ* lungs at E18.5 revealed similar sites of *Fgf10* expression (Fig. 11A''-C''; *n = 8*). The expression of the eYFP reporter from the IRES sequence could not be detected in any of the embryos or lungs. Tomato-positive cells were not detected in *Fgf10*$^{iCre/+}$; *Tomato*$^{flox/+}$ lungs from corn oil-injected females (Data not shown; *n = 6*).

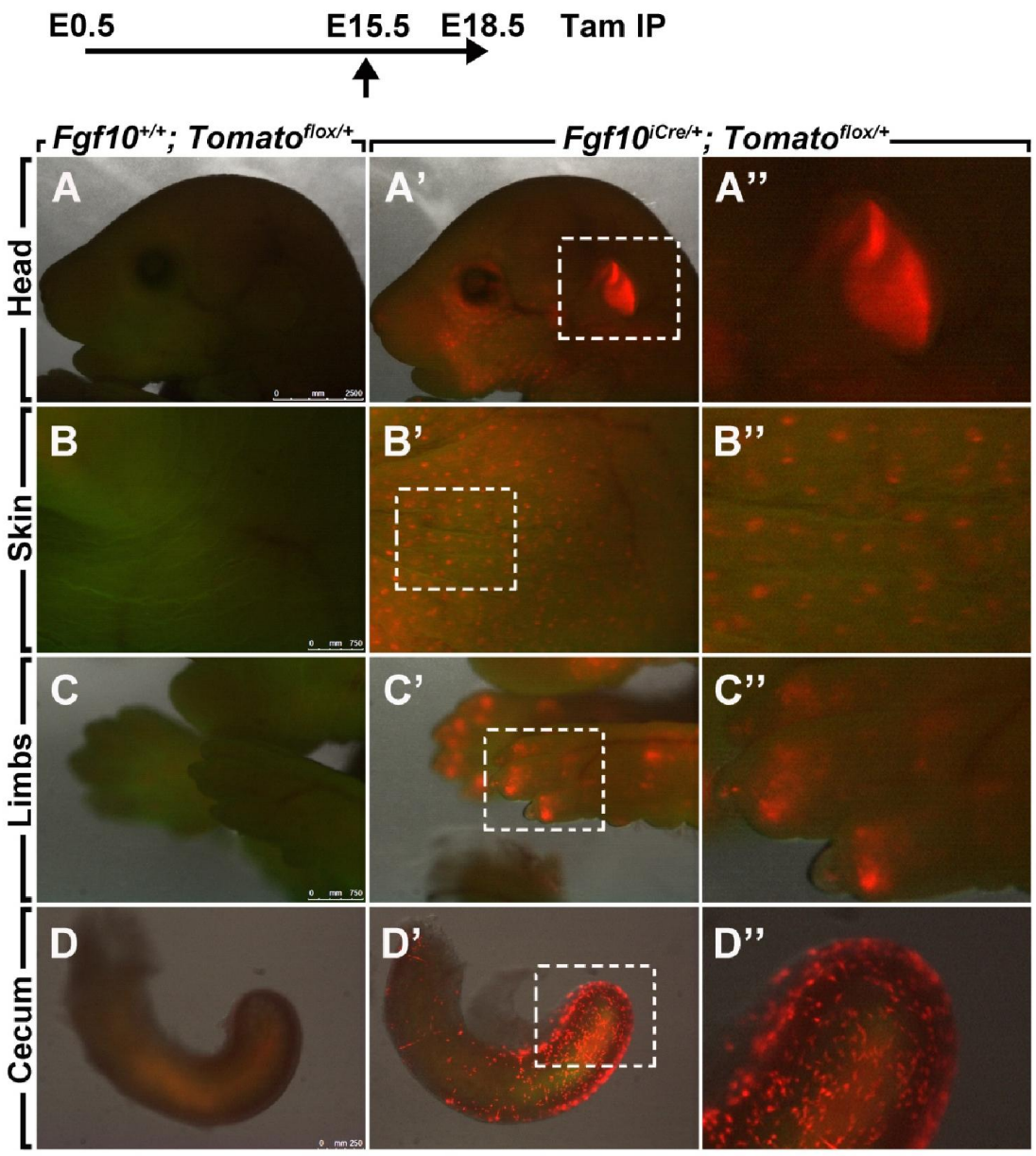

Figure 10. Tomato expression in E18.5 *Fgf10$^{iCre/+}$; Tomato$^{flox/+}$* embryos.
Recombination was induced at E15.5 by a single IP injection of tamoxifen. Note the absence of Tomato expression in *Fgf10$^{+/+}$; Tomato$^{flox/+}$* embryos (**A-D**). Tomato-positive cells are detected in the ear, skin, limbs and cecum (**A'-D'**). (**A''-D''**) Higher magnifications of dotted boxes in (A'-D'). *n = 3*. Tam: Tamoxifen.

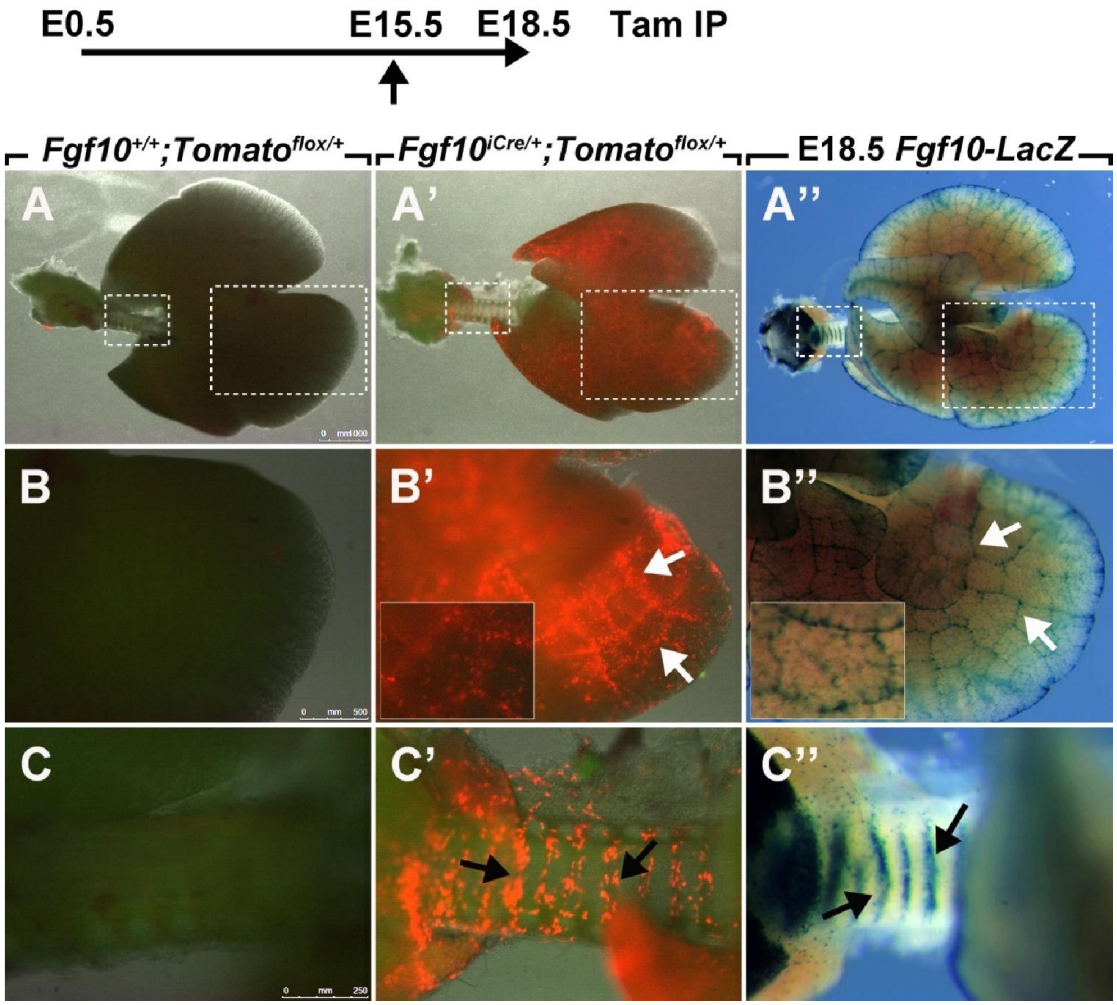

Figure 11. Tomato expression in E18.5 *Fgf10$^{iCre/+}$; Tomato$^{flox/+}$* lungs.
Recombination was induced at E15.5 by a single IP injection of tamoxifen. Note the absence of Tomato expression in *Fgf10$^{+/+}$; Tomato$^{flox/+}$* lungs (**A;** *n* = *3*). The regions in the dotted boxes are magnified in (**B**) and (**C**). Tomato-positive cells are observed in the lung mesenchyme and interlobular septa of *Fgf10$^{iCre/+}$; Tomato$^{flox/+}$* lungs (white arrows) (**A', B';** *n* = *3*). Inset in B' shows high magnification of interlobular septa. Labeled cells in the trachea arrange in ring-like structures (black arrows) (**C';** *n* = *3*). (**A''-C'';** *n* = *8*) X-Gal staining of *Fgf10-LacZ* lungs at E18.5. Inset in B" shows high magnification of interlobular septa.

4.1.4. Inducible conditional gene inactivation

To test the potential use of this line for gene inactivation studies, *Fgf10$^{iCre/+}$; Tomato$^{flox/flox}$* mice were crossed with mice carrying a *'floxed'* version of *Fgf10*

(*Fgf10*$^{flox/flox}$). Cre activity was induced by tamoxifen food from E8.5 to E14.5. By using the *Tomato*^{flox} reporter as readout of Cre activity, recombination was observed in the limbs, lungs and ceca (Fig. 12C, D, G, H, L; *n* = *3*; penetrance = 100%). *Fgf10*$^{iCre/flox}$*; Tomato*$^{flox/+}$ embryos suffered from diverse developmental abnormalities (*n* = *3*; penetrance = 100%). A formation defect characterized by webbed digits was observed at the level of the forelimbs as compared to their *Fgf10*$^{+/flox}$*; Tomato*$^{flox/+}$ control littermates. The phenotype was quantified by measuring the periphery of the digits (Fig. 12H vs. E, M; $P < 0.0001$). Hindlimbs did not show any obvious abnormalities. The lung showed an abnormal shape and suffered from branching simplification as illustrated by the reduced number of terminal buds in the accessory lobe (Fig. 12C vs. B, G vs. F, J; $P < 0.05$). The cecum, on the other hand, was shorter in *Fgf10*$^{iCre/flox}$*; Tomato*$^{flox/+}$ embryos as compared to littermate controls (Fig. 12L vs. I, K; $P < 0.05$).

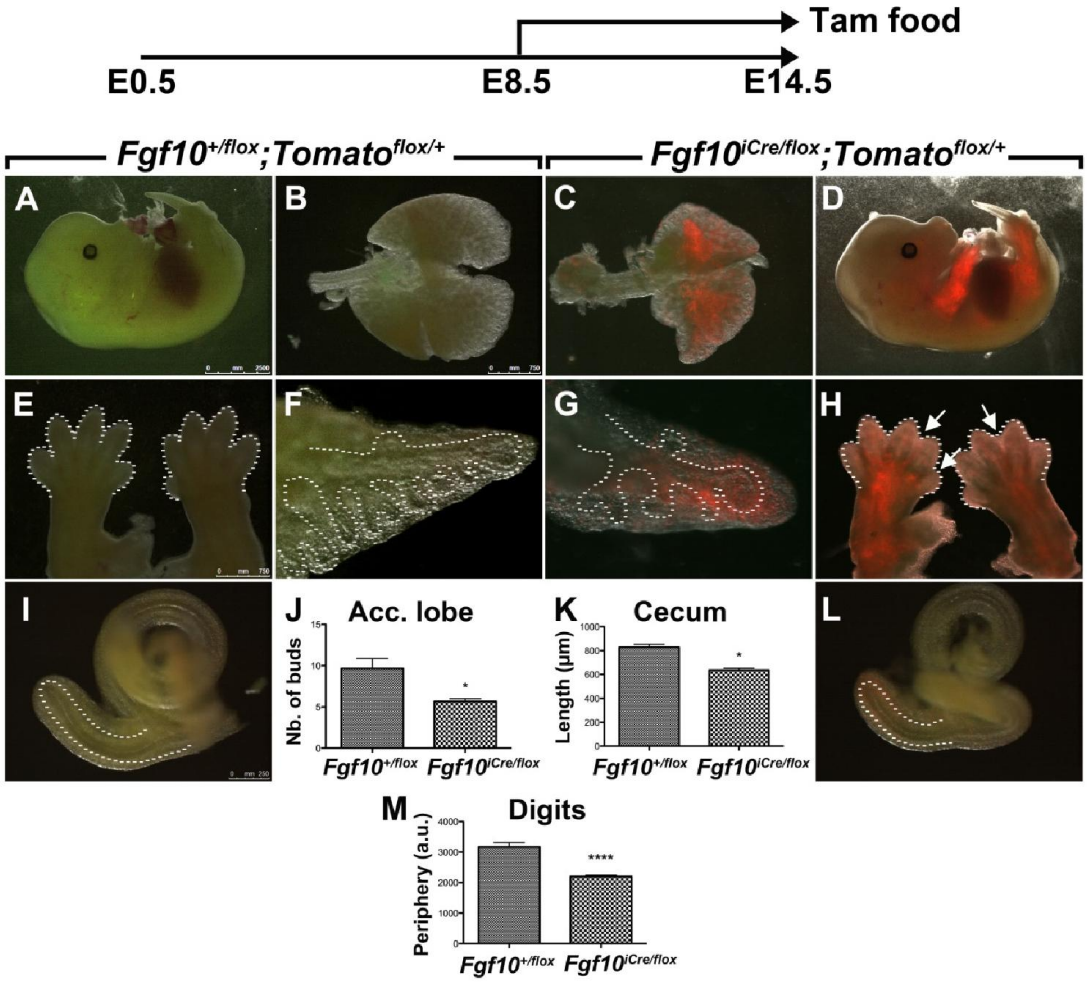

Figure 12. Inducible conditional *Fgf10* inactivation using *Fgf10^{iCre}* driver line. Cre was activated by tamoxifen food from E8.5 to E14.5 in *Fgf10$^{iCre/flox}$; Tomato$^{flox/+}$* embryos. Labeled cells are present in the limbs, lung and cecum (**D, G, H, L**). Note the webbing of the digits in the forelimbs (arrows indicate webbing sites and dashed lines indicate peripheries) (**H vs. E, M**) and the hypomorph-like phenotype in the cecum (**L vs. I, K**). *Fgf10$^{iCre/flox}$; Tomato$^{flox/+}$* lungs show a deformed shape (**C vs. B**) as well as branching simplification (**G vs. F, J**). Dashed lines indicate the epithelium in the lung (**F, G**) and cecum (**I, L**). *n = 3*. Data are shown as average values ± S.E.M. * $P < 0.05$; **** $P < 0.0001$. Embryonic tissues were kindly provided by Dr. Denise Al Alam (CHLA, CA, USA, Protocol number 31-11).

4.1.5. Mismatch between *Cre* and *Fgf10* expression levels

In order to investigate the expression levels of *Cre* from the *Fgf10*^{iCre} locus, timed-pregnant females carrying *Fgf10*$^{iCre/+}$ embryos were sacrificed at different developmental stages and *Fgf10* and *Cre* expression levels were assessed by qPCR by comparing mRNA abundance from different stages to E11.5. *Fgf10* expression levels progressively increased in *Fgf10*$^{iCre/+}$ embryos from E11.5 ($n = 5$) to E13.5 ($n = 3$; $P < 0.01$) and E18.5 ($n = 7$; $P < 0.001$) and were maintained postnatally at P2 ($n = 2$; $P < 0.05$), P12 ($n = 4$; $P < 0.0001$) and P161 ($n = 3$; $P < 0.001$); however, *Cre* expression levels, from the same embryos, showed a slower increase from E11.5 ($n = 5$) to E13.5 ($n = 3$; $P < 0.05$) and E18.5 ($n = 7$; $P < 0.01$) and then dropped postnatally at P2 ($n = 2$; $P < 0.05$), P12 ($n = 4$; $P < 0.001$) and P161 ($n = 3$; $P < 0.001$) (Fig. 13A). In spite of low *Cre* expression levels postnatally, single IP injections of tamoxifen at P1 or P4 led to significant recombination in *Fgf10*$^{iCre/+}$*; Tomato*$^{flox/+}$ lungs at P6 and P60 respectively (Fig. 13D-G; $n = 4$; penetrance = 100%). Induction in P1 *Tomato*$^{flox/+}$ pups (single transgenics) did not reveal any recombination at P10 (Fig. 13B, C; $n = 2$). Finally, serial tamoxifen IP injections (one daily injection for one week), followed by a ten-day tamoxifen diet and ten-day normal diet, revealed recombination in the trachea and lung of *Fgf10*$^{iCre/+}$*; Tomato*$^{flox/+}$ adult mice (Fig. 13H, I; $n = 3$; penetrance = 100%).

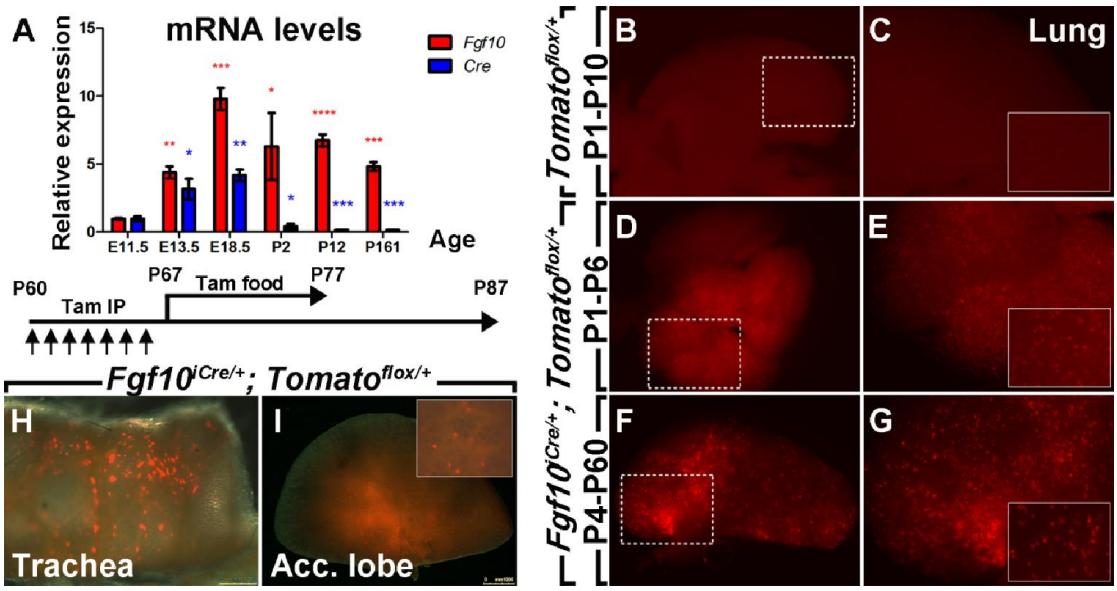

Figure 13. Mismatch between *Cre* and *Fgf10* expression levels in *Fgf10*$^{iCre/+}$ embryos.

(**A**) *Fgf10* and *Cre* relative mRNA levels as determined by qPCR. For RNA preparation, whole embryos were used at E11.5 (*n* = *5*) and E13.5 (*n* = *3*) whereas lungs were used at E18.5 (*n* = *7*), P2 (*n* = *2*), P12 (*n* = *4*) and P161 (*n* = *3*). *Fgf10* expression levels increase throughout development and are maintained postnatally while *Cre* levels slowly increase throughout development and are minimal postnatally. (**B**) Induction in P1 *Tomato*$^{flox/+}$ pups reveals no recombination at P10 in the lung (*n* = *2*). The area in the dotted box is magnified in (**C**). Inset in C shows high magnification with unlabeled cells. (**D-G;** *n* = *4*) Induction in P1 and P4 *Fgf10*$^{iCre/+}$*; Tomato*$^{flox/+}$ pups reveals recombination at P6 and P60 in the lung respectively. Insets in E and G show high magnification with labeled cells. (**H, I;** *n* = *3*) Tamoxifen-induced recombination in lungs from *Fgf10*$^{iCre/+}$*; Tomato*$^{flox/+}$ adult mice. Labeled cells are detected in the trachea and lung lobes. Inset in I shows high magnification with labeled cells. Data are shown as average values ± S.E.M. * $P < 0.05$; ** $P < 0.01$; *** $P < 0.001$; **** $P < 0.0001$. Reference gene: *β-actin*. Tamoxifen-treated lungs were kindly provided by Dr. Denise Al Alam (CHLA, CA, USA).

The 3 kb region downstream of *Fgf10* transcriptional start site, which was deleted upon homologous recombination, was analyzed for putative regulatory elements by comparing transcription factor binding sites conserved

between mice and humans (using rVista, http://rvista.dcode.org). The analysis revealed the presence of several conserved transcription factor binding site-dense regions (Fig. 14A). Interestingly, the 716 bp stretch at the 3' end of the deleted region contains putative binding sites for SMAD4, NKX2.5, TBX5 and ISL1. Furthermore, the deleted region was analyzed for lung-related histone modifications using UCSC Genome Browser (http://genome.ucsc.edu). The analysis revealed the presence of a dense H3K4me3 (histone H3 trimethylated at Lys4) modification site overlapping exon 1-intron 1 boundary (Fig. 14B).

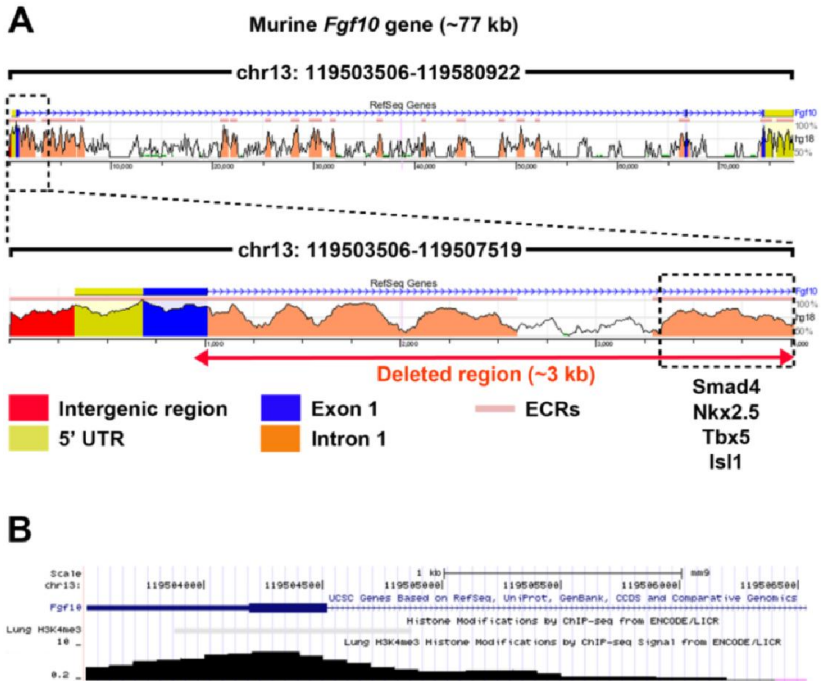

Figure 14. Bioinformatic screening for putative regulatory elements 3 kb downstream of *Fgf10* ATG.

(**A**) The screening reveals regions that are rich in transcription factor binding sites conserved between mice and humans (as predicted by rVista; http://rvista.dcode.org). Lung-related transcription factor binding sites within the 3' end of the deleted sequence are shown. (**B**) Screening for lung-related H3K4me3 modification sites (as predicted by UCSC Genome Browser; http://genome.ucsc.edu). A dense H3K4me3 modification site is predicted in the region overlapping exon 1-intron 1 boundary of *Fgf10* gene. Abbreviations: ECRs: Evolutionary conserved regions; UTR: Untranslated region.

4.2. *Fgf10*-positive cells constitute a progenitor cell population during lung development and represent a subpopulation of resident mesenchymal stem cells during postnatal life

4.2.1. *Fgf10*-positive cells are amplified and migrate during early lung development *ex vivo*

In order to study the behavior of *Fgf10*-positive cells during the pseudoglandular stage of lung development, pregnant mice carrying *Fgf10*$^{iCre/+}$; *Tomato*$^{flox/+}$ embryos received a single IP injection of tamoxifen at E11.5 and embryos were harvested at E12.5. Lungs were cultured in an air-liquid interphase and bright field/fluorescence time-lapse imaging was carried out for 72 h (Fig. 15; *n* = *3*). Lineage-labeled cells were originally detected as small populations in the distal mesenchyme and were mostly abundant in the accessory lobe (Fig. 15A, A', A''). During the first 24 h of culture, Tomato-positive cells amplified exponentially and populated other regions of the growing lung (Fig. 15C, C', C'', I). At the end of the three-day culture, lineage-labeled cells were highly abundant and dispersed throughout the lung mesenchyme (Fig. 15D, D', D''). After *ex vivo* culture, lungs were fixed, processed and stained for αSMA (Fig. 15E-H). An average of 81 ± 0.2 (*n* = *3*) Tomato-positive cells was detected per 5 µm section (Fig. 15F, F', J). A subpopulation of *Fgf10*-positive cells (5.67 ± 0.57 cells; *n* = *3*) appeared in the PBSMC layer (Fig. 15H, H', J).

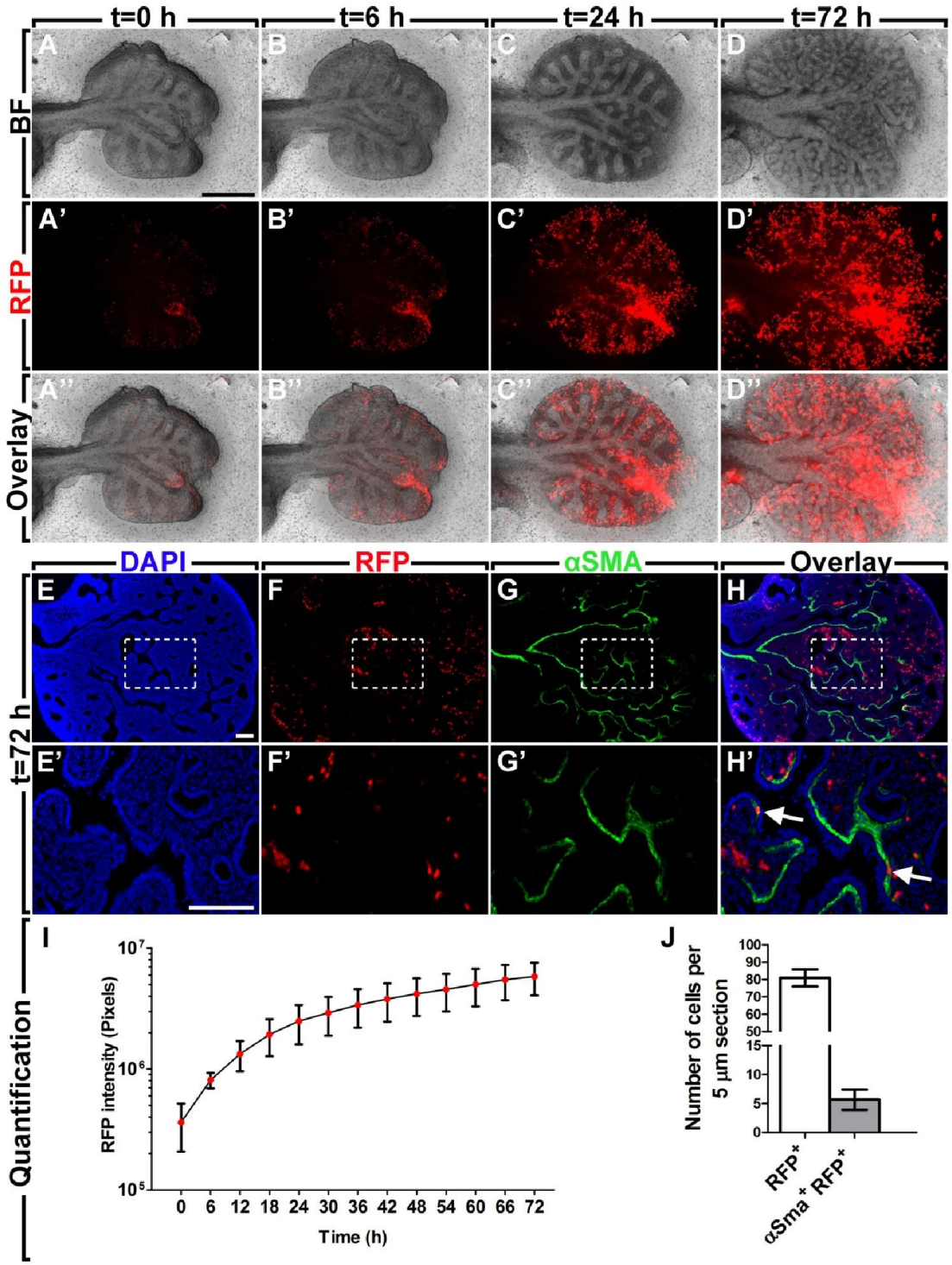
t=0 h
t=6 h
t=24 h
t=72 h
BF
RFP
Overlay
A
B
C
D
A'
B'
C'
D'
A''
B''
C''
D''
DAPI
RFP
αSMA
Overlay
t=72 h
E
F
G
H
E'
F'
G'
H'
Quantification
I
RFP intensity (Pixels)
Time (h)
J
Number of cells per 5 µm section
RFP+
αSma+ RFP+

Figure 15. Time-lapse imaging of E12.5 lungs from *Fgf10*$^{iCre/+}$; *Tomato*$^{flox/+}$ embryos.
Recombination was induced *in vivo* by a single IP injection of tamoxifen at E11.5. (**A-D**) Bright field imaging of the E12.5 lung undergoing branching morphogenesis. (**A'-D'**) Fluorescence imaging of Tomato-positive cells through the RFP channel showing the progressive amplification and migration of lineage labeled cells. Note the high Tomato expression in the accessory lobe. (**A''-D''**) Overlay of BF and fluorescent images. (**E-H**) Immunofluorescence detection of αSMA (green) in the *Fgf10*$^{iCre/+}$; *Tomato*$^{flox/+}$ lung after 72 h of culture. The areas in white boxes are magnified in (**E'-H'**). A subpopulation of lineage-labeled cells lies in the parabronchial smooth muscle cell layer (white arrows in H'). (**I**) Quantification of the RFP signal over time. Lineage-labeled cells show exponential amplification during the first 24 h followed by linear amplification for the following two days. (**J**) Quantification of lineage-labeled cells after αSMA immunostaining. *n = 3*. Data are shown as average values ± S.E.M. Scale bars: (A-D) 500 µm; (E-H) 100 µm; (E'-H') 100 µm. BF: Bright field.

4.2.2. *Fgf10*-positive cells are progenitors for parabronchial and vascular smooth muscle cells *in vivo*

To study the commitment of *Fgf10*-positive cells to the smooth muscle lineage *in vivo*, pregnant mice carrying *Fgf10*$^{iCre/+}$; *Tomato*$^{flox/+}$ embryos received a single IP injection of tamoxifen at E10.5 and embryonic lungs were harvested at E13.5, E15.5 and E18.5 (Fig. 16A-C). Because Tomato-positive cells were mostly abundant in the accessory lobe, this lobe was chosen for immunostaining. αSMA staining of *Fgf10*$^{iCre/+}$; *Tomato*$^{flox/+}$ lungs revealed a subpopulation of Tomato-positive cells in the PBSMC layer at all three developmental stages (Fig. 16D-F). Among total Tomato-positive cells, Tomato-positive PBSMCs were significantly abundant at E13.5 (14.03 ± 1.31% of total Tomato-positive cells; *n = 3*) (Fig. 16D, J) and E15.5 (18.47 ± 3.75%; *n = 3*) (Fig. 16E, K) but declined at E18.5 (7.51 ± 0.72%; *n = 3*) (Fig. 16F, L). Another population of Tomato-positive cells was identified in the vascular smooth muscle cell (VSMC) compartment at E15.5 (3.44 ± 0.96%; *n = 3*) (Fig. 16H, K) and E18.5 (4.88 ± 0.83%; *n = 3*) (Fig. 16I, L). A third population of lineage-labeled cells was observed in the vicinity of

parabronchial and vascular smooth muscle cells at all three stages (Fig. 16J-L). These cells did not stain for the neuronal marker β-III Tubulin (data not shown). The various lineage-labeled cell populations, classified according to αSMA staining, are summarized in Table 7.

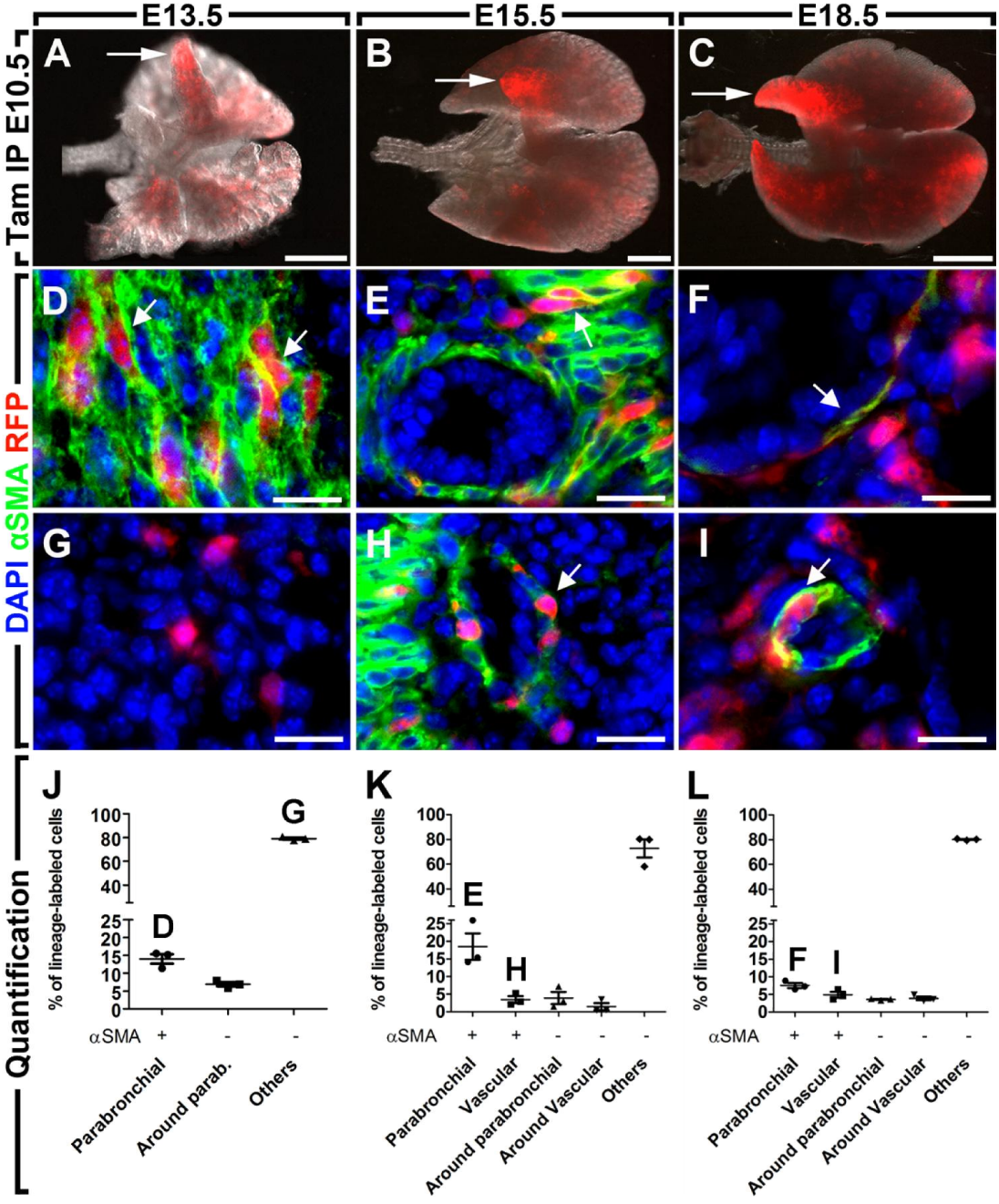

Figure 16. Contribution of *Fgf10*-positive cells labeled at E10.5 to the smooth muscle lineage *in vivo*.
(**A-C**) Overlay of BF and fluorescent images of the lung at E13.5, E15.5 and E18.5. Note the strong RFP signal in the accessory lobe at all three stages (white arrows). (**D-F**) αSMA staining (green) on the accessory lobes of the lungs from the upper panel showing RFP^+ cells in the PBSMC layer at all three stages (white arrows). The endogenous Tomato signal was detected via the RFP channel. (**G**) High magnification of $αSma^-$ RFP^+ cells at E13.5. (**H, I**) αSMA staining showing RFP^+ cells in the VSMC compartment at E15.5 and E18.5 (white arrows). (**J-L**) Quantification of multiple RFP^+ populations based on αSMA staining. *n = 3*. Data are shown as average values ± S.E.M. Scale bars: (A) 500 μm; (B) 1000 μm; (C) 750 μm; (D-I) 25 μm.

Table 7. Classification of *Fgf10*-expressing cell populations labeled at E10.5 according to *αSma* expression.
Data are shown as average values ± S.E.M. Abbreviations: ND: Not determined; PBSMCs: Parabronchial smooth muscle cells; VSMCs: Vascular smooth muscle cells.

Time of harvest	E13.5	E15.5	E18.5
Total RFP^+ cells counted per sample	278 ± 25	254 ± 33.84	392.33 ± 51.11
% RFP^+ PBSMCs	14.03 ± 1.31%	18.47 ± 3.75%	7.51 ± 0.72%
% RFP^+ VSMCs	ND	3.44 ± 0.96%	4.88 ± 0.83%
% RFP^+ β-III Tub^- cells around PBSMCs	6.92 ± 0.56%	3.87 ± 1.72%	3.56 ± 0.12%
% RFP^+ β-III Tub^- cells around VSMCs	ND	1.45 ± 0.99%	3.86 ± 0.52%
% other RFP^+ cells	79.05 ± 1.20%	72.77 ± 7.32%	80.19 ± 0.38%

4.2.3. *Fgf10*-positive cells from early pseudoglandular stage are potent progenitors *in vivo*

The genetic model used in this study revealed that only a minor proportion of *Fgf10*-positive cells commit to the smooth muscle lineage (Fig. 16J-L). *Fgf10* is known to be expressed by adipocyte precursors and *Fgf10*-null neonates suffer from impaired development of the white adipose tissue (Yamasaki et al., 1999; Sakaue et al., 2002). Thus, we decided to investigate whether *Fgf10*-positive cells give rise to an adipose-related cell lineage in the lung, the lipofibroblasts. *Fgf10*-positive cells were labeled during early pseudoglandular stage (E11.5) and lungs were harvested at E12.5, E15.5 and E18.5 (Fig. 17A-C). Since lipofibroblasts start to emerge in the lung at E15.5 (Al Alam and El Agha, in progress), αSMA and ADRP immunostaining was performed at E18.5. For convenience, the left lung lobe was used to carry out immunofluorescence staining and quantification (Fig. 17D). An average of 450 ± 10.12 (*n = 3*) Tomato-positive cells was counted per sample and a minor proportion of RFP^+ cells stained for αSMA around the epithelium (5.68 ± 0.39%; *n = 3*) (Fig. 17E, F) and within vascular walls (4.31 ± 0.23%; *n = 3*) (Fig. 17E, G). Similarly to *Fgf10*-positive cells labeled at E10.5, a population of $αSma^- RFP^+$ cells was identified in the vicinity of PBSMCs (10.17 ± 0.88%; *n = 3*) (Fig. 17E, H) and VSMCs (3.92 ± 0.72%; *n = 3*) (Fig. 17E). These cells did not express the neuronal marker *β-III Tubulin* (Fig. S1). Interestingly, a significant population of RFP^+ cells stained for ADRP (29.96 ± 5.17%; *n = 3*) (Fig. 17E, I). The remaining population of RFP^+ cells (45.97 ± 4.2%; *n = 3*) that did not stain for αSMA or ADRP was characterized by its big size and the presence of filopodia (Fig. 17E, J, K). The lungs were also stained for other markers like CD45 and CD31 but no overlap was observed between these markers and the RFP signal (Fig. S1).

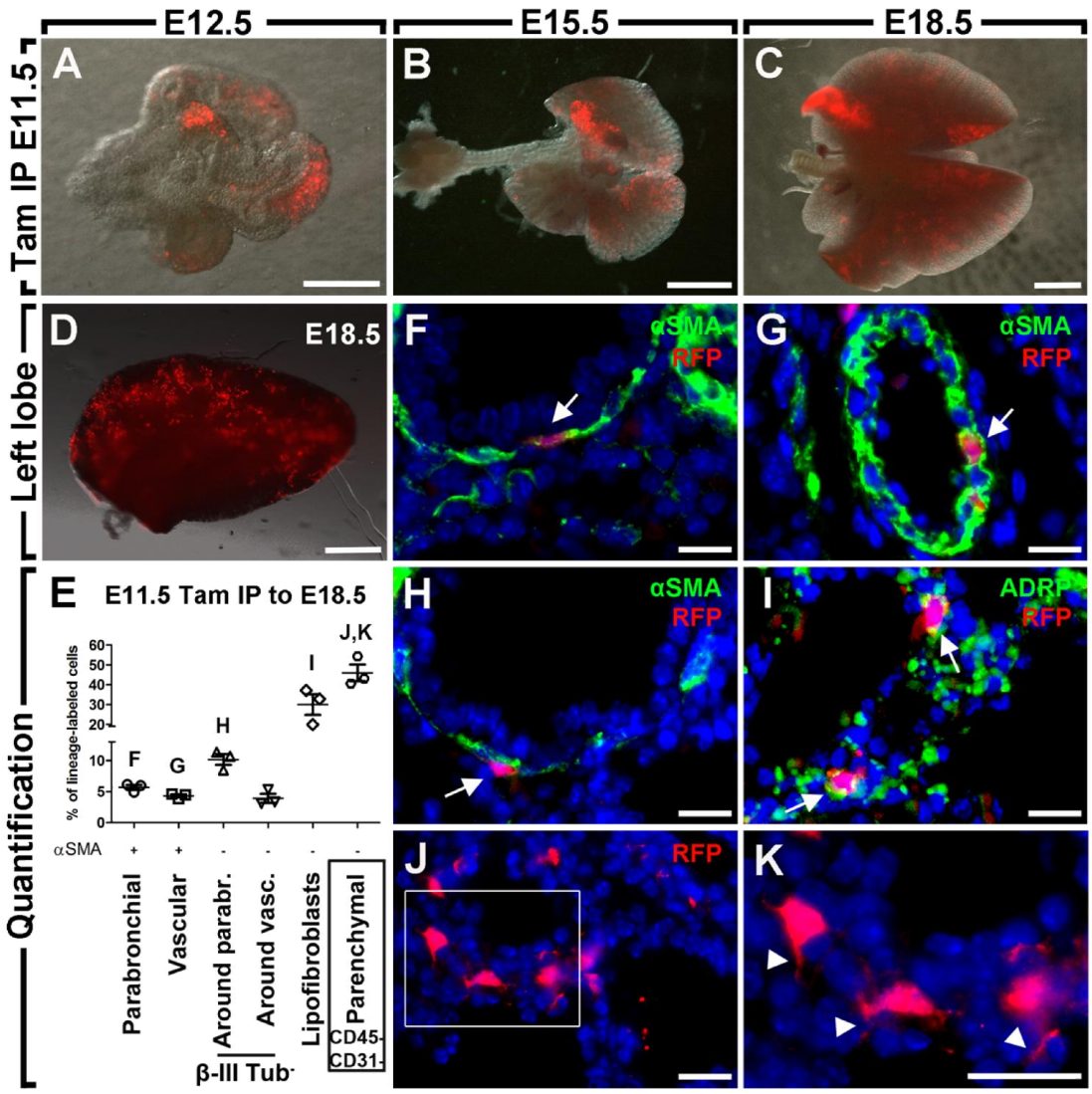

Figure 17. *In vivo* lineage tracing of *Fgf10*-positive cells labeled at E11.5.
(**A-C**) Overlay of BF and fluorescent images of the lung at E12.5, E15.5 and E18.5. (**D**) Overlay of BF and fluorescent images of the left lung lobe at E18.5. (**E**) Quantification of RFP$^+$ populations. (**F-H**) αSMA staining showing RFP$^+$ cells in the PBSMC layer (F), vascular walls (G) and around PBSMCs (H). (**I**) Immunofluorescence staining showing Adrp$^+$ RFP$^+$ cells. (**J**) Big RFP$^+$ cells with filopodia are present in the lung parenchyma. The area in the white box is magnified in (**K**). *n = 3*. Data are shown as average values ± S.E.M. Scale bars: (A) 250 µm; (B,C) 1000 µm; (D) 500 µm; (F-K) 12.5 µm.

4.2.4. *Fgf10*-positive cells from late pseudoglandular stage are progenitors for lipofibroblasts *in vivo*

Fgf10-positive cells from E11.5 showed to be precursor cells for PBSMCs, VSMCs and lipofibroblasts at E18.5 (Fig. 17). However, the commitment of these early progenitors to the smooth muscle lineage showed a decline beyond E15.5 (Fig. 16J-L). To further investigate this observation and to test whether lipofibroblast progenitors are restricted to early developmental stages, *Fgf10*-positive cells were labeled at E15.5 and embryonic lungs were harvested at E16.5 and E18.5 (Fig. 18). RFP expression was low at E16.5 (Fig. 18A; *n* = *3*) and was more pronounced at E18.5 (Fig. 18B). The left lung lobe was used to carry out immunofluorescence staining and quantification (Fig. 18D). An average of 499 ± 71.04 (*n* = *3*) Tomato-positive cells was counted per sample at E18.5. αSMA staining showed minimal overlap with the RFP signal in the parabronchial (0.26 ± 0.03%; *n* = *3*) and vascular (0.75 ± 0.34%; *n* = *3*) compartments (Fig. 18E). Significant numbers of αSma^{-} RFP^{+} cells around PBSMCs (10.33 ± 1.65%; *n* = *3*) (Fig. 18E, F) and VSMCs (4.99 ± 0.32%; *n* = *3*) (Fig. 18E, G) were detected. ADRP staining revealed a considerable proportion of $Adrp^{+}$ RFP^{+} cells (39.98 ± 8.28%; *n* = *3*) (Fig. 18E, H, I). Similarly to cells labeled at E11.5, αSma^{-} $Adrp^{-}$ β-III Tub^{-} $CD45^{-}$ $CD31^{-}$ cells (43.69 ± 8.32%; *n* = *3*) were also observed (Fig. 18E, J, K and Fig. S2).

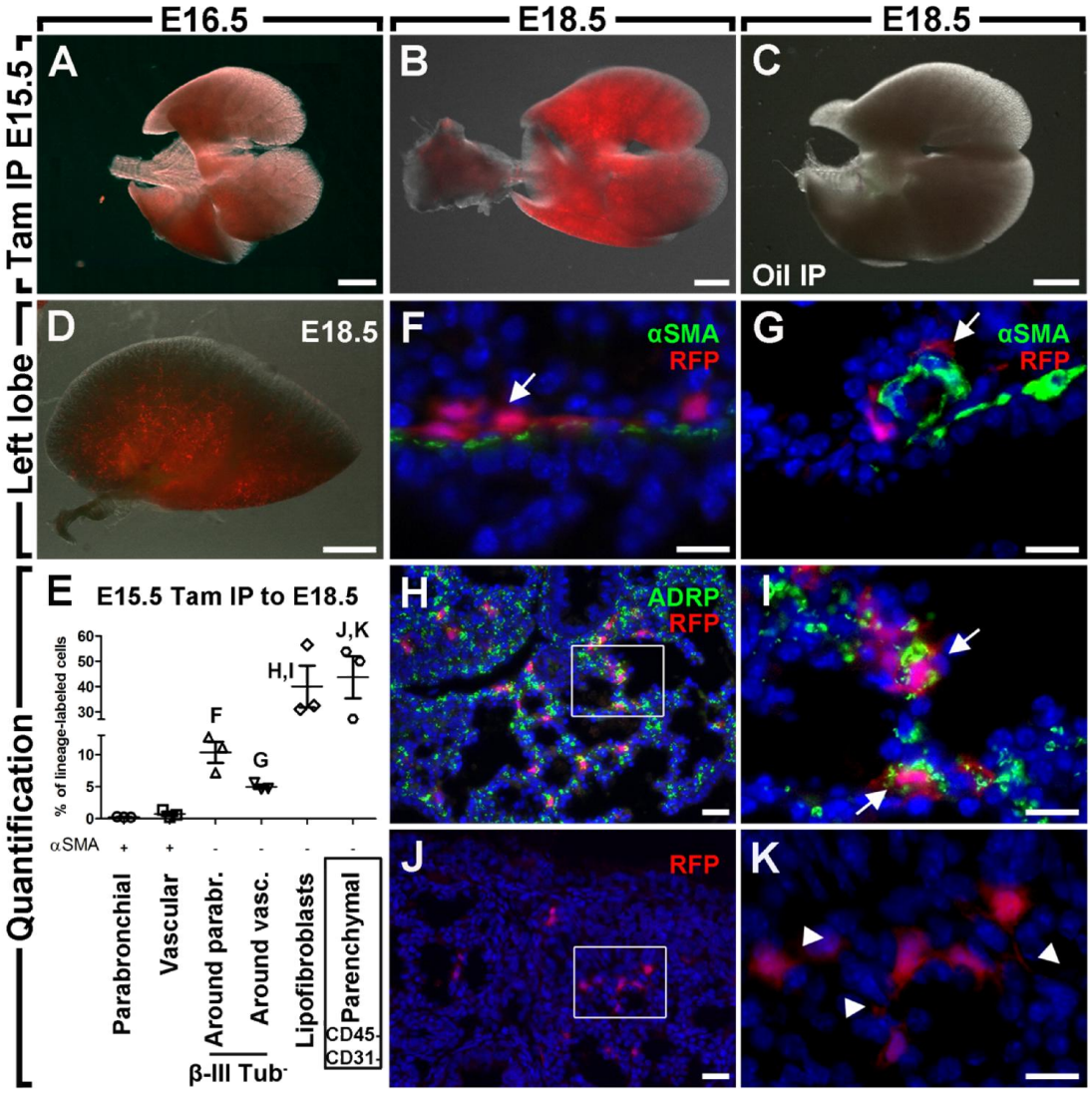

Figure 18. *In vivo* lineage tracing of *Fgf10*-positive cells labeled at E15.5.
(**A,B**) Overlay of BF and fluorescent images of the lung at E16.5 and E18.5. The RFP signal is more intense at E18.5. (**C**) Overlay of BF and fluorescent images of an E18.5 lung exposed to corn oil instead of tamoxifen. Note the absence of Tomato expression. (**D**) Overlay of BF and fluorescent images of the left lung lobe at E18.5. (**E**) Quantification of RFP^+ populations. (**F, G**) αSMA staining showing $αSma^-$ RFP^+ cells around PBSMCs (F) and VSMCs (G). (**H**) ADRP immunostaining showing RFP^+ cells expressing *Adrp*. The area in the white box is magnified in (**I**). (**J**) Big RFP^+ cells with filopodia are present in the lung parenchyma. The area in the white box is magnified in (**K**). *n = 3*. Data are shown as average values ± S.E.M. Scale bars: (A, D) 750 µm; (B, C) 1000 µm; (H, J) 25 µm; (I, K) 12.5 µm.

4.2.5. *Fgf10* expression identifies lipofibroblast rather than alveolar myofibroblast progenitors during alveologenesis

The alveolar stage of lung development is known for the prevalence of alveolar myofibroblasts. These cells, in addition to lipofibroblasts, are believed to play a critical role in secondary septa formation and alveolar maturation during postnatal alveolarization. To determine whether *Fgf10*-positive cells contribute to these lineages postnatally, pregnant mice carrying *Fgf10*$^{iCre/+}$; *Tomato*$^{flox/+}$ embryos were left to develop to term and then fed tamoxifen-containing pellets starting postnatal day 2 (P2). At P14, pups were sacrificed, lungs were harvested and processed, and the left lung lobe was used for immunostaining (Fig. 19). No Tomato signal was detected in lungs from *Fgf10*$^{+/+}$; *Tomato*$^{flox/+}$ pups (Fig. 19A, L) whereas the signal was abundant in the *Fgf10*$^{iCre/+}$; *Tomato*$^{flox/+}$ counterparts (Fig. 19B), especially near the main bronchus (Fig. 19C). An average of 141 ± 40 (*n* = *3*) Tomato-positive cells was counted per *Fgf10*$^{iCre/+}$; *Tomato*$^{flox/+}$ sample. αSMA immunostaining revealed a subpopulation of lineage-labeled cells expressing *αSma* (19.70 ± 1.88%; *n* = *3*) (Fig. 19D-H, M). These cells were located in the lung parenchyma and not at the tips of secondary septa where alveolar myofibroblasts are present. On the other hand, ADRP immunostaining showed that a major proportion of *Fgf10*-expressing cells gives rise to lipofibroblasts (67.74 ± 1.27%; *n* = *3*) (Fig. 19I-K, M).

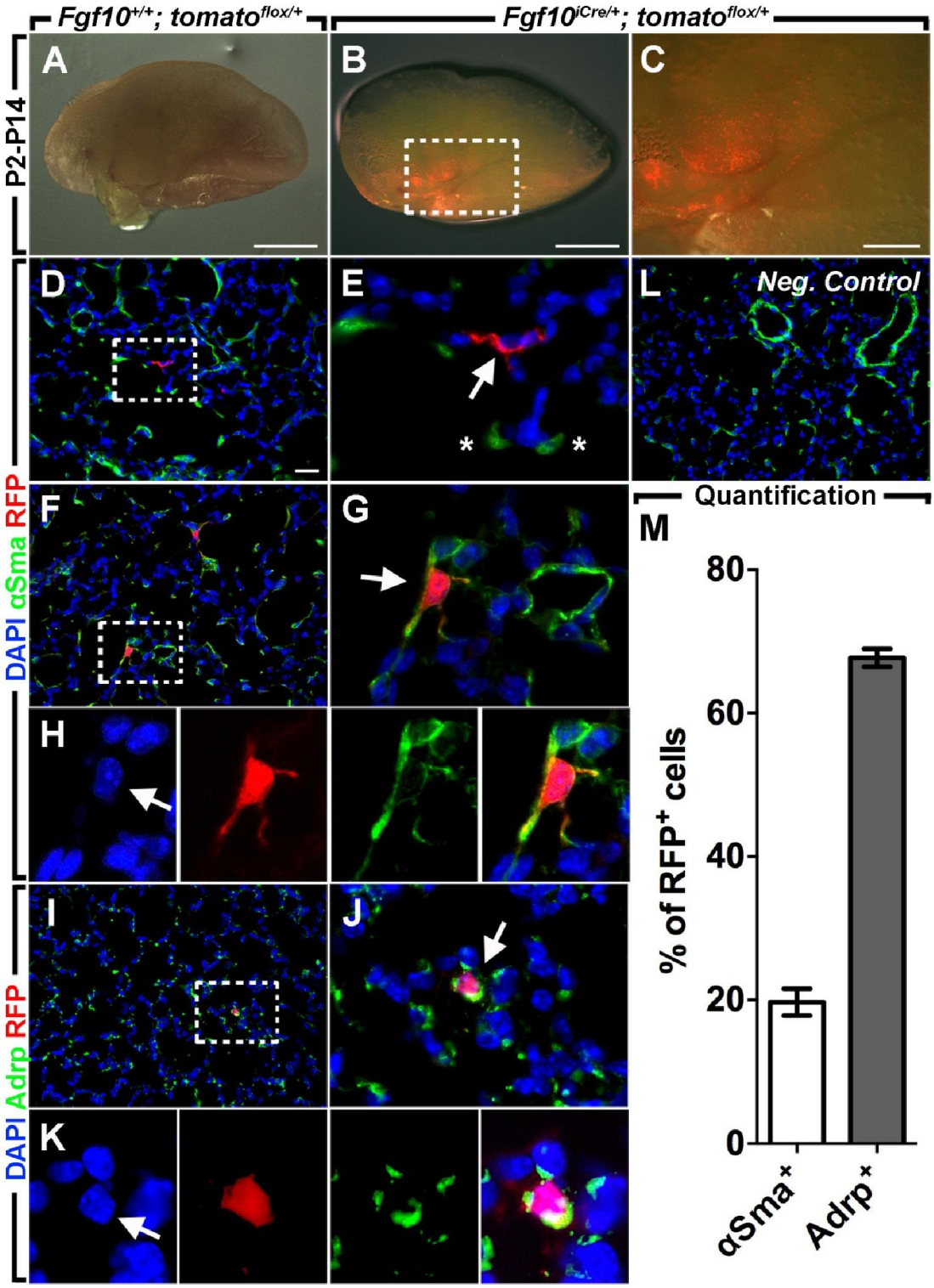
Fgf10+/+; tomatoflox/+
Fgf10iCre/+; tomatoflox/+
P2-P14
A
B
C
D
E
L
Neg. Control
DAPI αSma RFP
F
G
Quantification
M
H
DAPI Adrp RFP
I
J
K
80
60
40
20
0
% of RFP+ cells
αSma+
Adrp+

Figure 19. *Fgf10*-positive cells preferentially give rise to lipofibroblasts rather than alveolar myofibroblasts during alveologenesis.
Nursing mother mice were fed tamoxifen-containing pellets from P2 to P14. (**A**) Whole-mount fluorescence imaging of the left lung lobe from an *Fgf10*$^{+/+}$; *Tomato*$^{flox/+}$ pup. Note the absence of the Tomato signal. (**B**) Representative image of the left lung lobe from *Fgf10*$^{iCre/+}$; *Tomato*$^{flox/+}$ pups. Note the strong Tomato signal around the mainstem bronchus. The area in the dotted box is magnified in (**C**). (**D**) Immunostaining for αSMA showing an αSma^{-} RFP^{+} cell. The area in the dotted box is magnified in (**E**). The asterisks mark alveolar myofibroblasts in the secondary septa. (**F**) Immunostaining for αSMA showing an αSma^{+} RFP^{+} cell (white arrow). The area in the dotted box is magnified in (**G**). (**H**) Single-channel fluorescent images of the αSma^{+} RFP^{+} cell shown in (G). (**I**) Immunostaining for ADRP showing an Adrp^{+} RFP^{+} cell. The area in the dotted box is magnified in (**J**). (**K**) Single-channel fluorescent images of the Adrp^{+} RFP^{+} cell shown in (J). (**L**) Immunostaining for αSMA on an *Fgf10*$^{+/+}$; *Tomato*$^{flox/+}$ lung. Note the absence of the Tomato signal. (**M**) Quantification of lineage-labeled cells according to *αSma* and *Adrp* expression. *n = 3*. Data are shown as average values ± S.E.M. Scale bars: (A, B) 2.5 mm; (C) 750 μm; (D-L) 25 μm.

4.2.6. *Fgf10*-positive cells express resident MSC markers

Fgf10-expressing cells were labeled at E11.5 or E15.5 and lungs were harvested at E18.5. Lungs were dissociated into single cell suspensions and stained for CD45, CD31, EpCAM, PDGFRα, c-Kit and Sca-1. 50,000-100,000 cells were analyzed per sample per timepoint using a FACSAria III cell sorter (Fig. 20).

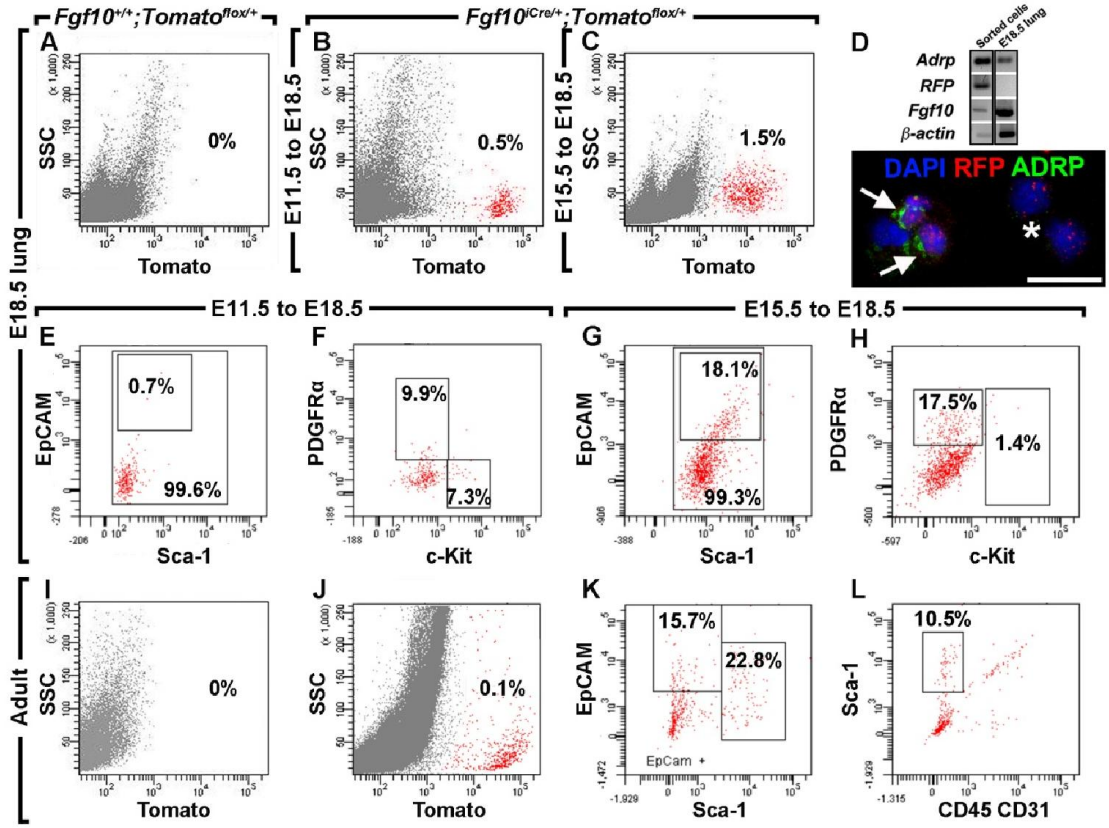

M Summary

Labeling at E11.5

Total cells $\xrightarrow{0.5\%}$ Fgf10⁺ cells $\xrightarrow{99.6\%}$ Sca-1^{low} $\xrightarrow{0.7\%}$ EpCam⁺; $\xrightarrow{9.9\%}$ Pdgfrα⁺

Labeling at E15.5

Total cells $\xrightarrow{1.5\%}$ Fgf10⁺ cells $\xrightarrow{99.3\%}$ Sca-1^{low} $\xrightarrow{18.1\%}$ EpCam⁺; $\xrightarrow{17.5\%}$ Pdgfrα⁺

Labeling during adulthood

Total cells $\xrightarrow{0.1\%}$ Fgf10⁺ cells $\xrightarrow{10.5\%}$ MSCs (CD45⁻ CD31⁻ Sca-1⁺)

N

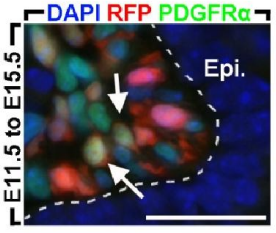

Figure 20. Flow cytometry analysis of *Fgf10*-positive cells labeled during embryonic development or postnatally.
(**A**) E18.5 lungs from *Fgf10*$^{+/+}$; *Tomato*$^{flox/+}$ embryos show no Tomato signal. (**B, C**) Tomato-positive cells account for ~0.5 and ~1.5% of the total E18.5 lung suspension when labeled at E11.5 and E15.5 respectively. (**D**) RT-PCR and immunostaining of sorted *Fgf10*-positive cells (labeled at E15.5) showing high expression of *Adrp* (white arrows). Note the presence of Adrp^{-} cells (asterisk). Wild type E18.5 lungs were used as negative and positive controls for *RFP* and *Adrp* expression respectively. (**E, F**) 99.6% of *Fgf10*-expressing cells labeled at E11.5 coexpress low levels of *Sca-1* (Sca-1^{low}) and 0.7% of these cells coexpress *EpCam*. 9.9 and 7.3% of lineage-labeled cells express *Pdgfrα* and *c-Kit* respectively. (**G, H**) 99.3% of *Fgf10*-expressing cells labeled at E15.5 coexpress low levels of *Sca-1* (Sca-1^{low}) and 18.1% of these cells coexpress *EpCam.* 17.5% of these cells coexpress *Pdgfrα* and very little overlap *with c-Kit* expression is detected (1.4%). (**I**) Lungs from *Fgf10*$^{+/+}$; *Tomato*$^{flox/+}$ adult mice show no Tomato signal. (**J**) Tomato-positive cells account for ~0.1% of the total adult lung. (**K**) 15.7 and 22.8% of lineage-labeled cells coexpress *EpCam* and *Sca-1* respectively. (**L**) A subpopulation of *Fgf10*-expressing cells (10.5%) shows the molecular signature of resident MSCs (CD45^{-} CD31^{-} Sca-1^{+}). (**M**) Summary of the flow cytometry analysis of *Fgf10*-expressing cells during embryonic lung development and postnatally. (**N**) Section of an E15.5 *Fgf10*$^{iCre/+}$; *Tomato*$^{flox/+}$ lung (labeled at E11.5) showing *Pdgfrα* expression. White arrows indicate RFP^{+} Pdgfrα^{+} cells and the dashed line marks the epithelial-mesenchymal boundary. *n* ≥ *2*. Scale bars: (D) 25 μm; (N) 12.5 μm.

No Tomato signal was detected in lungs from *Fgf10*$^{+/+}$; *Tomato*$^{flox/+}$ embryos (Fig. 20A). Whereas lineage-labeled cells from E11.5 accounted for ~0.5% of the total lung, those from E15.5 accounted for ~1.5% (Fig. 20B, C). Most *Fgf10*-positive cells from E11.5 and E15.5 were CD45^{-} CD31^{-} (data not shown). A subpopulation of *Fgf10*-positive cells from E11.5 and E15.5 also expressed the mesenchymal marker *Pdgfrα* at E18.5 (9.9 and 17.5% respectively) (Fig. 20F, H). Interestingly, almost no Tomato-positive cells from E11.5 and 18.1% from E15.5 stained for the pan-epithelial cell marker *EpCam* at E18.5 (Fig. 20E, G). *c-Kit* expression was very low at this stage (E18.5) but staining revealed 7.3 and 1.4% overlap with the Tomato signal in E11.5 and E15.5 timepoints respectively (Fig. 20F, H). Almost all lineage-labeled cells

from both timepoints expressed low levels of *Sca-1* (Sca-1^{low}) at E18.5 (Fig. 20E, G). RT-PCR and cytospin analysis of sorted *Fgf10*-positive cells (labeled at E15.5) showed high expression of *Adrp* (Fig. 20D), confirming the immunofluorescence data obtained from processed lung tissues (Figs. 17 and 18). Histological analysis of E15.5 *Fgf10$^{iCre/+}$; Tomato$^{flox/+}$* lungs (labeled at E11.5) showed a sub-population of RFP$^+$ Pdgfrα$^+$ cells (Fig. 20N).

Fgf10-expressing cells, labeled postnatally, represented ~0.1% of the total lung (a total of one million cells was analyzed) (Fig. 20J). 15.7 and 22.8% of RFP$^+$ cells stained for EpCAM and Sca-1 respectively (Fig 6K). A subpopulation (10.5%) of the total RFP$^+$ population exhibited the molecular signature of resident MSCs (CD45$^-$ CD31$^-$ Sca-1$^+$) (Fig. 20L).

4.2.7. *Fgf10*-expressing cells acquire myofibroblast characteristics during lung fibrosis

In order to study the role of *Fgf10*-positive progenitor cells in lung repair postnatally, four week-old *Fgf10$^{iCre/+}$; Tomato$^{flox/+}$* female mice were fed tamoxifen-containing pellets for four weeks and then received an IT injection of saline or bleomycin (3.5 U/Kg of body weight). Fourteen days later, mice were anesthetized and lung function measurement was performed. Lung fibrosis was confirmed in bleomycin-treated animals by deteriorated lung function parameters (decrease in compliance and increase in elastance and resistance) compared to saline-treated animals (Fig. 21F; *n* = *3*). H/E staining revealed the presence of dense fibrotic lesions in bleomycin-treated lungs compared to their saline counterparts (Fig. 21C, D). Interestingly, a three-fold increase in the number of *Fgf10*-expressing cells was detected in fibrotic lungs compared to control lungs (185 ± 27.54 vs 60 ± 9.81; *n* = *3*) (Fig. 21A, B, E).

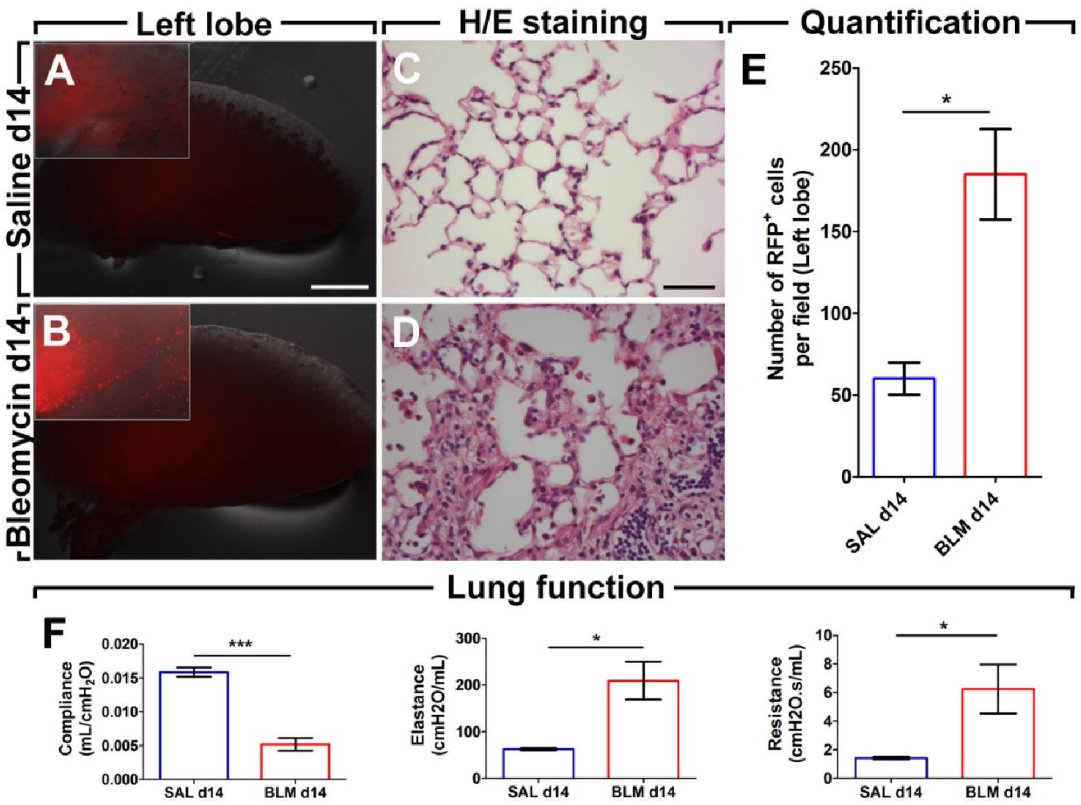

Figure 21. *Fgf10*-positive cells are amplified in bleomycin-treated lungs.
(**A, B**) Whole-mount fluorescence imaging of the left lobes from saline and bleomycin-treated *Fgf10*$^{iCre/+}$; *Tomato*$^{flox/+}$ lungs. High magnification images are shown in the insets. (**C, D**) H/E staining showing dense fibrotic lesions in bleomycin-treated lungs compared to saline-treated lungs. (**E**) Quantification of lineage-labeled cells in fibrotic and control lungs. (**F**) Lung function measurements confirming the presence of lung fibrosis in bleomycin-treated animals. *n = 3*. Data are shown as average values ± S.E.M. * $P < 0.05$; *** $P < 0.001$. Scale bars: (A, B) 2.5 cm; (C, D) 50 µm. Abbreviations: BLM: Bleomycin; SAL: Saline.

The lungs from saline and bleomycin-treated mice were immunostained for αSMA. Whereas none of the lineage-labeled cells stained for the myofibroblast marker in the saline group (Fig. 22A-C, G), 70.55 ± 2.86% (*n = 3*) of *Fgf10*-expressing cells stained for αSMA in bleomycin-treated lungs (Fig. 22D-G). Analysis of gene expression from bleomycin-treated lungs (day 14) showed an upregulation of myofibroblast markers (*αSma* and *Col1a1*) and a downregulation of lipofibroblast markers (*Adrp, Lipase* and *Pparg*) (Fig. 22H).

qPCR on biopsies from end-stage IPF patients also revealed a downregulation of lipofibroblast markers (*CEBPa, PPARg, Lipase* and *Resistin*) compared to donor biopsies (Fig. 22I).

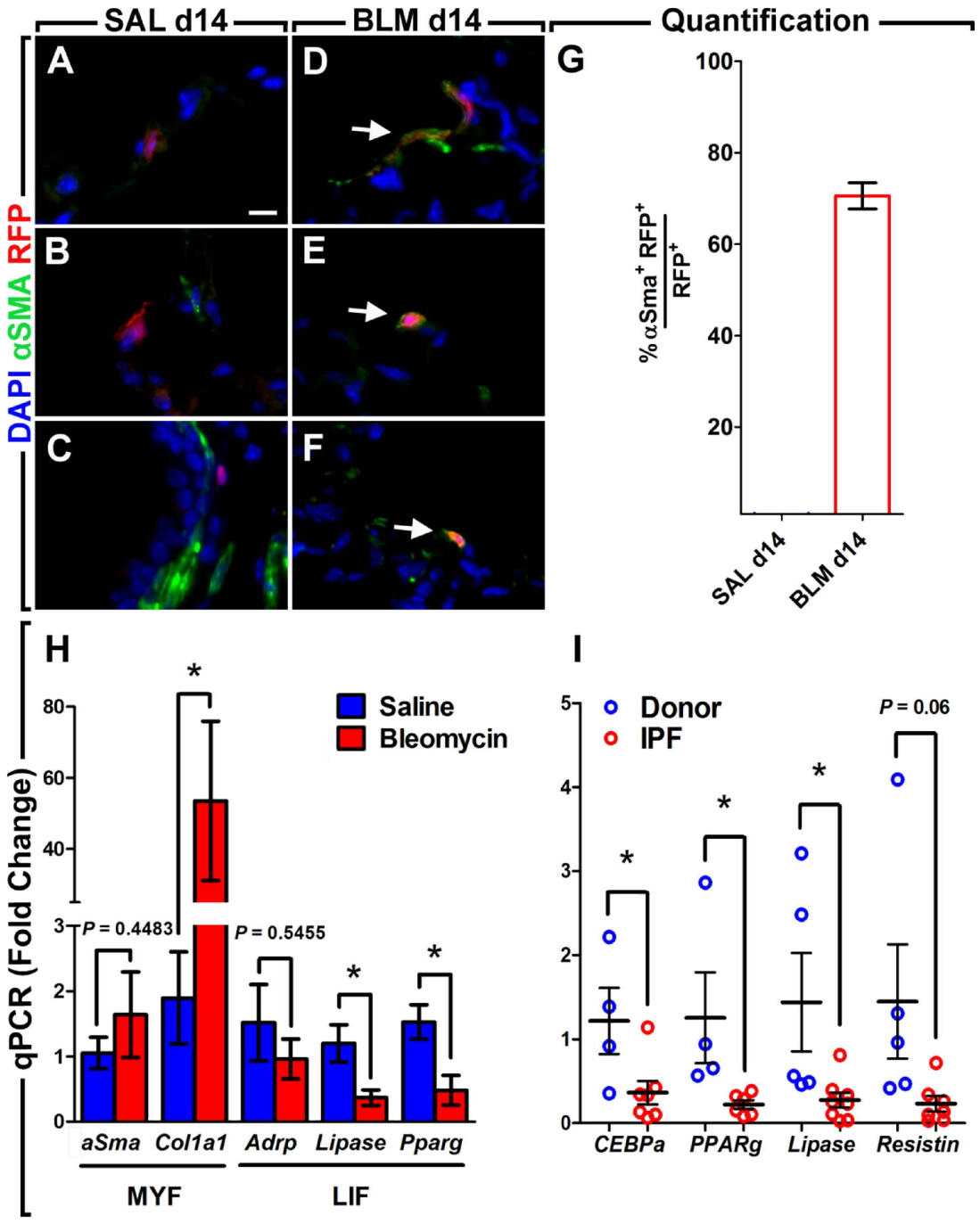

Figure 22. *Fgf10*-positive cells give rise to activated myofibroblasts in bleomycin-induced pulmonary fibrosis.
(**A-C**) A panel of representative images of lineage-labeled cells from saline-treated lungs. Note the absence of any overlap with the αSMA signal. (**D-F**) A panel of representative images of lineage-labeled cells from bleomycin-treated lungs. Note the overlap between the RFP and αSMA signals (white arrows). (**G**) Quantification of lineage-labeled myofibroblasts (*n = 3*). (**H**) qPCR analysis showing upregulation of myofibroblast markers (*αSma* and *Col1a1*) and downregulation of lipofibroblast markers (*Adrp, Lipase* and *Pparg*) in bleomycin-treated lungs ($3 \leq n \leq 6$) compared to saline-treated lungs ($3 \leq n \leq 8$). (**I**) qPCR analysis showing downregulation of lipofibroblast markers (*CEBPa, PPARg, Lipase* and *Resistin*) in end-stage IPF patients ($6 \leq n \leq 8$) compared to donors (*n = 4 or 5*). Data are shown as average values ± S.E.M. * $P < 0.05$. Reference genes: *Hprt* and *PBGD*. Scale bar: 10 μm. Abbreviations: IPF: Idiopathic pulmonary fibrosis; LIF: Lipofibroblasts; MYF: Myofibroblasts. cDNA from saline and bleomycin-treated lungs was kindly provided by Dr. Melanie Königshoff.

4.3. Role of *Fgf10* in lipofibroblast formation *in vivo* and *in vitro*

4.3.1. Decreased *Fgf10* expression correlates with decreased lipofibroblast formation *in vivo*

Our lineage tracing data demonstrate that *Fgf10*-expressing cells are both early and late progenitors for lipofibroblasts *in vivo*. To test whether *Fgf10* expression levels are critical for the formation of the lipofibroblast lineage, we crossed *Fgf10^{iCre}* mice with the previously described *Fgf10-LacZ* mice and pups were examined at P0. The resulting allelic combination of *Fgf10-LacZ/iCre* yields hypomorphic levels of *Fgf10* expression. *Fgf10-LacZ/iCre* pups were significantly smaller in size than their control littermates (*Fgf10-LacZ/+*) and their hindlimbs were severely truncated (Fig. 23A vs. C). *Fgf10-LacZ/iCre* lungs were smaller (Fig. 23B vs. D) and displayed thicker intersaccular walls as well as hemorrhagic areas upon histological analysis (Fig. 23E-H). Immunofluorescence for ADRP showed that mutant lungs exhibit impaired lipofibroblast formation as shown by decreased staining in the

mutants compared to the controls (Fig. 23I-L). In addition, gene expression analysis revealed an 80% decrease in *Fgf10* expression in hypomorphic lungs compared to their littermate controls (Fig. 23M; $n = 3$; $P < 0.01$). The decrease in *Fgf10* expression also correlated with a significant reduction in the expression levels of AEC II marker *Sftpc* (Fig. 23M; $n = 3$; $P < 0.01$) and endothelial cell marker *Flk1* (Fig. 23M; $n = 3$; $P < 0.01$). Interestingly, *αSma* expression was significantly upregulated in hypomorphic lungs compared to control lungs (Fig. 23M; $n = 3$; $P < 0.05$). The expression levels of lipofibroblast markers were also validated at the RNA level (Fig. 23N). *Zinc finger protein 423 (Zfp423)* (marker for committed pre-adipocytes) ($n = 3$; $P = 0.0953$), *Cebpb* ($n = 3$; $P < 0.05$) and *Pparg* ($n = 3$; $P < 0.05$) (markers for differentiating adipocytes) as well as *Adrp* ($n = 3$; $P < 0.01$) and *Lipase* ($n = 3$; $P < 0.01$) (markers for mature lipofibroblasts) showed a drastic decrease in mutant lungs compared to control lungs.

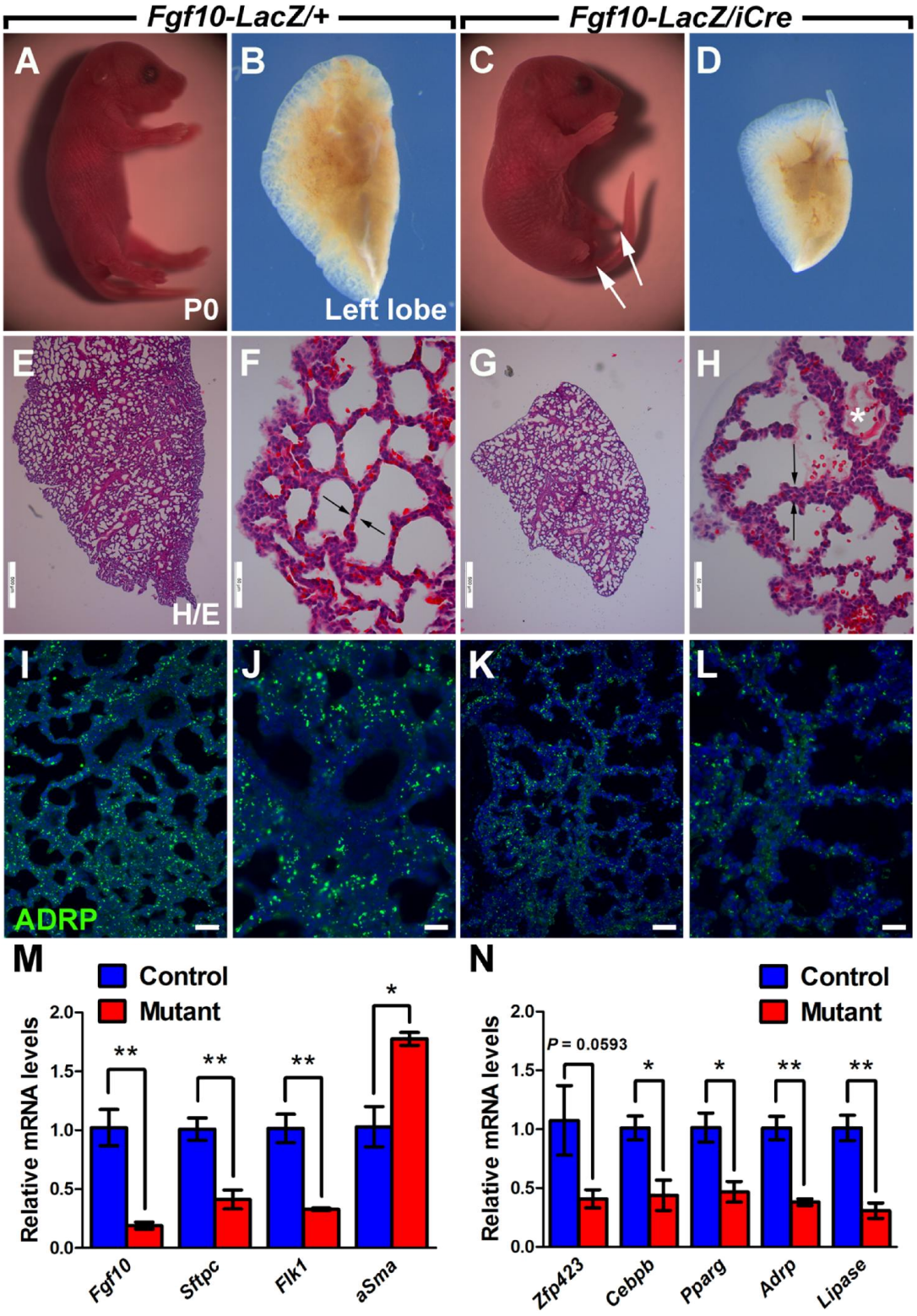
Fgf10-LacZ/+
Fgf10-LacZ/iCre
A
P0
B
Left lobe
C
D
E
H/E
F
G
H
*
I
ADRP
J
K
L
M
Control
Mutant
Relative mRNA levels
2.0
1.5
1.0
0.5
0.0
**
**
**
*
Fgf10
Sftpc
Flk1
aSma
N
Control
Mutant
Relative mRNA levels
P = 0.0593
*
*
**
**
Zfp423
Cebpb
Pparg
Adrp
Lipase

Figure 23. *Fgf10* dosage is critical for lipofibroblast formation *in vivo*.
(**A-D**) *Fgf10-LacZ/iCre* pups are smaller in size compared to *Fgf10-LacZ/+* control pups. Note the severe truncation of the hindlimbs (white arrows) as well as the hypoplastic lungs from the hypomorphic pups. (**E-H**) H/E staining of control and hypomorphic lungs. Note the thickening of intersaccular walls (black arrows) and hemorrhagic areas (white asterisk) in the mutant lungs. (**I-L**) ADRP immunostaining showing decreased *Adrp* expression in hypomorphic lungs compared to their control counterparts. (**M**) qPCR analysis showing significant downregulation of *Fgf10, Sftpc* and *Flk1* as well as upregulation of *αSma* in hypomorphic lungs compared to littermate controls. (**N**) qPCR analysis showing significant downregulation of markers of adipocyte precursors as well as mature lipofibroblasts. *n = 3*. Data are shown as average values ± S.E.M. * $P < 0.05$; ** $P < 0.01$. Reference gene: *Hprt*. Scale bars: (E, G) 500 μm; (F, H, I, K) 50 μm; (J, L) 25 μm.

4.3.2. FGF10 acts on embryonic mesenchymal cells and induces the expression of lipofibroblast markers *in vitro*

FGF10 has so far been believed to signal only to the epithelium expressing FGFR2b. However, the contribution of *Fgf10*-positive cells to various mesenchymal lineages raised the question whether FGF10 can also signal to mesenchymal cells in the developing lung. To address this issue, primary culture of E19.5 rat lung mesenchyme was prepared and treated with rhFGF10. P-ERK and αSMA immunostaining revealed that embryonic lung fibroblasts respond to exogenous FGF10 by activating the MAPK/ERK pathway and downregulating *αSma* expression (Fig. 24A, B). Western blotting revealed that treatment with increasing concentrations of rhFGF10 resulted in increased expression of PTHrP receptor, PPARγ, C/EBPα and Leptin (Fig. 24C).

In order to determine whether FGF10 signaling in the mesenchyme triggers lipofibroblast formation in human fibroblasts, we used the well-established embryonic human lung fibroblast cell line WI-38. Treatment of these cells with increasing concentrations of rhFGF10 triggered the expression of lipofibroblast markers PPARγ, Leptin and C/EBPα (Fig. 24D). RT-PCR

revealed that WI-38 cells and rat lung fibroblasts (Passage 3) express *Fgfr1b* rather than *Fgfr2b* while rat lung fibroblasts (Passage 1) express *Fgfr1b* as well as *Fgfr2b* (Fig. 24E). Sorted *Fgf10*-positive cells (labeled at E14.5) from E18.5 embryonic mouse lungs were also treated with rhFGF10. The treatment resulted in the activation of the MAPK/ERK pathway (Fig. 24F, G). RT-PCR showed that these cells express *Fgfr1b* rather than *Fgfr2b* similarly to rat lung fibroblasts (Passage 3) and WI-38 cell line. These cells showed to also express low levels of *Fgfr1/2c* (Fig. 24H).

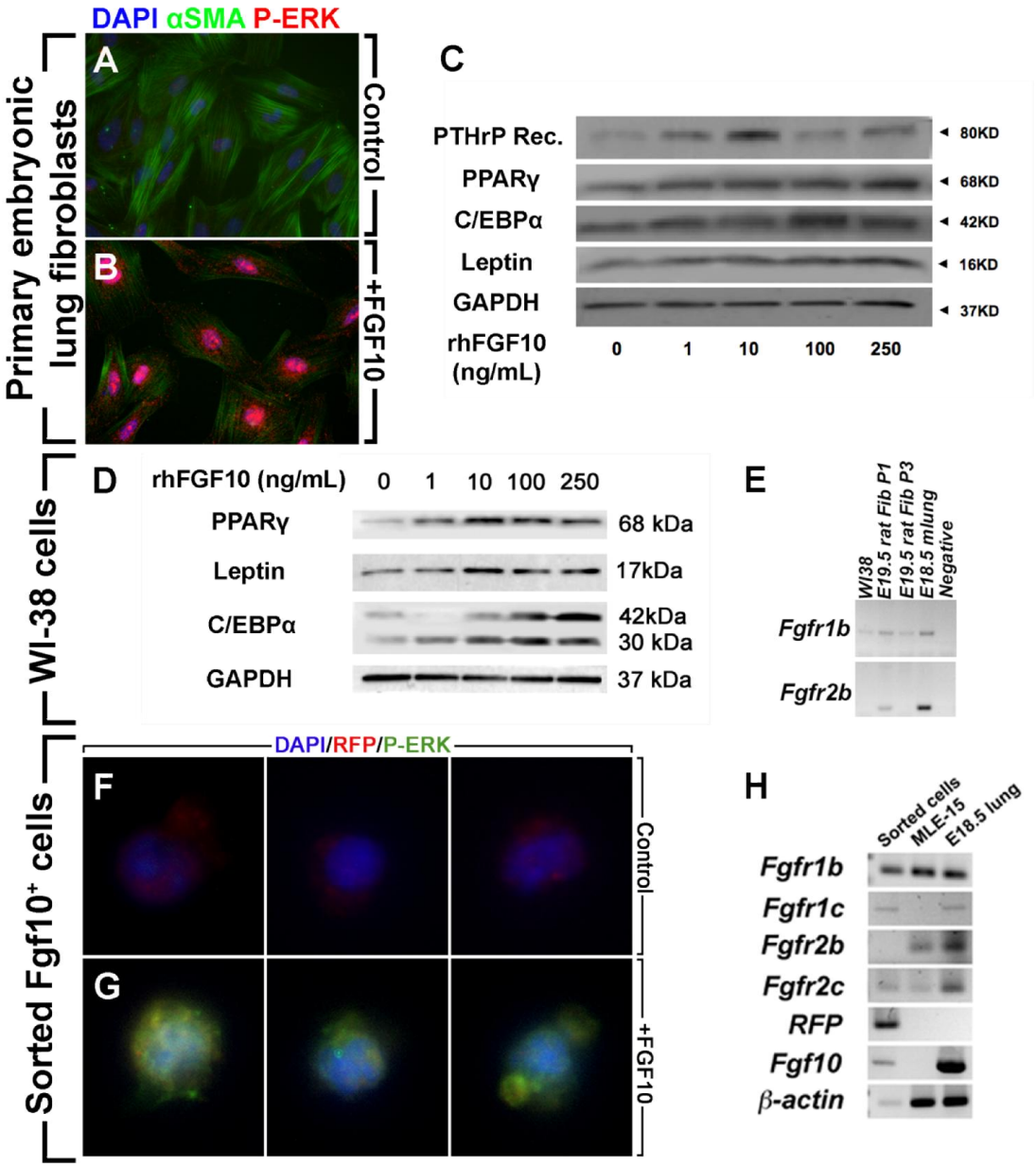

Figure 24. Embryonic lung fibroblasts respond to exogenous FGF10 and upregulate lipofibroblast markers *in vitro*.

(**A-B**) Immunofluorescence staining for αSMA and P-ERK showing activation of the MAPK/ERK pathway and downregulation of *αSma* expression in rhFGF10-treated embryonic rat lung fibroblasts. (**C**) Western blots showing upregulation of lipofibroblast markers (PTHrP receptor, PPARγ, C/EBPα and Leptin) upon treatment with increasing concentrations of rhFGF10. GAPDH was used as a loading control. (**D**) Western blots showing upregulation of lipofibroblast markers (PPARγ, Leptin and C/EBPα) in WI-38 cells upon treatment with rhFGF10. (**E**) RT-PCR showing that WI-38 cells and embryonic rat lung fibroblasts (Passage 3) express *Fgfr1b* rather than *Fgfr2b*. Passage 1 embryonic rat lung fibroblasts express both *Fgfr1b* and *Fgfr2b*. E18.5 mouse lung homogenates were used as a positive control. (**F, G**) Sorted *Fgf10*-positive cells respond to rhFGF10 treatment by activation of MAPK/ERK pathway. (**H**) RT-PCR showing that *Fgf10*-positive cells express *Fgfr1b* rather than *Fgfr2b* as well as low levels of *Fgfr1/2c*. MLE-15 cells and E18.5 lungs were used as controls for the expression of epithelial and mesenchymal isoforms of *Fgfr1/2*. Data were kindly provided by Drs. Virender K. Rehan (UCLA, CA, USA) and Denise Al Alam (CHLA, CA, USA).

5. Discussion

5.1. Validation of *Fgf10*^{iCre} knock-in mouse line

FGF10 is a morphogen that is critical for the embryonic development of many organs including the lung, duodenum, cecum, colon, pancreas, limb and mammary placodes. *Fgf10* knockout mice suffer from agenesis of the corresponding organs, thus limiting any real use of these mice in studying the behavior or lineage commitment of *Fgf10*-positive cells. On the other hand, due to the stability of β-galactosidase, the *Fgf10-LacZ* transgenic line allows non-inducible transient tracing of *Fgf10*-positive cells in many organs. However, the gold standard for an optimal lineage tracing tool relies on the inducibility of constitutive cell labeling via the controlled activation of Cre recombinase. Then, short- and long-term lineage commitment can be investigated. Therefore, the data obtained with the *Fgf10-LacZ* line should always be validated using the proper Cre inducible line. Nevertheless, this line has helped identify the progeny of *Fgf10*-positive cells in the heart, lung, gut, mammary glands, brain (Kelly et al., 2001; Mailleux et al., 2005; Veltmaat et al., 2006; Ramasamy et al., 2007; Hajihosseini et al., 2008; Parsa et al., 2008) and limbs (Hajihosseini and Bellusci, unpublished results). Thus, the *Fgf10*^{iCre} knock-in line represents a novel tool that bypasses the pitfalls associated with the *Fgf10-LacZ* transgenic line. This is because *Fgf10*-positive cells are exclusively labeled upon tamoxifen injection, after which labeled cells can be traced and characterized. A previous report has shown that intraperitoneally administered tamoxifen reaches effective levels in the embryonic circulation within 12 hours, after which it is cleared from the pregnant mouse within 12 hours (Nakamura et al., 2006). This 24-hour time frame allows accurate labeling of *Fgf10*-positive cells.

In the first part of this study, we induced recombination in pregnant females carrying *Fgf10*$^{iCre/+}$*; Tomato*$^{flox/+}$ embryos at E15.5. At E18.5, lineage-labeled cells were found in the ears of the embryos (Fig. 10A") and this observation is consistent with previously published reports that describe the role of FGF10 in inner ear formation (Alvarez et al., 2003). Moreover, labeled cells were

observed in the skin (Fig. 10B") where FGF10 is known to be expressed in the dermal papillae (Hamada et al., 1999). In the lung, labeled cells were dispersed throughout the mesenchyme (Fig. 11A'). However, the signal was more pronounced in interlobular septa (Fig. 11B'). Further studies need to be performed in order to explain this observation. As for the trachea, labeled cells were arranged in discrete ring-like structures (Fig. 11C'). This pattern is consistent with previously published reports about the role of FGF10 in tracheal cartilage ring formation in mice (Tiozzo et al., 2009; Sala et al., 2011). We also used *Fgf10-LacZ* lungs from the same stage (E18.5) to validate our data. As expected, X-Gal staining of *Fgf10-LacZ* lungs revealed similar sites of *Fgf10* expression (Fig. 11A''-C'').

For functional inactivation studies, we generated E14.5 $Fgf10^{iCre/flox}$; $Tomato^{flox/+}$ embryos in which Cre had been activated since E8.5. By virtue of the embedded $Tomato^{flox}$ reporter, we were able to locate recombination sites and thus, we restricted our diagnostic to those specific sites. An abnormal phenotype, characterized by webbing of the digits, was observed in the forelimbs (Fig. 12H vs. E, M). This finding agrees with previous reports about the involvement of *Fgf10* misregulation in digit abnormalities such as syndactyly [(Liu et al., 2002); (Al Alam and Bellusci, in revision)]. Moreover, $Fgf10^{iCre/flox}$; $Tomato^{flox/+}$ lungs showed clear developmental abnormalities characterized by a deformed shape as well as branching simplification (Fig. 12C vs. B, G vs. F, J). This phenotype is similar to that obtained by Abler et al. who used a general mesenchymal driver line $(Dermo1^{Cre})$ to perform conditional gene inactivation of *Fgf10* (Abler et al., 2009). Last but not least, our research group has previously demonstrated that the gut is a major site of *Fgf10* expression and that *Fgf10*-null embryos suffered from cecal atresia. Our data agrees with this finding as $Fgf10^{iCre/flox}$; $Tomato^{flox/+}$ embryos suffered from a hypomorph-like phenotype at the level of the cecum upon partial loss of function of *Fgf10* (Fig. 12L vs. I, K).

One drawback of the $Fgf10^{iCre}$ line is the mismatch between *Cre* and *Fgf10* expression levels as examined at different developmental stages by qPCR (Fig. 13A). To understand the inefficient expression of *Cre* from the $Fgf10^{iCre}$

locus, we performed a bioinformatic analysis for the 3 kb deleted sequence downstream of ATG codon of exon 1 of *Fgf10* gene using online tools (Fig. 14). The analysis revealed the presence of H3K4me3 site overlapping exon 1-intron 1 boundary. This histone modification is known to be associated with the 5' end of actively transcribed genes (Santos-Rosa et al., 2002). On the other hand, several conserved binding sites for lung-related transcription factors were detected, including binding sites for SMAD4, NKX2.5, TBX5 and ISL1. TBX5 is thought to directly control *Fgf10* expression in the lung mesenchyme (Cebra-Thomas et al., 2003). Moreover, a recent report has shown that ISL1 regulates *FGF10* transcription within the second heart field by binding to an enhancer element in intron 1 of *FGF10* gene (Golzio et al., 2012). Altogether, these data suggest the presence of key regulatory elements in intron 1 critical for the maintenance of *Fgf10* expression over time. Nonetheless, this line allows targeting a subset of *Fgf10*-positive cells after birth allowing to study the lineage commitment of these cells during homeostasis and during the repair process after injury.

Alternative strategies that would bypass potential consequences on *Cre* expression levels include fusion of Cre-ERT2 in frame with the ATG codon of *Fgf10* without deleting intronic sequences, thus preserving putative regulatory elements and matching *Cre* expression levels to endogenous *Fgf10*. Another approach would be the insertion of IRES-Cre-ERT2 in the 3' UTR downstream of *Fgf10* stop codon. In this case, *Fgf10* would still be expressed at physiological levels but *Cre* expression levels would depend greatly on the activity of the IRES element.

In conclusion, the *Fgf10*^{iCre} knock-in line described in this study is a novel tool that allows labeling and tracking of *Fgf10*-positive cells. The mosaic recombination pattern, as illustrated by the *Tomato*^{flox} reporter, makes this line convenient for clonal analysis, especially when a partial loss of function approach is desired. This tool can potentially bring insight on the role of *Fgf10*-positive progenitor cells in development and repair after injury.

5.2. Lineage tracing of *Fgf10*-positive progenitor cells during embryonic lung development

The embryonic lung mesenchyme consists of cells that belong to distinct lineages including myogenic, adipogenic, chondrogenic, neuronal and other lineages. Most of these cell types arise from endogenous (or resident) progenitor populations while few (eg. nerve cells) arise from exogenous sources (the neural crest). Moreover, there is strong evidence suggesting that hematopoietic cells in the mesenchyme derive from non-bone marrow-derived resident progenitors (Lugus et al., 2009). Cell fate determination likely arises from a complex network of autocrine and paracrine signals leading to the proliferation and differentiation of lineage-restricted as well as multipotent progenitor cell populations.

Most of the mesenchymal cell types that populate the lung start to emerge during early phases of embryonic lung development (Table 2). One of the early markers of the lung mesenchyme is *Fgf10*. During early lung development, *Fgf10* is expressed in the distal (sub-mesothelial) mesenchyme and it acts on the opposite epithelium expressing *Fgfr2b* (Bellusci, Grindley, et al., 1997). *Fgf10* maintains epithelial cells in a progenitor-like state and induces epithelial branching and migration. Loss of function of *Fgf10* results in branching simplification and decreased numbers of epithelial progenitors. Although the primary target of FGF10 is the epithelium, severe mesenchymal abnormalilties are also observed when FGF10 signaling is attenuated (Ramasamy et al., 2007).

Our research group has shown that *Fgf10*-expressing cells are highly dynamic and they relocate around the growing epithelial buds and give rise to PBSMCs on the proximal side of the epithelial tree (Mailleux et al., 2005). In the latter study, distal mesenchymal tissue from *Fgf10-LacZ* lungs was grafted into the corresponding position in wild type lungs and the lungs were allowed to grow *ex vivo*. *LacZ*-positive cells were eventually detected alongside the growing epithelium giving rise to PBSMCs. β-Catenin signaling was shown to control

the proliferation but not the differentiation of these PBSMC progenitors (De Langhe et al., 2008).

The dynamic expression pattern of *Fgf10* in the lung mesenchyme throughout development suggests that *Fgf10*-expressing cells behave differently at different developmental stages. Here, we used the *Fgf10*^{iCre} knock-in mouse line, combined with the *Tomato*^{flox} reporter line, to permanently label *Fgf10*-positive cells (as well as their descendants) and study their fate in a time-controlled manner. Initially, cells were labeled at E11.5 and lungs were harvested at E12.5 (Fig. 15). Time-lapse imaging on intact embryonic lungs showed that *Fgf10*-expressing cells possess high mitotic and migratory capabilities. These cells, initially located in the distal mesenchyme, amplified and migrated greatly throughout the mesenchyme over the 72 h-culture period. However, it cannot be excluded that remaining traces of tamoxifen can also induce Cre activity, and thus RFP expression, *ex vivo*. In agreement with what our group has previously shown (Mailleux et al., 2005), a subpopulation of *Fgf10*-positive cells was eventually embedded within the PBSMC layer.

Lineage tracing of *Fgf10*-positive cells from E10.5 showed that the smooth muscle program in these cells is mostly active between E11.5 and E15.5, beyond which the cells seem to commit to other lineages (Fig. 16). Interestingly, we show for the first time that these cells are also progenitors for VSMCs. Que et al. have previously shown that mesothelial *Wt1*-positive cells are progenitors for VSMCs but not PBSMCs (Que et al., 2008). Here, we provide evidence for the presence of an *Fgf10*-expressing progenitor cell population that is capable of generating both lineages.

The domain of *Fgf10* expression in the embryonic lung has been thoroughly studied. Northern blotting and qPCR data show that *Fgf10* transcripts progressively accumulate in the embryonic lung between E11.5 and E18.5 (Bellusci, Grindley, et al., 1997; El Agha et al., 2012). *In situ* hybridization and X-Gal staining of *Fgf10-LacZ* lungs show that *Fgf10* expression is restricted to the tips of the distal mesenchyme until E14.5, after which the expression becomes dispersed throughout the mesenchyme (Mailleux et al., 2005; Ramasamy et al., 2007; El Agha et al., 2012; Tiozzo et al., 2012). Our lineage

tracing data reveal two distinct populations of progenitor cells, each of which is characterized by a distinct pattern in terms of cell localization as well as differentiation potential. When labeled at E11.5, these cells reside mostly in the distal mesenchyme at E18.5 (especially observed in the accessory lobe) and contribute to myogenic (PBSMCs and VSMCs) as well as adipogenic lineages (lipofibroblasts) (Fig. 17). On the contrary, *Fgf10*-positive cells are more dispersed at E18.5 when labeled at E15.5 and they give rise to adipogenic - but not myogenic – lineages (Fig. 18). An interesting subpopulation of αSma^{-} RFP^{+} cells adjacent to parabronchial and vascular smooth muscle cells was observed in both progenitor populations. Initially, we thought that these cells could have a neuronal nature since *Fgf10* is known to be involved in neurogenesis (Hajihosseini et al., 2008; Haan et al., 2013). However, β-III Tubulin immunostaining did not show any overlap with the lineage label (Figs. S1 and S2). The progenies of these two progenitor cell populations are summarized in Figure 25 and Table 8.

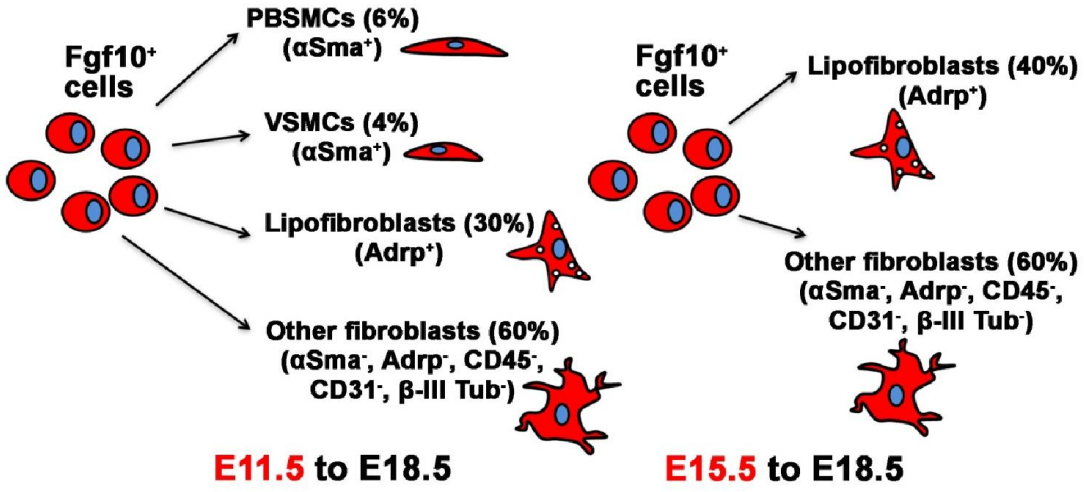

Figure 25. *Fgf10*-positive cells from E11.5 and E15.5 represent two distinct populations of mesenchymal progenitors.
Fgf10-positive cells labeled at E11.5 give rise to PBSMCs, VSMCs and lipofibroblasts at E18.5. *Fgf10*-positive cells labeled at E15.5 give rise to lipofibroblasts at E18.5.

Table 8. The differentiation potential of *Fgf10*-positive progenitor cells becomes progressively restricted during embryonic lung development.
Comparison between the lineage commitment of *Fgf10*-positive cells when labeled at E11.5 and E15.5. Whereas both populations give rise to lipofibroblasts at E18.5, cells from E11.5 - but not E15.5 - give rise to PBSMCs and VSMCs *in vivo. n = 3.*

	Time of labeling	E11.5	E15.5	P value
Analysis at E18.5	**Total RFP$^+$ cells counted per sample**	450 ± 10.12	499 ± 71.04	-
	% RFP$^+$ PBSMCs	5.68 ± 0.39%	0.26 ± 0.03%	0.0002
	% RFP$^+$ VSMCs	4.31 ± 0.23%	0.75 ± 0.34%	0.001
	% RFP$^+$ β-III Tub$^-$ cells around PBSMCs	10.17 ± 0.88%	10.33 ± 1.65%	0.9346
	% RFP$^+$ β-III Tub$^-$ cells around VSMCs	3.92 ± 0.72%	4.99 ± 0.32%	0.2436
	% RFP$^+$ Lipofibroblasts	29.96 ± 5.17%	39.98 ± 8.28%	0.3629
	% other RFP$^+$ cells	45.97 ± 4.2%	43.69 ± 8.32%	0.8192

The role of *Fgf10* in the formation of adipogenic lineages has already been demonstrated. *Fgf10*-null neonates suffer from impaired development of the white adipose tissue (Yamasaki et al., 1999; Sakaue et al., 2002). *In vitro*, *Fgf10* is involved in the differentiation of pre-adipocytes to adipocytes. This is demonstrated by the ability of FGF10-blocking antibodies to inhibit insulin-mediated adipogenesis in NIH3T3-L1 cells (Sakaue et al., 2002). Here, we show, for the first time, that *Fgf10*-expressing cells are precursor cells for lipofibroblasts in the embryonic and postnatal lung. We also generated the *Fgf10-LacZ/iCre* hypomorphic allele (equivalent to *Fgf10-LacZ/-* allele) and

the phenotype of the pups and lungs recapitulated what our group has previously published (Ramasamy et al., 2007). Moreover, we also show that hypomorphic *Fgf10* newborns suffer from decreased lipofibroblast formation (Fig. 23). Interestingly, lungs from these pups reveal severe downregulation of early, intermediate and late markers of adipogenesis (*Zfp423, Cebpb, Pparg, Adrp* and *Lipase*), suggesting that *Fgf10* dosage is critical not only for the formation of lipofibroblasts during late lung development but also for the maintenance of early lipofibroblast progenitors. Thus, we provide direct evidence for the involvement of *Fgf10* in the formation of lipofibroblasts in the developing lung. We propose a model in which FGF10 is involved in amplifying committed pre-adipocytes ($ZFP423^{+}$) and potentiating the differentiation process into mature adipocytes (Fig. 26).

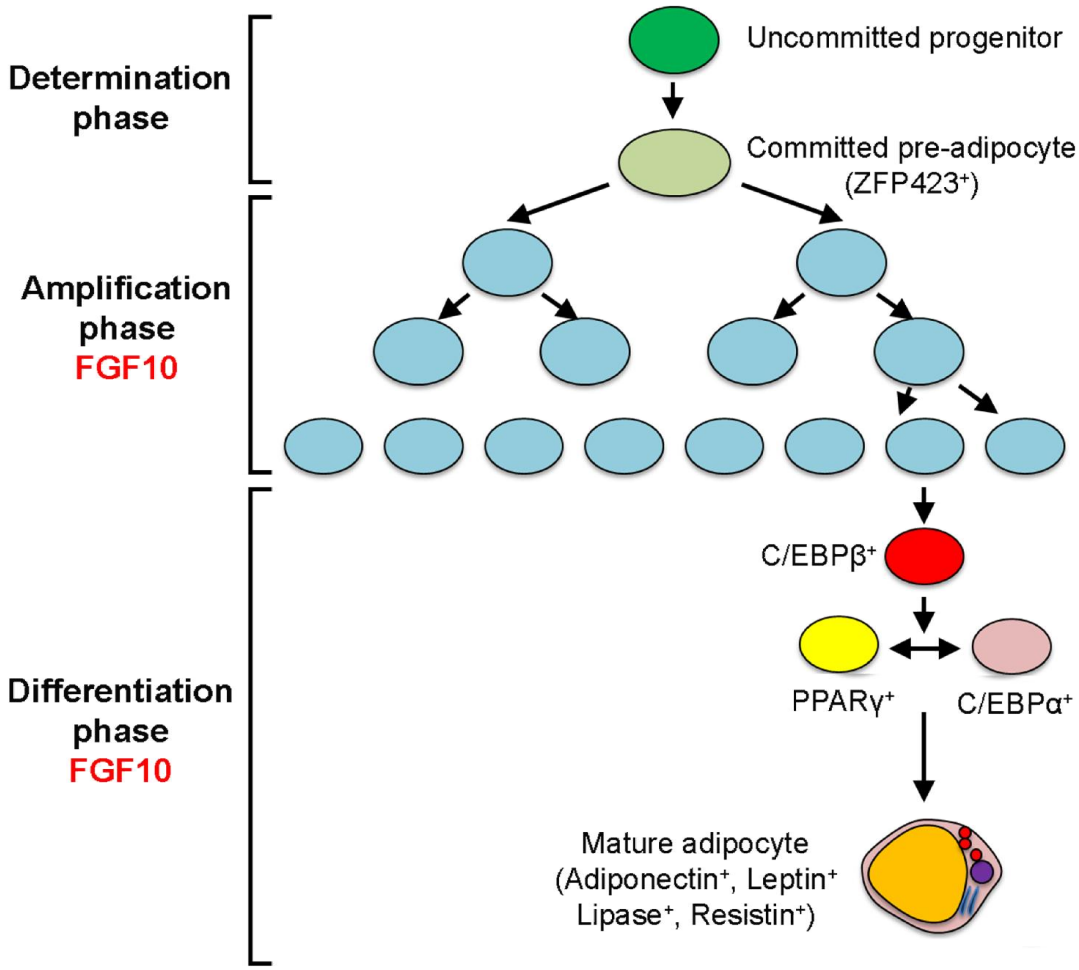

Figure 26. Model for the involvement of FGF10 in adipogenesis.
ZFP423 is a transcription factor that identifies committed pre-adipocytes (Gupta et al., 2012). During the differentiation of pre-adipocytes, C/EBPβ is upregulated followed by C/EBPα and PPARγ upregulation [Reviewed in (Rosen, 2005)]. The proposed model shows that FGF10 is involved in the amplification of committed pre-adipocytes (ZFP423$^+$) and enhancing the differentiation from C/EBPβ$^+$ cells, to C/EBPα$^+$ and PPARγ$^+$ cells and finally to mature adipocytes. ZFP423: Zinc finger protein 423.

FGF10 has so far been believed to signal only to the epithelium expressing *Fgfr2b*. Here, we demonstrate that exogenous FGF10 acts on embryonic human and rodent fibroblasts to induce the lipofibroblast phenotype (Fig. 24). Thus, we demonstrate that paracrine FGF10 signaling triggers the formation

of lipofibroblasts *in vitro*. RT-PCR on mesenchymal cells showed that FGFR1b seems to mediate the action of exogenous FGF10 on these cells.

In order to gain more insight into the expansion pattern of *Fgf10*-positive cells during embryonic development, cells were labeled at E11.5 or E18.5 and lineage-labeled cells were analyzed by FACS at E18.5. Whereas *Fgf10*-positive cells labeled at E11.5 accounted for 0.5% of the total lung at E18.5, those labeled at E15.5 represented 1.5% of the total E18.5 lung (Fig. 20). This indicates that during embryonic lung development, not all *Fgf10*-expressing cells derive from *Fgf10*-positive mother cells; rather, the *Fgf10*-expressing domain expands by *de novo* induction of *Fgf10*-expression (Fig. 27). Moreover, flow cytometry analysis revealed that a minor subpopulation of early *Fgf10*-positive progenitors (labeled at E11.5) acquires *Pdgfrα* at later developmental stages. On the other hand, a subpopulation of late *Fgf10*-positive progenitors (labeled at E15.5) acquires *Pdgfrα* as well as pan-epithelial cell marker *EpCam*. Interestingly, both populations express low levels of *Sca-1* (Sca-1^{low}) at E18.5.

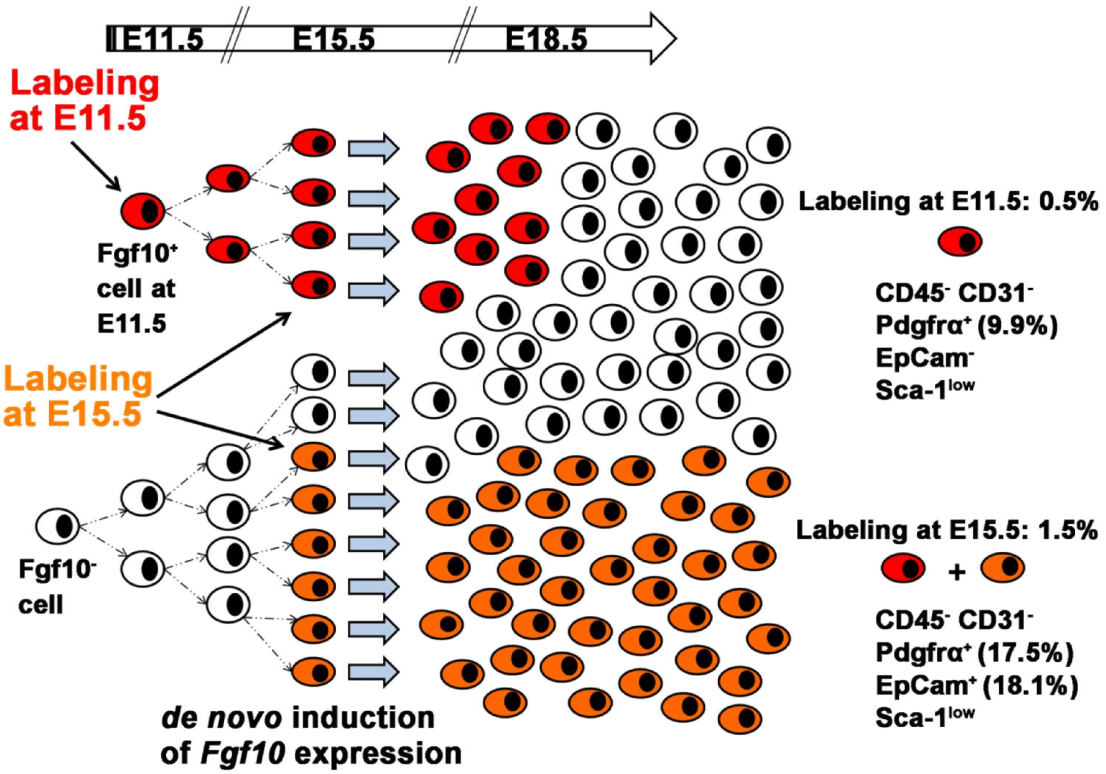

Figure 27. Model for the expansion of *Fgf10*-expressing cells during embryonic lung development.
Cells labeled at E11.5 account for ~0.5% of the total lung at E18.5. At E15.5, *Fgf10* expression is induced in fibroblasts that do not derive from the original *Fgf10*-expressing cell population. When tamoxifen is injected at E15.5, *Fgf10*-expressing cells, derived from the E11.5 *Fgf10*-positive ancestors, and *Fgf10*-expressing cells that start expressing *Fgf10* at E15.5 are labeled. The combination of both lineages accounts for ~1.5% of the total lung at E18.5.

5.3. The role of *Fgf10*-positive progenitor cells in lung homeostasis and repair during postnatal life

5.3.1. *Fgf10*-positive cells during the alveolar stage of lung development

Alveolar myofibroblasts and lipofibroblasts are two cell lineages that are highly abundant during postnatal alveolarization. These cell types play important roles in the formation of functional alveoli in newborns. Alveolar myofibroblasts (not to be confused with activated myofibroblasts that prevail in

lung fibrosis) are contractile *αSma*-expressing fibroblasts that reside at the tips of secondary septa. These cells produce an elastin precursor, tropoelastin. Elastin is required for initiation and progression of secondary septa formation (Vaccaro and Brody, 1978; Noguchi et al., 1989; Yamada et al., 2005). These cells transiently populate the lung during alveologenesis and are believed to undergo programmed cell death (or apoptosis) leading to their disappearance from the adult lung (Bruce et al., 1999). Fibroblasts expressing *Pdgfrα* (receptor for PDGF-A) are believed to be progenitors for alveolar myofibroblasts. *Pdgfa*-null newborns lack alveolar myofibroblasts and suffer from failure in alveolarization (Boström et al., 1996; Lindahl et al., 1997).

On the other hand, lipofibroblasts are lipid-containing interstitial fibroblasts that are also involved in alveolar maturation. These cells supply AEC II with triglycerides that are required for the synthesis of pulmonary surfactant. AEC II secrete PTHrP that is critical for the induction and maintenance of the lipofibroblast phenotype through the PPARγ pathway. Disruption of PTHrP signaling leads to lipofibroblast-to-myofibroblast transdifferentiation and defective alveologenesis (Torday et al., 2003; Rubin et al., 2004; Torday and Rehan, 2007; Rehan and Torday, 2012). Although the number of lipofibroblasts peaks around two weeks of age, a significant number of these cells persists in the adult lung (Rehan et al., 2006).

In this study, the contribution of *Fgf10*-positive progenitor cells to these two lineages was addressed. When labeled during the alveolar stage of lung development, most *Fgf10*-expressing cells gave rise to lipofibroblasts whereas a minor population gave rise to myofibroblasts (Fig. 19). These myofibroblasts did not localize at the tips of secondary septa where alveolar myofibroblasts are known to prevail. Yet, it has been shown that FGFR2b ligands are required for the differentiation of alveolar myofibroblast progenitors during homeostasis (Perl and Gale, 2009) as well as regeneration after pneumonectomy (Chen et al., 2012). Moreover, Ramasamy et al. have shown that *Fgf10*-hypomorphic lungs have impaired septation/alveolarization postnatally (Ramasamy et al., 2007). Thus, we conclude that although a minor population of *Fgf10*-expressing cells gives rise to *αSma*-positive fibroblasts,

Fgf10-positive cells are not progenitors for alveolar myofibroblasts *in vivo*. However, paracrine signaling between *Fgf10*-positive cells and *Pdgfrα*-positive progenitors is likely necessary for the formation of the alveolar myofibroblast lineage during the alveolar stage of lung development. Our data suggest that alveolar myofibroblasts are unlikely to derive from *Fgf10*-expressing lipofibroblasts during the first two weeks after birth.

5.3.2. *Fgf10*-positive cells during homeostasis and disease

Fgf10-positive cells were examined during lung homeostasis in the adult mouse. Despite the low efficiency of the $Fgf10^{iCre}$ line in labeling *Fgf10*-expressing cells postnatally, FACS analysis of disaggregated adult lungs revealed that these cells constitute ~0.1% of the whole lung. A subpopulation of *Fgf10*-expressing cells (10.5% of total *Fgf10*-expressing cells) exhibits the molecular signature ($CD45^-$ $CD31^-$ $Sca\text{-}1^+$) of resident MSCs that were previously described by McQualter et al. (McQualter et al., 2009) (Fig. 20). In the latter study, the authors reported that the $CD45^-$ $CD31^-$ $Sca\text{-}1^+$ fraction of the adult lung represents a mesenchymal population of resident progenitor cells. These cells have shown to be precursors for myogenic and adipogenic lineages and are also critical for the growth of epithelial progenitors *in vitro*, likely via the FGF10/FGFR2b signaling pathway (McQualter et al., 2009, 2010). In their co-culture system, McQualter et al. have demonstrated that mesenchymal progenitors relocate around epithelial colonies giving rise to SMCs, thus recapitulating the behavior of *Fgf10*-expressing cells during embryonic lung development (Mailleux et al., 2005). Thus, our data support the findings of McQualter et al. and provide direct evidence that *Fgf10* expression identifies a subset of resident MSCs postnatally.

In order to study the role of *Fgf10*-positive progenitor cells in lung repair after injury, $Fgf10^{iCre/+}$; $Tomato^{flox/+}$ adult mice were fed tamoxifen-containing pellets before bleomycin was delivered intratracheally. After fourteen days, mice were anesthetized and lung function was measured. Lung function parameters on anesthetized animals and histology of the corresponding lungs confirmed the presence of lung fibrosis in bleomycin-treated mice compared to saline-treated controls. Interestingly, a three-fold increase in the number of

lineage-labeled cells was observed in bleomycin-challenged lungs (Fig. 21). Whereas the *Fgf10*-expressing pool did not contribute to *αSma*-positive fibroblasts under homeostatic conditions, most of lineage-labeled cells expressed *αSma* in bleomycin-treated lungs (Fig. 22).

Activated myofibroblasts are thought to arise from resident fibroblasts, circulating fibrocytes and AEC II by EMT during lung fibrosis. Recently, resident fibroblasts have shown to be the main repertoire for these cells. Rock et al. have demonstrated that activated myofibroblasts arise from multiple fibroblastic populations and that pericyte-like cells were abundant in fibrotic lesions but failed to express high levels of *αSma* (Rock et al., 2011). Hoyles et al. have demonstrated that knocking down high affinity type II TGF-β receptors in resident fibroblasts prevents their differentiation to activated myofibroblasts, resulting in attenuation of lung fibrosis (Hoyles et al., 2011). In this study, we show that *Fgf10*-positive progenitor cells are a source of activated myofibroblasts in bleomycin-induced pulmonary fibrosis. Gene expression analysis on bleomycin-treated lungs showed an upregulation of myofibroblast markers that also correlated with a downregulation of lipofibroblast markers compared to saline-treated lungs (Fig. 22). This suggests that these cells undergo lipofibroblast-to-myofibroblast transdifferentiation. Gene expression analysis on biopsies from end-stage IPF patients also showed a downregulation in lipofibroblast markers compared to donors, suggesting that this transdifferentiation is likely to occur during lung fibrosis in humans.

Lipofibroblast-to-myofibroblast transdifferentiation has already been demonstrated in the hyperoxia model of Bronchopulmonary dysplasia (BPD). Rehan and Torday have shown that fetal rat lung fibroblasts lose their adipogenic phenotype and transdifferentiate to myofibroblasts when exposed to hyperoxia *in vitro* (Rehan and Torday, 2003). It is also believed that injury to AEC II disrupts PTHrP signaling and causes neighboring fibroblasts to default to the myofibroblast phenotype (Torday and Rehan, 2007). TGF-β has also shown to induce subcutaneous adipocyte-to-myofibroblast differentiaton in skin fibrosis. Wnt signaling, particularly via Wnt3a ligand, is suggested to

mediate TGF-β-induced mesenchymal fibrogenic responses and loss of adipose tissue in skin fibrosis (Akhmetshina et al., 2012; Wei et al., 2012). Similarly, there is evidence suggesting that functional Wnt signaling is increased in injured epithelial cells as well as fibrotic foci in IPF (Chilosi et al., 2003; Königshoff et al., 2008). On the other hand, the ability of PPARγ agonists (eg. Rosiglitazone) to attenuate TGF-β-mediated fibrosis has been demonstrated *in vitro* (Burgess et al., 2005) and *in vivo* (Genovese et al., 2005; Wu et al., 2009; Jin et al., 2012).

Our research group has previously shown that *Fgf10* overexpression in AEC II is preventive and therapeutic against bleomycin-induced pulmonary fibrosis in mice. Analysis of the Bronchoalveolar lavage fluid (BALF) from those mice revealed a decrease in the levels of endogenous bioactive TGF-β1. Tunel assays showed increased survival of AEC II despite bleomycin administration (Gupte et al., 2009).

Thus, we conclude that under homeostatic conditions, *Fgf10*-expressing cells give rise to lipofibroblasts in the lung. During pulmonary fibrosis, these cells transdifferentiate to activated myofibroblasts. Treatment with FGF10 could help reverse the transdifferentiation and restore the lipofibroblast phenotype.

5.4. Future perspectives and stem cell therapy in regenerative medicine

The use of recombinant human FGFs, produced in *Escherichia coli (E. coli)*, to treat human diseases has already been implemented more than a decade ago. Palifermin (trade name Kepivance®, Amgen Inc., CA, USA) contains a truncated form of human Keratinocyte growth factor (KGF or FGF7) and is used to treat and prevent oral mucositis (mouth sores) and dysphagia (difficulty in swallowing) in hematologic cancer patients undergoing severe chemotherapy and radiation therapy prior to bone marrow transplantation (FDA approval in 2004). Palifermin is introduced intravenously and helps to regenerate the mucosal barrier. Palifermin has also shown to induce alveolar maintenance programs in elastase-induced emphysema in mice (Yildirim et al., 2010).

On the other hand, Repifermin contains a truncated form of KGF2 (or FGF10) and was developed by Human Genome Sciences (Rockville, MD, USA) and GlaxoSmithKline (London, UK) to treat wounds, oral and intestinal mucositis and inflammatory bowel diseases (Wheeler, 2001). Repifermin has shown to accelerate healing of skin wounds (Soler et al., 1999) and colitis (Meerveld et al., 2003) in animals as well as healing of chronic venous ulcers in humans (Robson et al., 2001). However, it did not show to be effective in treating active ulcerative colitis in clinical trials (Sandborn et al., 2003) and thus, the development of this drug was ceased in 2004. Yet, attempts to enhance its unfolding temperature (Derrick et al., 2007) and ensure sustained release (Huang and Berkland, 2009) have shown to significantly increase the bioavailability and efficiency of Repifermin. This suggests that this drug could be revived and possibly tested in lung regeneration after injury.

To date, Pirfenidone (InterMune Inc., Brisbane, CA, USA) is the only available drug that is prescribed for treating IPF patients. Although it was implemented in clinical trials fourteen years ago, the mechanism of action for Pirfenidone is still unknown. Unfortunately, clinical trials have shown that the effects of Pirfenidone on IPF patients are subtle in terms of improving quality of life, symptoms and survival [Reviewed in (Jenkins, 2013; Raghu and Thickett, 2013)].

On the other hand, the use of stem cells in regenerative medicine seems to be promising. Isolation of MSCs was first reported in 1976 and these cells were described as an adherent, clonogenic, non-phagocytic and fibroblastic-like population of bone marrow cells (Friedenstein et al., 1976). MSCs not only give rise to multiple mesenchymal and non-mesenchymal lineages, but also have immunomodulatory properties which makes them a good candidate for regenerative medicine as their allogeneic transplantation bypasses host immune rejection [Reviewed in (Patel et al., 2013)]. Bone-marrow-derived as well as placental MSCs are currently being tested and considered in clinical trials for treating patients with PAH, ALI, IPF, COPD/emphysema and asthma [www.clinicaltrials.gov and reviewed in (Trounson et al., 2011)].

Interestingly, non-bone marrow-derived (or resident) MSCs were reported in almost all postnatal organs and tissues (Da Silva Meirelles et al., 2006). It is believed that these cells are involved in normal as well as aberrant repair following injury. Failure of resident MSCs to promote tissue repair in pathological conditions is likely due to the fact that their microenvironmental niche is compromised (Scadden, 2006; Beers and Morrisey, 2011). These microenvironments influence MSC properties like lineage commitment, anti-inflammatory properties, T-cell activation and differentiation to myofibroblasts [Reviewed in (Foronjy and Majka, 2012)].

The role of resident lung MSCs in lung fibrosis was demonstrated by Jun et al. The authors have shown that these cells are depleted in bleomycin-induced pulmonary fibrosis and administration of *ex vivo*-cultured resident lung MSCs attenuates lung fibrosis. These cells reduce the number of inflammatory cells in the BALF and inhibit T-cell proliferation (Jun et al., 2011).

The reported work establishes *Fgf10* as a marker for a subset of resident MSCs in the lung. Our finding that recombinant FGF10 acts on mesenchymal cells to induce/maintain the lipofibroblast phenotype suggests that pre-treating isolated MSCs with FGF10 prior to their administration could be of great use in treating advanced-stage IPF patients.

6. Summary

FGF10 belongs to a family of evolutionary-conserved peptides that are involved in embryonic organogenesis as well as postnatal homeostasis. During embryonic lung development, *Fgf10*-expressing cells define the domain for directional growth of epithelial buds and thus orchestrate branching morphogenesis. Disruption of FGF10 signaling not only leads to failure in branching but also to malformation of various mesenchymal lineages.

Here, we generated a knock-in mouse line that allows lineage tracing of *Fgf10*-expressing cells during development and postnatally in a time-controlled manner. Our **validation** studies show that:

- The *Fgf10*^{iCre} knock-in line faithfully reports *Fgf10* expression in many organs and tissues during embryonic development
- The insertion of Cre-ERT2 cassette in exon 1 led to the deletion of intronic sequences that are critical for the maintenance of *Fgf10* expression over time. In spite of that, prolonged tamoxifen exposure enables the labeling of a considerable number of *Fgf10*-expressing cells in the postnatal lung.

Our findings from the **lineage tracing** studies demonstrate that:

- *Fgf10*-expressing cells are potent mesenchymal progenitors *in vivo*
- *Fgf10*-expressing cells from early lung development give rise to parabronchial and vascular smooth muscle cells as well as lipofibroblasts during late development
- *Fgf10*-expressing cells from late lung development and postnatally are precursors for lipofibroblasts rather than alveolar myofibroblasts

- During adult life, these cells represent a subpopulation of resident MSCs that, upon bleomycin injury, give rise to activated myofibroblasts
- Recombinant FGF10 is capable of acting on mesenchymal cells to induce the lipofibroblast phenotype
- Our findings suggest that these cells can be a potential target for treating lung fibrosis in humans.

Thus, we propose a model in which *Fgf10*-expressing cells represent a population of resident mesenchymal stem cells that reside in the adult lung. Under homeostatic conditions, these cells give rise to lipofibroblasts. Injury to AEC II leads to a decrease in PTHrP/PPARγ signaling and increase in TGF-β and Wnt signaling, leading to their transdifferentiation to activated myofibroblasts (Fig. 28).

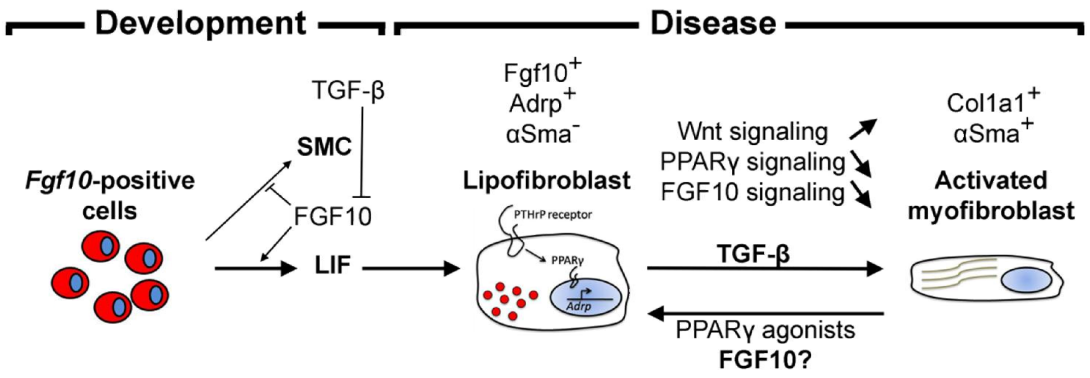

Figure 28. Model for the role of FGF10 in identifying early lipofibroblast progenitors and controlling their fate during development and disease.
During embryonic development, *Fgf10*-positive cells give rise to lipofibroblasts and to a less extent smooth muscle cells (El Agha et al., *Fgf10*-positive cells represent a progenitor cell population during lung development and postnatally; in revision). Gain of function of FGF10 signaling in the mesenchyme inhibits smooth muscle formation (De Langhe et al., 2006) whereas loss of function of *Fgf10* leads to decreased lipofibroblast formation (Fig. 23). TGF-β acts as a negative regulator of *Fgf10* expression [Reviewed in (Cardoso and Lu, 2006)]. During disease, *Fgf10*-expressing lipofibroblasts (αSma^- $Adrp^+$) transdifferentiate to activated myofibroblasts ($Col1a1^+$ αSma^+) likely due to increased TGF-β and Wnt signaling and decreased PTHrP/PPARγ and FGF10 signaling. The proposed therapeutic approach attempts to push activated myofibroblasts back to the lipofibroblast phenotype by PPARγ agonists and possibly FGF10. LIF: Lipofibroblasts.

7. Zusammenfassung

FGF10 gehört zu einer Peptidfamilie, die im Laufe der Evolution stark konserviert wurde. Diese Peptide sind sowohl an der embryonalen Organogenese als auch an der postnatalen Homöostase beteiligt. *Fgf10*-exprimierende Zellen bestimmen das zielgerichtete Wachstum der epithelialen Lungenknospen und definieren somit die morphogenetische Entwicklung der Lunge in der Embryonalperiode. Eine Unterbrechung des FGF10 Signalweges führt nicht nur zur fehlerhaften Entwicklung der Verästelung des Bronchialbaumes, sondern auch zur Malformation verschiedener anderer mesenchymalen Zelllinien.

In der vorliegenden Arbeit wurde eine knock-in Mauslinie generiert, mit deren Hilfe *Fgf10*-exprimierende Zellen sowohl während der prä- als auch während der postnatalen Entwicklung zu einem beliebigen Zeitpunkt nachverfolgt werden können. Die Experimente zur **Validierung** ergaben folgende Resultate:

- Die *Fgf10*^{iCre} knock-in Mauslinie zeigt die *Fgf10* Expression während der Embryonalentwicklung in zahlreichen Organen und Geweben zuverlässig an

- Die Insertion der Cre-ERT2 Kassette in das Exon 1 von *Fgf10* führte zur Deletion derjenigen Intronsequenzen, welche für die Aufrechterhaltung der *Fgf10* Expression von Bedeutung sind. Dennoch ist es möglich, mittels Zugabe von Tamoxifen über einen längeren Zeitraum hinweg eine erhebliche Anzahl von *Fgf10*-exprimierenden Zellen in der postnatalen Lunge zu markieren.

Die Untersuchungen zum **Lineage Tracing** zeigten auf:

- *Fgf10*-exprimierende Zellen sind *in vivo* potente mesenchymale Progenitorzellen

- Aus *Fgf10*-exprimierenden Zellen der frühen Phase der Lungenentwicklung entstehen im Laufe der späten Lungenentwicklung parabronchiale und vaskuläre glatte Muskelzellen sowie Lipofibroblasten

- Postnatal und während der Spätphase der Lungenentwicklung fungieren *Fgf10*-exprimierende Zellen als Progenitorzellen für Lipofibroblasten. Ihre Transdifferenzierung zu Alveolar-Myofibroblasten wurde nicht beobachtet

- In der adulten Phase stellen *Fgf10*-exprimierende Zellen eine Unterpopulation residenter mesenchymaler Stammzellen (MSC) dar, welche sich bei Schädigung durch Bleomycin zu aktivierten Myofibroblasten entwickeln

- Rekombinantes FGF10 ist in der Lage, in mesenchymalen Zellen einen Phänotypus der Lipofibroblasten zu induzieren

- Die erzielten Ergebnisse deuten darauf hin, dass *Fgf10*-exprimierende Zellen einen potentiellen therapeutischen Ansatz für die Behandlung der Fibrose beim Menschen darstellen können.

Daher wird ein Modell vorgeschlagen, bei dem *Fgf10*-exprimierende Zellen in der adulten Lunge eine Zellpopulation von residenten mesenchymalen Stammzellen repräsentieren. Unter homöostatischen Bedingungen entwickeln sich aus dieser Zellpopulation Lipofibroblasten. Eine Schädigung von Typ II Alveolarzellen führt zur Verminderung des PTHrP/PPARγ- und einer Zunahme der TGF-ß und Wnt Signalwege, wodurch sie zu aktivierten Myofibroblasten transdifferenzieren (Abb. 28).

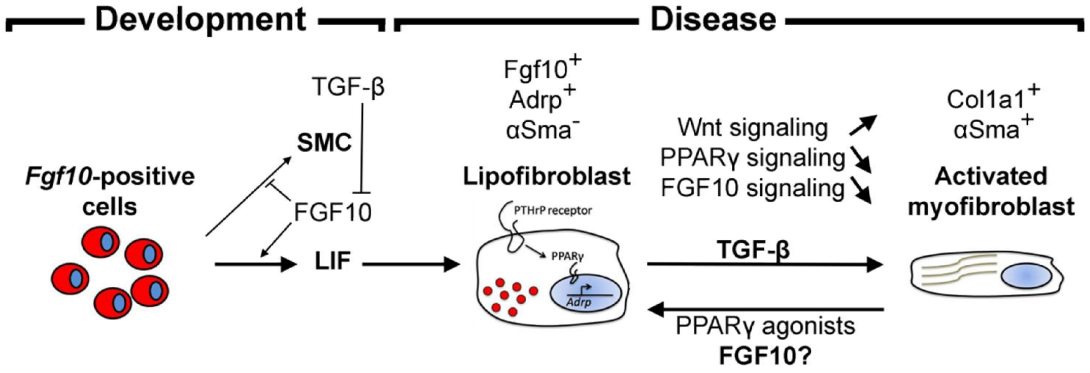

Abbildung 28. Bedeutung von FGF10 zur Identifizierung früher Lipofibroblasten-Progenitorzellen und dessen Einfluss auf physiologische und krankhafte Prozesse.

Aus *Fgf10*-positiven Zellen entstehen im Laufe der embryonalen Entwicklung Lipofibroblasten und - in geringem Umfang - glatte Muskelzellen (El Agha et al., *Fgf10*-positive cells represent a progenitor cell population during lung development and postnatally; in Überarbeitung). Eine Aktivierung der FGF10 Signalwege (Gain-of-function) im Mesenchym inhibiert die Entwicklung glatter Muskelzellen (De Langhe et al., 2006), während ein Verlust von *Fgf10* zu einer reduzierten Entwicklung von Lipofibroblasten führt (Abb. 23). TGF-ß fungiert als negativer Regulator der *Fgf10* Expression [Reviewed in (Cardoso and Lu, 2006)]. In krankhaften Prozessen transdifferenzieren *Fgf10*-exprimierende Lipofibroblasten (αSma^{-} $Adrp^{+}$) zu aktivierten Myofibroblasten ($Col1a1^{+}$ αSma^{+}). Es wird vermutet, dass dies einerseits auf eine zunehmende Aktivierung der TGF-ß und Wnt Signalwege zurückzuführen ist und andererseits auf eine Verminderung der PTHrP/PPARγ und FGF10 Signalwege. Die Rückbildung von aktivierten Myofibroblasten zu Lipofibroblast-phänotypischen Zellen mittels Anwendung von PPARγ Agonisten und möglicherweise FGF10 wäre ein potentieller therapeutischer Ansatz. LIF: Lipofibroblasten.

8. References

Abler, L.L., Mansour, S.L., Sun, X., 2009. Conditional gene inactivation reveals roles for Fgf10 and Fgfr2 in establishing a normal pattern of epithelial branching in the mouse lung. Dev Dyn 238, 1999–2013.

Adamson, I.Y., Bowden, D.H., 1974. The type 2 cell as progenitor of alveolar epithelial regeneration. A cytodynamic study in mice after exposure to oxygen. Lab Invest 30, 35–42.

Affolter, M., Bellusci, S., Itoh, N., Shilo, B., Thiery, J.P., Werb, Z., 2003. Tube or not tube: remodeling epithelial tissues by branching morphogenesis. Dev Cell 4, 11–18.

Akhmetshina, A., Palumbo, K., Dees, C., Bergmann, C., Venalis, P., Zerr, P., Horn, A., Kireva, T., Beyer, C., Zwerina, J., Schneider, H., Sadowski, A., Riener, M.-O., MacDougald, O. a, Distler, O., Schett, G., Distler, J.H.W., 2012. Activation of canonical Wnt signalling is required for TGF-β-mediated fibrosis. Nature communications 3, 735.

Al Alam, D., Green, M., Tabatabai Irani, R., Parsa, S., Danopoulos, S., Sala, F.G., Branch, J., El Agha, E., Tiozzo, C., Voswinckel, R., Jesudason, E.C., Warburton, D., Bellusci, S., 2011. Contrasting expression of canonical Wnt signaling reporters TOPGAL, BATGAL and Axin2(LacZ) during murine lung development and repair. PLoS One 6, e23139.

Alvarez, Y., Alonso, M.T., Vendrell, V., Zelarayan, L.C., Chamero, P., Theil, T., Bosl, M.R., Kato, S., Maconochie, M., Riethmacher, D., Schimmang, T., 2003. Requirements for FGF3 and FGF10 during inner ear formation. Development 130, 6329–6338.

Armelin, H.A., 1973. Pituitary extracts and steroid hormones in the control of 3T3 cell growth. Proc Natl Acad Sci U S A 70, 2702–2706.

Beenken, A., Mohammadi, M., 2009. The FGF family: biology, pathophysiology and therapy. Nat Rev Drug Discov 8, 235–253.

Beers, M.F., Morrisey, E.E., 2011. The three R's of lung health and disease: repair, remodeling, and regeneration. The Journal of clinical investigation 121, 2065–73.

Bellusci, S., Furuta, Y., Rush, M.G., Henderson, R., Winnier, G., Hogan, B.L., 1997. Involvement of Sonic hedgehog (Shh) in mouse embryonic lung growth and morphogenesis. Development 124, 53–63.

Bellusci, S., Grindley, J., Emoto, H., Itoh, N., Hogan, B.L., 1997. Fibroblast growth factor 10 (FGF10) and branching morphogenesis in the embryonic mouse lung. Development 124, 4867–4878.

Berg, T., Rountree, C.B., Lee, L., Estrada, J., Sala, F.G., Choe, A., Veltmaat, J.M., De Langhe, S., Lee, R., Tsukamoto, H., Crooks, G.M., Bellusci, S., Wang, K.S., 2007. Fibroblast growth factor 10 is critical for liver growth during embryogenesis and controls hepatoblast survival via beta-catenin activation. Hepatology 46, 1187–1197.

Bhatt, A.J., Amin, S.B., Chess, P.R., Watkins, R.H., Maniscalco, W.M., 2000. Expression of vascular endothelial growth factor and Flk-1 in developing and glucocorticoid-treated mouse lung. Pediatr Res 47, 606–613.

Bhushan, A., Itoh, N., Kato, S., Thiery, J.P., Czernichow, P., Bellusci, S., Scharfmann, R., 2001. Fgf10 is essential for maintaining the proliferative capacity of epithelial progenitor cells during early pancreatic organogenesis. Development 128, 5109–5117.

Borthwick, D.W., Shahbazian, M., Krantz, Q.T., Dorin, J.R., Randell, S.H., 2001. Evidence for stem-cell niches in the tracheal epithelium. Am J Respir Cell Mol Biol 24, 662–670.

Boström, H., Willetts, K., Pekny, M., Levéen, P., Lindahl, P., Hedstrand, H., Pekna, M., Hellström, M., Gebre-Medhin, S., Schalling, M., Nilsson, M.,

Kurland, S., Törnell, J., Heath, J.K., Betsholtz, C., 1996. PDGF-A signaling is a critical event in lung alveolar myofibroblast development and alveogenesis. Cell 85, 863–73.

Bruce, M.C., Honaker, C.E., Cross, R.J., 1999. Lung fibroblasts undergo apoptosis following alveolarization. American journal of respiratory cell and molecular biology 20, 228–36.

Burgess, H.A., Daugherty, L.E., Thatcher, T.H., Lakatos, H.F., Ray, D.M., Redonnet, M., Phipps, R.P., Sime, P.J., 2005. PPARgamma agonists inhibit TGF-beta induced pulmonary myofibroblast differentiation and collagen production: implications for therapy of lung fibrosis. American journal of physiology. Lung cellular and molecular physiology 288, L1146–53.

Burns, R.C., Fairbanks, T.J., Sala, F., De Langhe, S., Mailleux, A., Thiery, J.P., Dickson, C., Itoh, N., Warburton, D., Anderson, K.D., Bellusci, S., 2004. Requirement for fibroblast growth factor 10 or fibroblast growth factor receptor 2-IIIb signaling for cecal development in mouse. Dev Biol 265, 61–74.

Burri, P.H., 2006. Structural aspects of postnatal lung development - alveolar formation and growth. Biol Neonate 89, 313–322.

Cardoso, W. V, 2000. Lung morphogenesis revisited: old facts, current ideas. Dev Dyn 219, 121–130.

Cardoso, W. V, Lu, J., 2006. Regulation of early lung morphogenesis: questions, facts and controversies. Development 133, 1611–1624.

Casey, J.P., Magalhaes, T., Conroy, J.M., Regan, R., Shah, N., et al., 2012. A novel approach of homozygous haplotype sharing identifies candidate genes in autism spectrum disorder. Human genetics 131, 565–79.

Cebra-Thomas, J.A., Bromer, J., Gardner, R., Lam, G.K., Sheipe, H., Gilbert, S.F., 2003. T-box gene products are required for mesenchymal induction

of epithelial branching in the embryonic mouse lung. Dev Dyn 226, 82–90.

Chapman, H.A., Li, X., Alexander, J.P., Brumwell, A., Lorizio, W., Tan, K., Sonnenberg, A., Wei, Y., Vu, T.H., 2011. Integrin alpha6beta4 identifies an adult distal lung epithelial population with regenerative potential in mice. J Clin Invest 121, 2855–2862.

Chen, L., Acciani, T., Le Cras, T., Lutzko, C., Perl, A.-K.T., 2012. Dynamic regulation of platelet-derived growth factor receptor α expression in alveolar fibroblasts during realveolarization. American journal of respiratory cell and molecular biology 47, 517–27.

Chilosi, M., Poletti, V., Zamò, A., Lestani, M., Montagna, L., Piccoli, P., Pedron, S., Bertaso, M., Scarpa, A., Murer, B., Cancellieri, A., Maestro, R., Semenzato, G., Doglioni, C., 2003. Aberrant Wnt/beta-catenin pathway activation in idiopathic pulmonary fibrosis. The American journal of pathology 162, 1495–502.

Clark, J.C., Tichelaar, J.W., Wert, S.E., Itoh, N., Perl, A.K., Stahlman, M.T., Whitsett, J.A., 2001. FGF-10 disrupts lung morphogenesis and causes pulmonary adenomas in vivo. Am J Physiol Lung Cell Mol Physiol 280, L705–15.

Colvin, J.S., White, A.C., Pratt, S.J., Ornitz, D.M., 2001. Lung hypoplasia and neonatal death in Fgf9-null mice identify this gene as an essential regulator of lung mesenchyme. Development 128, 2095–2106.

Crapo, J.D., Barry, B.E., Gehr, P., Bachofen, M., Weibel, E.R., 1982. Cell number and cell characteristics of the normal human lung. Am Rev Respir Dis 126, 332–337.

Da Silva Meirelles, L., Chagastelles, P.C., Nardi, N.B., 2006. Mesenchymal stem cells reside in virtually all post-natal organs and tissues. Journal of cell science 119, 2204–13.

De Langhe, S.P., Carraro, G., Tefft, D., Li, C., Xu, X., Chai, Y., Minoo, P., Hajihosseini, M.K., Drouin, J., Kaartinen, V., Bellusci, S., 2008. Formation and differentiation of multiple mesenchymal lineages during lung development is regulated by beta-catenin signaling. PLoS One 3, e1516.

De Langhe, S.P., Carraro, G., Warburton, D., Hajihosseini, M.K., Bellusci, S., 2006. Levels of mesenchymal FGFR2 signaling modulate smooth muscle progenitor cell commitment in the lung. Dev Biol 299, 52–62.

De Moerlooze, L., Spencer-Dene, B., Revest, J.M., Hajihosseini, M., Rosewell, I., Dickson, C., 2000. An important role for the IIIb isoform of fibroblast growth factor receptor 2 (FGFR2) in mesenchymal-epithelial signalling during mouse organogenesis. Development 127, 483–492.

Del Moral, P.-M., De Langhe, S.P., Sala, F.G., Veltmaat, J.M., Tefft, D., Wang, K., Warburton, D., Bellusci, S., 2006. Differential role of FGF9 on epithelium and mesenchyme in mouse embryonic lung. Developmental biology 293, 77–89.

Del Moral, P.M., Sala, F.G., Tefft, D., Shi, W., Keshet, E., Bellusci, S., Warburton, D., 2006. VEGF-A signaling through Flk-1 is a critical facilitator of early embryonic lung epithelial to endothelial crosstalk and branching morphogenesis. Dev Biol 290, 177–188.

deMello, D.E., Sawyer, D., Galvin, N., Reid, L.M., 1997. Early fetal development of lung vasculature. Am J Respir Cell Mol Biol 16, 568–581.

Derrick, T., Grillo, A.O., Vitharana, S.N., Jones, L., Rexroad, J., Shah, A., Perkins, M., Spitznagel, T.M., Middaugh, C.R., 2007. Effect of polyanions on the structure and stability of repifermin (keratinocyte growth factor-2). Journal of pharmaceutical sciences 96, 761–76.

Ding, B.-S., Nolan, D.J., Guo, P., Babazadeh, A.O., Cao, Z., Rosenwaks, Z., Crystal, R.G., Simons, M., Sato, T.N., Worgall, S., Shido, K., Rabbany, S.Y., Rafii, S., 2011. Endothelial-derived angiocrine signals induce and sustain regenerative lung alveolarization. Cell 147, 539–53.

El Agha, E., Al Alam, D., Carraro, G., MacKenzie, B., Goth, K., De Langhe, S.P., Voswinckel, R., Hajihosseini, M.K., Rehan, V.K., Bellusci, S., 2012. Characterization of a novel fibroblast growth factor 10 (Fgf10) knock-in mouse line to target mesenchymal progenitors during embryonic development. PLoS One 7, e38452.

Entesarian, M., Dahlqvist, J., Shashi, V., Stanley, C.S., Falahat, B., Reardon, W., Dahl, N., 2007. FGF10 missense mutations in aplasia of lacrimal and salivary glands (ALSG). Eur J Hum Genet 15, 379–382.

Entesarian, M., Matsson, H., Klar, J., Bergendal, B., Olson, L., Arakaki, R., Hayashi, Y., Ohuchi, H., Falahat, B., Bolstad, A.I., Jonsson, R., Wahren-Herlenius, M., Dahl, N., 2005. Mutations in the gene encoding fibroblast growth factor 10 are associated with aplasia of lacrimal and salivary glands. Nat Genet 37, 125–127.

Evans, M.J., Cabral, L.J., Stephens, R.J., Freeman, G., 1975. Transformation of alveolar type 2 cells to type 1 cells following exposure to NO2. Exp Mol Pathol 22, 142–150.

Fairbanks, T.J., De Langhe, S., Sala, F.G., Warburton, D., Anderson, K.D., Bellusci, S., Burns, R.C., 2004. Fibroblast growth factor 10 (Fgf10) invalidation results in anorectal malformation in mice. J Pediatr Surg 39, 360–365.

Fairbanks, T.J., Kanard, R.C., De Langhe, S.P., Sala, F.G., Del Moral, P.M., Warburton, D., Anderson, K.D., Bellusci, S., Burns, R.C., 2004. A genetic mechanism for cecal atresia: the role of the Fgf10 signaling pathway. J Surg Res 120, 201–209.

Fairbanks, T.J., Kanard, R.C., Del Moral, P.M., Sala, F.G., De Langhe, S.P., Lopez, C.A., Veltmaat, J.M., Warburton, D., Anderson, K.D., Bellusci, S., Burns, R.C., 2005. Colonic atresia without mesenteric vascular occlusion. The role of the fibroblast growth factor 10 signaling pathway. J Pediatr Surg 40, 390–396.

Foronjy, R.F., Majka, S.M., 2012. The Potential for Resident Lung Mesenchymal Stem Cells to Promote Functional Tissue Regeneration: Understanding Microenvironmental Cues. Cells 1, 874–885.

Friedenstein, A.J., Gorskaja, J.F., Kulagina, N.N., 1976. Fibroblast precursors in normal and irradiated mouse hematopoietic organs. Experimental hematology 4, 267–74.

Garcia, O., Carraro, G., Navarro, S., Bertoncello, I., McQualter, J., Driscoll, B., Jesudason, E., Warburton, D., 2012. Cell-based therapies for lung disease. Br Med Bull 101, 147–161.

Gebb, S.A., Shannon, J.M., 2000. Tissue interactions mediate early events in pulmonary vasculogenesis. Dev Dyn 217, 159–169.

Genovese, T., Cuzzocrea, S., Di Paola, R., Mazzon, E., Mastruzzo, C., Catalano, P., Sortino, M., Crimi, N., Caputi, A.P., Thiemermann, C., Vancheri, C., 2005. Effect of rosiglitazone and 15-deoxy-Delta12,14-prostaglandin J2 on bleomycin-induced lung injury. The European respiratory journal : official journal of the European Society for Clinical Respiratory Physiology 25, 225–34.

Giangreco, A., Reynolds, S.D., Stripp, B.R., 2002. Terminal bronchioles harbor a unique airway stem cell population that localizes to the bronchoalveolar duct junction. Am J Pathol 161, 173–182.

Giangreco, A., Shen, H., Reynolds, S.D., Stripp, B.R., 2004. Molecular phenotype of airway side population cells. American journal of physiology. Lung cellular and molecular physiology 286, L624–30.

Goldfarb, M., Schoorlemmer, J., Williams, A., Diwakar, S., Wang, Q., Huang, X., Giza, J., Tchetchik, D., Kelley, K., Vega, A., Matthews, G., Rossi, P., Ornitz, D.M., D'Angelo, E., 2007. Fibroblast growth factor homologous factors control neuronal excitability through modulation of voltage-gated sodium channels. Neuron 55, 449–463.

Golzio, C., Havis, E., Daubas, P., Nuel, G., Babarit, C., Munnich, A., Vekemans, M., Zaffran, S., Lyonnet, S., Etchevers, H.C., 2012. ISL1 Directly Regulates FGF10 Transcription during Human Cardiac Outflow Formation. PLoS One 7, e30677.

Goodell, M.A., Brose, K., Paradis, G., Conner, A.S., Mulligan, R.C., 1996. Isolation and functional properties of murine hematopoietic stem cells that are replicating in vivo. J Exp Med 183, 1797–1806.

Gospodarowicz, D., 1975. Purification of a fibroblast growth factor from bovine pituitary. J Biol Chem 250, 2515–2520.

Gospodarowicz, D., Bialecki, H., Greenburg, G., 1978. Purification of the fibroblast growth factor activity from bovine brain. J Biol Chem 253, 3736–3743.

Greif, D.M., Kumar, M., Lighthouse, J.K., Hum, J., An, A., Ding, L., Red-Horse, K., Espinoza, F.H., Olson, L., Offermanns, S., Krasnow, M. a, 2012. Radial construction of an arterial wall. Developmental cell 23, 482–93.

Grunert, S., Jechlinger, M., Beug, H., 2003. Diverse cellular and molecular mechanisms contribute to epithelial plasticity and metastasis. Nat Rev Mol Cell Biol 4, 657–665.

Gupta, R.K., Mepani, R.J., Kleiner, S., Lo, J.C., Khandekar, M.J., Cohen, P., Frontini, A., Bhowmick, D.C., Ye, L., Cinti, S., Spiegelman, B.M., 2012. Zfp423 expression identifies committed preadipocytes and localizes to adipose endothelial and perivascular cells. Cell metabolism 15, 230–9.

Gupte, V. V, Ramasamy, S.K., Reddy, R., Lee, J., Weinreb, P.H., Violette, S.M., Guenther, A., Warburton, D., Driscoll, B., Minoo, P., Bellusci, S., 2009. Overexpression of fibroblast growth factor-10 during both inflammatory and fibrotic phases attenuates bleomycin-induced pulmonary fibrosis in mice. Am J Respir Crit Care Med 180, 424–436.

Haan, N., Goodman, T., Najdi-Samiei, a., Stratford, C.M., Rice, R., El Agha, E., Bellusci, S., Hajihosseini, M.K., 2013. Fgf10-Expressing Tanycytes Add New Neurons to the Appetite/Energy-Balance Regulating Centers of the Postnatal and Adult Hypothalamus. Journal of Neuroscience 33, 6170–6180.

Hajihosseini, M.K., De Langhe, S., Lana-Elola, E., Morrison, H., Sparshott, N., Kelly, R., Sharpe, J., Rice, D., Bellusci, S., 2008. Localization and fate of Fgf10-expressing cells in the adult mouse brain implicate Fgf10 in control of neurogenesis. Mol Cell Neurosci 37, 857–868.

Hamada, K., Ozawa, K., Itami, S., Yoshikawa, K., 1999. Human fibroblast growth factor 10 expression in dermal papilla cells, outer root sheath cells and keratinocytes. Exp Dermatol 8, 347–349.

Harada, H., Toyono, T., Toyoshima, K., Yamasaki, M., Itoh, N., Kato, S., Sekine, K., Ohuchi, H., 2002. FGF10 maintains stem cell compartment in developing mouse incisors. Development 129, 1533–1541.

Hattori, Y., Yamasaki, M., Konishi, M., Itoh, N., 1997. Spatially restricted expression of fibroblast growth factor-10 mRNA in the rat brain. Brain Res Mol Brain Res 47, 139–146.

Hokuto, I., Perl, A.K., Whitsett, J.A., 2003. Prenatal, but not postnatal, inhibition of fibroblast growth factor receptor signaling causes emphysema. J Biol Chem 278, 415–421.

Hokuto, I., Perl, A.K., Whitsett, J.A., 2004. FGF signaling is required for pulmonary homeostasis following hyperoxia. Am J Physiol Lung Cell Mol Physiol 286, L580–7.

Hong, K.U., Reynolds, S.D., Watkins, S., Fuchs, E., Stripp, B.R., 2004. In vivo differentiation potential of tracheal basal cells: evidence for multipotent and unipotent subpopulations. Am J Physiol Lung Cell Mol Physiol 286, L643–9.

Hotta, Y., Nakamura, H., Konishi, M., Murata, Y., Takagi, H., Matsumura, S., Inoue, K., Fushiki, T., Itoh, N., 2009. Fibroblast growth factor 21 regulates lipolysis in white adipose tissue but is not required for ketogenesis and triglyceride clearance in liver. Endocrinology 150, 4625–4633.

Hoyles, R.K., Derrett-Smith, E.C., Khan, K., Shiwen, X., Howat, S.L., Wells, A.U., Abraham, D.J., Denton, C.P., 2011. An essential role for resident fibroblasts in experimental lung fibrosis is defined by lineage-specific deletion of high-affinity type II transforming growth factor beta receptor. Am J Respir Crit Care Med 183, 249–261.

Huang, M., Berkland, C., 2009. Controlled release of repifermin from polyelectrolyte complexes stimulates endothelial cell proliferation. Journal of pharmaceutical sciences 98, 268–80.

Itoh, N., 2007. The Fgf families in humans, mice, and zebrafish: their evolutional processes and roles in development, metabolism, and disease. Biol Pharm Bull 30, 1819–1825.

Itoh, N., Ornitz, D.M., 2004. Evolution of the Fgf and Fgfr gene families. Trends Genet 20, 563–569.

Itoh, N., Ornitz, D.M., 2008. Functional evolutionary history of the mouse Fgf gene family. Dev Dyn 237, 18–27.

Itoh, N., Ornitz, D.M., 2011. Fibroblast growth factors: from molecular evolution to roles in development, metabolism and disease. J Biochem 149, 121–130.

Jaskoll, T., Abichaker, G., Witcher, D., Sala, F.G., Bellusci, S., Hajihosseini, M.K., Melnick, M., 2005. FGF10/FGFR2b signaling plays essential roles during in vivo embryonic submandibular salivary gland morphogenesis. BMC Dev Biol 5, 11.

Jenkins, G., 2013. Pirfenidone should be prescribed for patients with idiopathic pulmonary fibrosis. Thorax 0.

Jin, G.Y., Bok, S.M., Han, Y.M., Chung, M.J., Yoon, K.-H., Kim, S.R., Lee, Y.C., 2012. Effectiveness of rosiglitazone on bleomycin-induced lung fibrosis: Assessed by micro-computed tomography and pathologic scores. European journal of radiology 81, 1901–6.

Jun, D., Garat, C., West, J., Thorn, N., Chow, K., Cleaver, T., Sullivan, T., Torchia, E.C., Childs, C., Shade, T., Tadjali, M., Lara, A., Nozik-Grayck, E., Malkoski, S., Sorrentino, B., Meyrick, B., Klemm, D., Rojas, M., Wagner, D.H., Majka, S.M., 2011. The pathology of bleomycin-induced fibrosis is associated with loss of resident lung mesenchymal stem cells that regulate effector T-cell proliferation. Stem cells (Dayton, Ohio) 29, 725–35.

Kanard, R.C., Fairbanks, T.J., De Langhe, S.P., Sala, F.G., Del Moral, P.M., Lopez, C.A., Warburton, D., Anderson, K.D., Bellusci, S., Burns, R.C., 2005. Fibroblast growth factor-10 serves a regulatory role in duodenal development. J Pediatr Surg 40, 313–316.

Kappel, A., Ronicke, V., Damert, A., Flamme, I., Risau, W., Breier, G., 1999. Identification of vascular endothelial growth factor (VEGF) receptor-2 (Flk-1) promoter/enhancer sequences sufficient for angioblast and endothelial cell-specific transcription in transgenic mice. Blood 93, 4284–4292.

Kelly, R.G., Brown, N.A., Buckingham, M.E., 2001. The arterial pole of the mouse heart forms from Fgf10-expressing cells in pharyngeal mesoderm. Dev Cell 1, 435–440.

Kim, C.F., Jackson, E.L., Woolfenden, A.E., Lawrence, S., Babar, I., Vogel, S., Crowley, D., Bronson, R.T., Jacks, T., 2005. Identification of bronchioalveolar stem cells in normal lung and lung cancer. Cell 121, 823–835.

Kim, K.K., Kugler, M.C., Wolters, P.J., Robillard, L., Galvez, M.G., Brumwell, A.N., Sheppard, D., Chapman, H.A., 2006. Alveolar epithelial cell

mesenchymal transition develops in vivo during pulmonary fibrosis and is regulated by the extracellular matrix. Proc Natl Acad Sci U S A 103, 13180–13185.

Klar, J., Blomstrand, P., Brunmark, C., Badhai, J., Hakansson, H.F., Brange, C.S., Bergendal, B., Dahl, N., 2011. Fibroblast growth factor 10 haploinsufficiency causes chronic obstructive pulmonary disease. J Med Genet 48, 705–709.

Königshoff, M., Balsara, N., Pfaff, E.-M., Kramer, M., Chrobak, I., Seeger, W., Eickelberg, O., 2008. Functional Wnt signaling is increased in idiopathic pulmonary fibrosis. PloS one 3, e2142.

Kurosu, H., Choi, M., Ogawa, Y., Dickson, A.S., Goetz, R., Eliseenkova, A. V, Mohammadi, M., Rosenblatt, K.P., Kliewer, S.A., Kuro-o, M., 2007. Tissue-specific expression of betaKlotho and fibroblast growth factor (FGF) receptor isoforms determines metabolic activity of FGF19 and FGF21. J Biol Chem 282, 26687–26695.

Lama, V.N., Phan, S.H., 2006. The extrapulmonary origin of fibroblasts: stem/progenitor cells and beyond. Proc Am Thorac Soc 3, 373–376.

Langsdorf, A., Radzikinas, K., Kroten, A., Jain, S., Ai, X., 2011. Neural crest cell origin and signals for intrinsic neurogenesis in the mammalian respiratory tract. Am J Respir Cell Mol Biol 44, 293–301.

Lebeche, D., Malpel, S., Cardoso, W. V, 1999. Fibroblast growth factor interactions in the developing lung. Mechanisms of development 86, 125–36.

Li, S., Wang, Y., Zhang, Y., Lu, M.M., DeMayo, F.J., Dekker, J.D., Tucker, P.W., Morrisey, E.E., 2012. Foxp1/4 control epithelial cell fate during lung development and regeneration through regulation of anterior gradient 2. Development 139, 2500–2509.

Lindahl, P., Karlsson, L., Hellström, M., Gebre-Medhin, S., Willetts, K., Heath, J.K., Betsholtz, C., 1997. Alveogenesis failure in PDGF-A-deficient mice is coupled to lack of distal spreading of alveolar smooth muscle cell progenitors during lung development. Development (Cambridge, England) 124, 3943–53.

Liu, Y., Liu, C., Yamada, Y., Fan, C.M., 2002. Growth arrest specific gene 1 acts as a region-specific mediator of the Fgf10/Fgf8 regulatory loop in the limb. Development 129, 5289–5300.

Lu, J., Izvolsky, K.I., Qian, J., Cardoso, W. V, 2005. Identification of FGF10 targets in the embryonic lung epithelium during bud morphogenesis. J Biol Chem 280, 4834–4841.

Lugus, J.J., Park, C., Ma, Y.D., Choi, K., 2009. Both primitive and definitive blood cells are derived from Flk-1+ mesoderm. Blood 113, 563–6.

Mailleux, A.A., Kelly, R., Veltmaat, J.M., De Langhe, S.P., Zaffran, S., Thiery, J.P., Bellusci, S., 2005. Fgf10 expression identifies parabronchial smooth muscle cell progenitors and is required for their entry into the smooth muscle cell lineage. Development 132, 2157–2166.

Mailleux, A.A., Spencer-Dene, B., Dillon, C., Ndiaye, D., Savona-Baron, C., Itoh, N., Kato, S., Dickson, C., Thiery, J.P., Bellusci, S., 2002. Role of FGF10/FGFR2b signaling during mammary gland development in the mouse embryo. Development 129, 53–60.

Makarenkova, H.P., Ito, M., Govindarajan, V., Faber, S.C., Sun, L., McMahon, G., Overbeek, P.A., Lang, R.A., 2000. FGF10 is an inducer and Pax6 a competence factor for lacrimal gland development. Development 127, 2563–2572.

McQualter, J.L., Bertoncello, I., 2012. Concise review: Deconstructing the lung to reveal its regenerative potential. Stem Cells 30, 811–816.

McQualter, J.L., Brouard, N., Williams, B., Baird, B.N., Sims-Lucas, S., Yuen, K., Nilsson, S.K., Simmons, P.J., Bertoncello, I., 2009. Endogenous fibroblastic progenitor cells in the adult mouse lung are highly enriched in the sca-1 positive cell fraction. Stem cells (Dayton, Ohio) 27, 623–33.

McQualter, J.L., Yuen, K., Williams, B., Bertoncello, I., 2010. Evidence of an epithelial stem/progenitor cell hierarchy in the adult mouse lung. Proceedings of the National Academy of Sciences of the United States of America 107, 1414–9.

Meerveld, B.G.-V., Venkova, K., Connolly, K., 2003. Efficacy of repifermin (keratinocyte growth factor-2) against abnormalities in gastrointestinal mucosal transport in a murine model of colitis. Journal of Pharmacy and Pharmacology 55, 67–75.

Metzger, R.J., Klein, O.D., Martin, G.R., Krasnow, M.A., 2008. The branching programme of mouse lung development. Nature 453, 745–750.

Miller, L.A., Wert, S.E., Clark, J.C., Xu, Y., Perl, A.K., Whitsett, J.A., 2004. Role of Sonic hedgehog in patterning of tracheal-bronchial cartilage and the peripheral lung. Dev Dyn 231, 57–71.

Milunsky, J.M., Zhao, G., Maher, T.A., Colby, R., Everman, D.B., 2006. LADD syndrome is caused by FGF10 mutations. Clin Genet 69, 349–354.

Morrisey, E.E., Hogan, B.L., 2010. Preparing for the first breath: genetic and cellular mechanisms in lung development. Dev Cell 18, 8–23.

Mucenski, M.L., Nation, J.M., Thitoff, A.R., Besnard, V., Xu, Y., Wert, S.E., Harada, N., Taketo, M.M., Stahlman, M.T., Whitsett, J.A., 2005. Beta-catenin regulates differentiation of respiratory epithelial cells in vivo. Am J Physiol Lung Cell Mol Physiol 289, L971–9.

Mucenski, M.L., Wert, S.E., Nation, J.M., Loudy, D.E., Huelsken, J., Birchmeier, W., Morrisey, E.E., Whitsett, J.A., 2003. beta-Catenin is

required for specification of proximal/distal cell fate during lung morphogenesis. J Biol Chem 278, 40231–40238.

Nakamura, E., Nguyen, M.T., Mackem, S., 2006. Kinetics of tamoxifen-regulated Cre activity in mice using a cartilage-specific CreER(T) to assay temporal activity windows along the proximodistal limb skeleton. Dev Dyn 235, 2603–2612.

Noguchi, A., Reddy, R., Kursar, J.D., Parks, W.C., Mecham, R.P., 1989. Smooth muscle isoactin and elastin in fetal bovine lung. Experimental lung research 15, 537–52.

Norgaard, G.A., Jensen, J.N., Jensen, J., 2003. FGF10 signaling maintains the pancreatic progenitor cell state revealing a novel role of Notch in organ development. Dev Biol 264, 323–338.

Nyeng, P., Norgaard, G.A., Kobberup, S., Jensen, J., 2007. FGF10 signaling controls stomach morphogenesis. Dev Biol 303, 295–310.

Nyeng, P., Norgaard, G.A., Kobberup, S., Jensen, J., 2008. FGF10 maintains distal lung bud epithelium and excessive signaling leads to progenitor state arrest, distalization, and goblet cell metaplasia. BMC Dev Biol 8, 2.

O'Hare, K.H., Sheridan, M.N., 1970. Electron microscopic observations on the morphogenesis of the albino rat lung, with special reference to pulmonary epithelial cells. The American journal of anatomy 127, 181–205.

Ohuchi, H., Hori, Y., Yamasaki, M., Harada, H., Sekine, K., Kato, S., Itoh, N., 2000. FGF10 acts as a major ligand for FGF receptor 2 IIIb in mouse multi-organ development. Biochem Biophys Res Commun 277, 643–649.

Ohuchi, H., Nakagawa, T., Yamamoto, A., Araga, A., Ohata, T., Ishimaru, Y., Yoshioka, H., Kuwana, T., Nohno, T., Yamasaki, M., Itoh, N., Noji, S., 1997. The mesenchymal factor, FGF10, initiates and maintains the outgrowth of the chick limb bud through interaction with FGF8, an apical ectodermal factor. Development 124, 2235–2244.

Ohuchi, H., Tao, H., Ohata, K., Itoh, N., Kato, S., Noji, S., Ono, K., 2003. Fibroblast growth factor 10 is required for proper development of the mouse whiskers. Biochem Biophys Res Commun 302, 562–567.

Ornitz, D.M., Itoh, N., 2001. Fibroblast growth factors. Genome Biol 2, REVIEWS3005.

Ornitz, D.M., Xu, J., Colvin, J.S., McEwen, D.G., MacArthur, C.A., Coulier, F., Gao, G., Goldfarb, M., 1996. Receptor specificity of the fibroblast growth factor family. J Biol Chem 271, 15292–15297.

Park, W.Y., Miranda, B., Lebeche, D., Hashimoto, G., Cardoso, W. V, 1998. FGF-10 is a chemotactic factor for distal epithelial buds during lung development. Dev Biol 201, 125–134.

Parsa, S., Kuremoto, K., Seidel, K., Tabatabai, R., Mackenzie, B., Yamaza, T., Akiyama, K., Branch, J., Koh, C.J., Al Alam, D., Klein, O.D., Bellusci, S., 2010. Signaling by FGFR2b controls the regenerative capacity of adult mouse incisors. Development 137, 3743–3752.

Parsa, S., Ramasamy, S.K., De Langhe, S., Gupte, V. V, Haigh, J.J., Medina, D., Bellusci, S., 2008. Terminal end bud maintenance in mammary gland is dependent upon FGFR2b signaling. Dev Biol 317, 121–131.

Patel, D.M., Shah, J., Srivastava, A.S., 2013. Therapeutic Potential of Mesenchymal Stem Cells in Regenerative Medicine. Stem Cells International 2013, 1–15.

Perl, A.K., Wert, S.E., Loudy, D.E., Shan, Z., Blair, P.A., Whitsett, J.A., 2005. Conditional recombination reveals distinct subsets of epithelial cells in trachea, bronchi, and alveoli. Am J Respir Cell Mol Biol 33, 455–462.

Perl, A.-K.T., Gale, E., 2009. FGF signaling is required for myofibroblast differentiation during alveolar regeneration. American journal of physiology. Lung cellular and molecular physiology 297, L299–308.

Peters, K., Werner, S., Liao, X., Wert, S., Whitsett, J., Williams, L., 1994. Targeted expression of a dominant negative FGF receptor blocks branching morphogenesis and epithelial differentiation of the mouse lung. EMBO J 13, 3296–3301.

Petiot, A., Conti, F.J., Grose, R., Revest, J.M., Hodivala-Dilke, K.M., Dickson, C., 2003. A crucial role for Fgfr2-IIIb signalling in epidermal development and hair follicle patterning. Development 130, 5493–5501.

Petiot, A., Perriton, C.L., Dickson, C., Cohn, M.J., 2005. Development of the mammalian urethra is controlled by Fgfr2-IIIb. Development 132, 2441–2450.

Phan, S.H., 2002. The myofibroblast in pulmonary fibrosis. Chest 122, 286S–289S.

Phillips, R.J., Burdick, M.D., Hong, K., Lutz, M.A., Murray, L.A., Xue, Y.Y., Belperio, J.A., Keane, M.P., Strieter, R.M., 2004. Circulating fibrocytes traffic to the lungs in response to CXCL12 and mediate fibrosis. J Clin Invest 114, 438–446.

Pirvola, U., Spencer-Dene, B., Xing-Qun, L., Kettunen, P., Thesleff, I., Fritzsch, B., Dickson, C., Ylikoski, J., 2000. FGF/FGFR-2(IIIb) signaling is essential for inner ear morphogenesis. J Neurosci 20, 6125–6134.

Pittenger, M.F., Mosca, J.D., McIntosh, K.R., 2000. Human mesenchymal stem cells: progenitor cells for cartilage, bone, fat and stroma. Curr Top Microbiol Immunol 251, 3–11.

Que, J., Wilm, B., Hasegawa, H., Wang, F., Bader, D., Hogan, B.L., 2008. Mesothelium contributes to vascular smooth muscle and mesenchyme during lung development. Proc Natl Acad Sci U S A 105, 16626–16630.

Raghu, G., Thickett, D.R., 2013. Pirfenidone for IPF: pro/con debate; the “con” viewpoint. Thorax 0, 2011–2014.

Ramasamy, S.K., Mailleux, A.A., Gupte, V. V, Mata, F., Sala, F.G., Veltmaat, J.M., Del Moral, P.M., De Langhe, S., Parsa, S., Kelly, L.K., Kelly, R., Shia, W., Keshet, E., Minoo, P., Warburton, D., Bellusci, S., 2007. Fgf10 dosage is critical for the amplification of epithelial cell progenitors and for the formation of multiple mesenchymal lineages during lung development. Dev Biol 307, 237–247.

Rawlins, E.L., Clark, C.P., Xue, Y., Hogan, B.L.M., 2009. The Id2+ distal tip lung epithelium contains individual multipotent embryonic progenitor cells. Development (Cambridge, England) 136, 3741–5.

Rawlins, E.L., Hogan, B.L.M., 2006. Epithelial stem cells of the lung: privileged few or opportunities for many? Development (Cambridge, England) 133, 2455–65.

Rawlins, E.L., Hogan, B.L.M., 2008. Ciliated epithelial cell lifespan in the mouse trachea and lung. American journal of physiology. Lung cellular and molecular physiology 295, L231–4.

Rehan, V., Torday, J., 2003. Hyperoxia augments pulmonary lipofibroblast-to-myofibroblast transdifferentiation. Cell biochemistry and biophysics 38, 239–50.

Rehan, V.K., Sugano, S., Wang, Y., Santos, J., Romero, S., Dasgupta, C., Keane, M.P., Stahlman, M.T., Torday, J.S., 2006. Evidence for the presence of lipofibroblasts in human lung. Experimental lung research 32, 379–93.

Rehan, V.K., Torday, J.S., 2012. PPARγ Signaling Mediates the Evolution, Development, Homeostasis, and Repair of the Lung. PPAR research 2012, 289867.

Revest, J.M., Suniara, R.K., Kerr, K., Owen, J.J., Dickson, C., 2001. Development of the thymus requires signaling through the fibroblast growth factor receptor R2-IIIb. J Immunol 167, 1954–1961.

Rice, R., Spencer-Dene, B., Connor, E.C., Gritli-Linde, A., McMahon, A.P., Dickson, C., Thesleff, I., Rice, D.P., 2004. Disruption of Fgf10/Fgfr2b-coordinated epithelial-mesenchymal interactions causes cleft palate. J Clin Invest 113, 1692–1700.

Robson, M.C., Phillips, T.J., Falanga, V., Odenheimer, D.J., Parish, L.C., Jensen, J.L., Steed, D.L., 2001. Randomized trial of topically applied repifermin (recombinant human keratinocyte growth factor-2) to accelerate wound healing in venous ulcers. Wound repair and regeneration : official publication of the Wound Healing Society [and] the European Tissue Repair Society 9, 347–52.

Rock, J.R., Barkauskas, C.E., Cronce, M.J., Xue, Y., Harris, J.R., Liang, J., Noble, P.W., Hogan, B.L., 2011. Multiple stromal populations contribute to pulmonary fibrosis without evidence for epithelial to mesenchymal transition. Proc Natl Acad Sci U S A 108, E1475–83.

Rock, J.R., Hogan, B.L., 2011. Epithelial progenitor cells in lung development, maintenance, repair, and disease. Annu Rev Cell Dev Biol 27, 493–512.

Rock, J.R., Onaitis, M.W., Rawlins, E.L., Lu, Y., Clark, C.P., Xue, Y., Randell, S.H., Hogan, B.L., 2009. Basal cells as stem cells of the mouse trachea and human airway epithelium. Proc Natl Acad Sci U S A 106, 12771–12775.

Rock, J.R., Randell, S.H., Hogan, B.L., 2010. Airway basal stem cells: a perspective on their roles in epithelial homeostasis and remodeling. Dis Model Mech 3, 545–556.

Rosen, E.D., 2005. The transcriptional basis of adipocyte development. Prostaglandins, leukotrienes, and essential fatty acids 73, 31–4.

Rosenfeld, M.G., Briata, P., Dasen, J., Gleiberman, A.S., Kioussi, C., Lin, C., O'Connell, S.M., Ryan, A., Szeto, D.P., Treier, M., 2000. Multistep signaling and transcriptional requirements for pituitary organogenesis in vivo. Recent Prog Horm Res 55, 1–4.

Rubin, L.P., Kovacs, C.S., De Paepe, M.E., Tsai, S.-W., Torday, J.S., Kronenberg, H.M., 2004. Arrested pulmonary alveolar cytodifferentiation and defective surfactant synthesis in mice missing the gene for parathyroid hormone-related protein. Developmental dynamics : an official publication of the American Association of Anatomists 230, 278–89.

Sabatini, F., Petecchia, L., Tavian, M., Jodon de Villeroché, V., Rossi, G. a, Brouty-Boyé, D., 2005. Human bronchial fibroblasts exhibit a mesenchymal stem cell phenotype and multilineage differentiating potentialities. Laboratory investigation; a journal of technical methods and pathology 85, 962–71.

Sakaue, H., Konishi, M., Ogawa, W., Asaki, T., Mori, T., Yamasaki, M., Takata, M., Ueno, H., Kato, S., Kasuga, M., Itoh, N., 2002. Requirement of fibroblast growth factor 10 in development of white adipose tissue. Genes Dev 16, 908–912.

Sala, F.G., Curtis, J.L., Veltmaat, J.M., Del Moral, P.M., Le, L.T., Fairbanks, T.J., Warburton, D., Ford, H., Wang, K., Burns, R.C., Bellusci, S., 2006. Fibroblast growth factor 10 is required for survival and proliferation but not differentiation of intestinal epithelial progenitor cells during murine colon development. Dev Biol 299, 373–385.

Sala, F.G., Del Moral, P.M., Tiozzo, C., Alam, D.A., Warburton, D., Grikscheit, T., Veltmaat, J.M., Bellusci, S., 2011. FGF10 controls the patterning of the tracheal cartilage rings via Shh. Development 138, 273–282.

Sandborn, W.J., Sands, B.E., Wolf, D.C., Valentine, J.F., Safdi, M., Katz, S., Isaacs, K.L., Wruble, L.D., Katz, J., Present, D.H., Loftus, E. V, Graeme-Cook, F., Odenheimer, D.J., Hanauer, S.B., 2003. Repifermin (keratinocyte growth factor-2) for the treatment of active ulcerative colitis: a randomized, double-blind, placebo-controlled, dose-escalation trial. Alimentary pharmacology & therapeutics 17, 1355–64.

Santos-Rosa, H., Schneider, R., Bannister, A.J., Sherriff, J., Bernstein, B.E., Emre, N.C., Schreiber, S.L., Mellor, J., Kouzarides, T., 2002. Active genes are tri-methylated at K4 of histone H3. Nature 419, 407–411.

Satoh, Y., Haraguchi, R., Wright, T., Mansour, S., Partanen, J., Hajihosseini, M., Eswarakumar, V., Lonai, P., Yamada, G., 2004. Regulation of external genitalia development by concerted actions of FGF ligands and FGF receptors. Anatomy and Embryology 208, 479–486.

Scadden, D.T., 2006. The stem-cell niche as an entity of action. Nature 441, 1075–9.

Schoch, K.G., Lori, A., Burns, K.A., Eldred, T., Olsen, J.C., Randell, S.H., 2004. A subset of mouse tracheal epithelial basal cells generates large colonies in vitro. Am J Physiol Lung Cell Mol Physiol 286, L631–42.

Schultz, C.J., Torres, E., Londos, C., Torday, J.S., 2002. Role of adipocyte differentiation-related protein in surfactant phospholipid synthesis by type II cells. American journal of physiology. Lung cellular and molecular physiology 283, L288–96.

Sekine, K., Ohuchi, H., Fujiwara, M., Yamasaki, M., Yoshizawa, T., Sato, T., Yagishita, N., Matsui, D., Koga, Y., Itoh, N., Kato, S., 1999. Fgf10 is essential for limb and lung formation. Nat Genet 21, 138–141.

Shakkottai, V.G., Xiao, M., Xu, L., Wong, M., Nerbonne, J.M., Ornitz, D.M., Yamada, K.A., 2009. FGF14 regulates the intrinsic excitability of cerebellar Purkinje neurons. Neurobiol Dis 33, 81–88.

Shan, L., Subramaniam, M., Emanuel, R.L., Degan, S., Johnston, P., Tefft, D., Warburton, D., Sunday, M.E., 2008. Centrifugal migration of mesenchymal cells in embryonic lung. Developmental dynamics : an official publication of the American Association of Anatomists 237, 750–7.

Shannon, J.M., Hyatt, B.A., 2004. Epithelial-mesenchymal interactions in the developing lung. Annu Rev Physiol 66, 625–645.

Shimada, T., Kakitani, M., Yamazaki, Y., Hasegawa, H., Takeuchi, Y., Fujita, T., Fukumoto, S., Tomizuka, K., Yamashita, T., 2004. Targeted ablation of Fgf23 demonstrates an essential physiological role of FGF23 in phosphate and vitamin D metabolism. J Clin Invest 113, 561–568.

Shimizu, T., Nettesheim, P., Ramaekers, F.C., Randell, S.H., 1992. Expression of “cell-type-specific” markers during rat tracheal epithelial regeneration. Am J Respir Cell Mol Biol 7, 30–41.

Simon, D.M., Mariani, T.J., 2007. Role of PPARs and Retinoid X Receptors in the Regulation of Lung Maturation and Development. PPAR research 2007, 91240.

Soler, P.M., Wright, T.E., Smith, P.D., Maggi, S.P., Hill, D.P., Ko, F., Jimenez, P. a, Robson, M.C., 1999. In vivo characterization of keratinocyte growth factor-2 as a potential wound healing agent. Wound repair and regeneration : official publication of the Wound Healing Society [and] the European Tissue Repair Society 7, 172–8.

Spooner, B.S., Wessells, N.K., 1970. Mammalian lung development: interactions in primordium formation and bronchial morphogenesis. J Exp Zool 175, 445–454.

Srinivasan, R.S., Dillard, M.E., Lagutin, O. V, Lin, F.-J., Tsai, S., Tsai, M.-J., Samokhvalov, I.M., Oliver, G., 2007. Lineage tracing demonstrates the venous origin of the mammalian lymphatic vasculature. Genes & development 21, 2422–32.

Stripp, B.R., Maxson, K., Mera, R., Singh, G., 1995. Plasticity of airway cell proliferation and gene expression after acute naphthalene injury. Am J Physiol 269, L791–9.

Summer, R., Fitzsimmons, K., Dwyer, D., Murphy, J., Fine, A., 2007. Isolation of an adult mouse lung mesenchymal progenitor cell population. American journal of respiratory cell and molecular biology 37, 152–9.

Tang, N., Marshall, W.F., McMahon, M., Metzger, R.J., Martin, G.R., 2011. Control of mitotic spindle angle by the RAS-regulated ERK1/2 pathway determines lung tube shape. Science (New York, N.Y.) 333, 342–5.

Tao, H., Shimizu, M., Kusumoto, R., Ono, K., Noji, S., Ohuchi, H., 2005. A dual role of FGF10 in proliferation and coordinated migration of epithelial leading edge cells during mouse eyelid development. Development 132, 3217–3230.

Thomson, A.A., Cunha, G.R., 1999. Prostatic growth and development are regulated by FGF10. Development 126, 3693–3701.

Tiozzo, C., Carraro, G., Al Alam, D., Baptista, S., Danopoulos, S., Li, A., Lavarreda-Pearce, M., Li, C., De Langhe, S., Chan, B., Borok, Z., Bellusci, S., Minoo, P., 2012. Mesodermal Pten inactivation leads to alveolar capillary dysplasia- like phenotype. The Journal of clinical investigation 122, 3862–72.

Tiozzo, C., De Langhe, S., Carraro, G., Alam, D.A., Nagy, A., Wigfall, C., Hajihosseini, M.K., Warburton, D., Minoo, P., Bellusci, S., 2009. Fibroblast growth factor 10 plays a causative role in the tracheal cartilage defects in a mouse model of Apert syndrome. Pediatr Res 66, 386–390.

Torday, J.S., Rehan, V.K., 2007. The evolutionary continuum from lung development to homeostasis and repair. American journal of physiology. Lung cellular and molecular physiology 292, L608–11.

Torday, J.S., Sun, H., Wang, L., Torres, E., 2002. Pre- and Postnatal Lung Development, Maturation, and Plasticity: Leptin mediates the parathyroid hormone-related protein paracrine stimulation of fetal lung maturation. Am J Physiol Lung Cell Mol Physiol 282, L405–410.

Torday, J.S., Torres, E., Rehan, V.K., 2003. The role of fibroblast transdifferentiation in lung epithelial cell proliferation, differentiation, and repair in vitro. Pediatric pathology & molecular medicine 22, 189–207.

Trounson, A., Thakar, R.G., Lomax, G., Gibbons, D., 2011. Clinical trials for stem cell therapies. BMC medicine 9, 52.

Tsao, P.N., Vasconcelos, M., Izvolsky, K.I., Qian, J., Lu, J., Cardoso, W. V, 2009. Notch signaling controls the balance of ciliated and secretory cell fates in developing airways. Development 136, 2297–2307.

Urakawa, I., Yamazaki, Y., Shimada, T., Iijima, K., Hasegawa, H., Okawa, K., Fujita, T., Fukumoto, S., Yamashita, T., 2006. Klotho converts canonical FGF receptor into a specific receptor for FGF23. Nature 444, 770–774.

Vaccaro, C., Brody, J.S., 1978. Ultrastructure of developing alveoli. I. The role of the interstitial fibroblast. The Anatomical record 192, 467–79.

Veltmaat, J.M., Relaix, F., Le, L.T., Kratochwil, K., Sala, F.G., Van Veelen, W., Rice, R., Spencer-Dene, B., Mailleux, A.A., Rice, D.P., Thiery, J.P., Bellusci, S., 2006. Gli3-mediated somitic Fgf10 expression gradients are required for the induction and patterning of mammary epithelium along the embryonic axes. Development 133, 2325–2335.

Volckaert, T., Dill, E., Campbell, A., Tiozzo, C., Majka, S., Bellusci, S., De Langhe, S.P., 2011. Parabronchial smooth muscle constitutes an airway epithelial stem cell niche in the mouse lung after injury. J Clin Invest 121, 4409–4419.

Warburton, D., Schwarz, M., Tefft, D., Flores-Delgado, G., Anderson, K.D., Cardoso, W. V, 2000. The molecular basis of lung morphogenesis. Mech Dev 92, 55–81.

Weaver, M., Batts, L., Hogan, B.L., 2003. Tissue interactions pattern the mesenchyme of the embryonic mouse lung. Dev Biol 258, 169–184.

Weaver, M., Yingling, J.M., Dunn, N.R., Bellusci, S., Hogan, B.L., 1999. Bmp signaling regulates proximal-distal differentiation of endoderm in mouse lung development. Development 126, 4005–4015.

Wei, J., Fang, F., Lam, A.P., Sargent, J.L., Hamburg, E., Hinchcliff, M.E., Gottardi, C.J., Atit, R., Whitfield, M.L., Varga, J., 2012. Wnt/β-catenin signaling is hyperactivated in systemic sclerosis and induces Smad-dependent fibrotic responses in mesenchymal cells. Arthritis and rheumatism 64, 2734–45.

Wheeler, G., 2001. Repifermin. Human Genome Sciences/GlaxoSmithKline. IDrugs : the investigational drugs journal 4, 813–9.

White, A.C., Lavine, K.J., Ornitz, D.M., 2007. FGF9 and SHH regulate mesenchymal Vegfa expression and development of the pulmonary capillary network. Development (Cambridge, England) 134, 3743–52.

White, A.C., Xu, J., Yin, Y., Smith, C., Schmid, G., Ornitz, D.M., 2006. FGF9 and SHH signaling coordinate lung growth and development through regulation of distinct mesenchymal domains. Development 133, 1507–1517.

Wu, M., Melichian, D.S., Chang, E., Warner-Blankenship, M., Ghosh, A.K., Varga, J., 2009. Rosiglitazone abrogates bleomycin-induced scleroderma and blocks profibrotic responses through peroxisome proliferator-activated receptor-gamma. The American journal of pathology 174, 519–33.

Wu, Q.-F., Yang, L., Li, S., Wang, Q., Yuan, X.-B., Gao, X., Bao, L., Zhang, X., 2012. Fibroblast growth factor 13 is a microtubule-stabilizing protein regulating neuronal polarization and migration. Cell 149, 1549–64.

Wuenschell, C.W., Sunday, M.E., Singh, G., Minoo, P., Slavkin, H.C., Warburton, D., 1996. Embryonic mouse lung epithelial progenitor cells co-express immunohistochemical markers of diverse mature cell lineages. J Histochem Cytochem 44, 113–123.

Yamada, M., Kurihara, H., Kinoshita, K., Sakai, T., 2005. Temporal expression of alpha-smooth muscle actin and drebrin in septal interstitial

cells during alveolar maturation. The journal of histochemistry and cytochemistry : official journal of the Histochemistry Society 53, 735–44.

Yamaguchi, T.P., Dumont, D.J., Conlon, R.A., Breitman, M.L., Rossant, J., 1993. flk-1, an flt-related receptor tyrosine kinase is an early marker for endothelial cell precursors. Development 118, 489–498.

Yamasaki, M., Emoto, H., Konishi, M., Mikami, T., Ohuchi, H., Nakao, K., Itoh, N., 1999. FGF-10 is a growth factor for preadipocytes in white adipose tissue. Biochem Biophys Res Commun 258, 109–112.

Yamasaki, M., Miyake, A., Tagashira, S., Itoh, N., 1996. Structure and expression of the rat mRNA encoding a novel member of the fibroblast growth factor family. J Biol Chem 271, 15918–15921.

Yildirim, A.O., Muyal, V., John, G., Müller, B., Seifart, C., Kasper, M., Fehrenbach, H., 2010. Palifermin induces alveolar maintenance programs in emphysematous mice. American journal of respiratory and critical care medicine 181, 705–17.

Yin, Y., Wang, F., Ornitz, D.M., 2011. Mesothelial- and epithelial-derived FGF9 have distinct functions in the regulation of lung development. Development 138, 3169–3177.

Yin, Y., White, A.C., Huh, S.H., Hilton, M.J., Kanazawa, H., Long, F., Ornitz, D.M., 2008. An FGF-WNT gene regulatory network controls lung mesenchyme development. Dev Biol 319, 426–436.

Yu, K., Xu, J., Liu, Z., Sosic, D., Shao, J., Olson, E.N., Towler, D.A., Ornitz, D.M., 2003. Conditional inactivation of FGF receptor 2 reveals an essential role for FGF signaling in the regulation of osteoblast function and bone growth. Development 130, 3063–3074.

Zhang, X., Ibrahimi, O.A., Olsen, S.K., Umemori, H., Mohammadi, M., Ornitz, D.M., 2006. Receptor specificity of the fibroblast growth factor family. The complete mammalian FGF family. J Biol Chem 281, 15694–15700.

9. Supplementary Material

Table S1. Clusters of differentiation and their functions in mice as described in the Protein Knowledgebase (UniProtKB, www.uniprot.org).
Abbreviations: BM: Bone marrow; EpCAM: Epithelial cell adhesion molecule; ECM: Extracellular matrix; ES cell: Embryonic stem cell; PDGFRα: Platelet-derived growth factor receptor alpha; PECAM-1: Platelet/endothelial cell adhesion molecule 1; VCAM-1: Vascular cell adhesion molecule 1.

Name	Protein name	Function(s)
CD24	Signal transducer CD24	Putative: Early thymocyte development
CD29	Integrin beta-1	Receptor for ECM proteins
CD31	PECAM-1	Leukocyte transendothelial migration
CD34	Hematopoietic progenitor cell antigen CD34	Putative: Attachment of stem cells to BM-ECM or directly to stromal cells
CD44	ECM receptor III	Putative: Involved in matrix adhesion
CD45	Receptor-type tyrosine protein phosphatase C or leukocyte common antigen	T cell activation
CD49f	Integrin alpha-6	Receptor for laminin Attachment of epithelial cells to basement membrane
CD90	THY-1 membrane glycoprotein	Putative: Cell-cell adhesion
CD104	Integrin beta-4	Receptor for laminin Critical structural role in the hemidesmosomes of epithelial cells
CD106	VCAM-1	Cell-cell recognition

		Leukocyte-endothelial cell adhesion
CD117	Mast/stem cell growth factor receptor Kit or c-Kit	Regulation of cell survival and proliferation, hematopoiesis and stem cell maintenance
CD140a	PDGFRα	Regulation of embryonic development, cell proliferation and cell survival
CD326	EpCAM	Putative: An immunological barrier for mucosal infection in the intestine. ES cell proliferation and differentiation

Table S2. Primers and probes used for qPCR and RT-PCR.
m: mouse; h: human.

Genes		Primers	UPL probes
		Taqman® assay	
Cre	Fwd	5'-GTTTTGCCGGGTCAGAAAA-3'	87
	Rev	5'-GGCGCGAGTTGATAGCTG-3'	
mFgf10	Fwd	5'-ATGACTGTTGACATCAGACTCCTT-3'	63
	Rev	5'-CACTGTTCAGCCTTTTGAGGA-3'	
mβ-actin	Fwd	5'-TGACAGGATGCAGAAGGAGA-3'	106
	Rev	5'-GCGTCAGGAGGAGCAATG-3'	
		SYBR® Green assay or RT-PCR	
mAdrp	Fwd	5'-CCTCAGCTCTCCTGTTAGGC-3'	-
	Rev	5'-CACTACTGCTGCTGCCATTT-3'	
mCebpb	Fwd	5'-TGATGCAATCCGGATCAA-3'	-

	Rev	5'-CACGTGTGTTGCGTCAGTC-3’	
mFgf10	Fwd	5’-ATGACTGTTGACATCAGACTCCTT-3’	-
	Rev	5’-CACTGTTCAGCCTTTTGAGGA-3’	
mFgfr1b	Fwd	5’-CCACAGGTCTGGTGACAGTGA-3’	-
	Rev	5’-CGGGAATTAATAGCTCGGATG-3’	
mFgfr1c	Fwd	5’-TCTGGCCTCTACGCTTGC-3’	-
	Rev	5’-CTTCCGAGGATGGGAGTG-3’	
mFgfr2b	Fwd	5’-CCCTACCTCAAGGTCCTGAA-3’	-
	Rev	5’-CATCCATCTCCGTCACATTG-3’	
mFgfr2c	Fwd	5’-TGCATGGTTGACAGTTCTGC-3’	-
	Rev	5’-TGCAGGCGATTAAGAAGACC-3’	
mFlk1	Fwd	5’-GGGGTATGGAGACGAGCTG-3’	-
	Rev	5’-GCACAGATCTGACTAAATTGCTG-3’	
mHprt	Fwd	5’-CCTAAGATGAGCGCAAGTTGAA-3’	-
	Rev	5’-CCACAGGACTAGAACACCTGCTAA-3’	
mLipase	Fwd	5’-GCGCTGGAGGAGTGTTTTT-3’	-
	Rev	5’-CCGCTCTCCAGTTGAACC-3’	
mPparg	Fwd	5’-GAAAGACAACGGACAAATCACC-3’	-
	Rev	5’-GGGGGTGATATGTTTGAACTTG-3’	
RFP	Fwd	5’-AAGGGCGAGATCAAGATGAG-3’	-
	Rev	5’-GACCTCGGCGTCGTAGTG-3’	
mSftpc	Fwd	5’-GGTCCTGATGGAGAGTCCAC-3’	-
	Rev	5’-GATGAGAAGGCGTTTGAGGT-3’	
mZfp423	Fwd	5’-GCGATCGGTGAAAGTTGAAG-3’	-
	Rev	5’-TCTCCTTCCAGGCCTCCT-3’	

mαSma	Fwd	5’-ACTCTCTTCCAGCCATCTTTCA-3’	-
	Rev	5’-ATAGGTGGTTTCGTGGATGC-3’	
mβ-actin	Fwd	5’-TGACAGGATGCAGAAGGAGA-3’	-
	Rev	5’-GCGTCAGGAGGAGCAATG-3’	
hCEBPa	Fwd	5'-GACATCAGCGCCTACATCG-3'	-
	Rev	5'-GGCTGTGCTGGAACAGGT-3'	
hLipase	Fwd	5'-GTGGCCGAGAGTGAGAACA-3'	-
	Rev	5'-GGAAGGAGTAGGTCTTATTTGTGG-3'	
hPBGD	Fwd	5'-TGTCTGGTAACGGCAATGCG-3'	-
	Rev	5'-CCCACGCGAATCACTCTCAT-3'	
hPPARg	Fwd	5'-TTGCTGTCATTATTCTCAGTGGA-3'	-
	Rev	5'-GAGGACTCAGGGTGGTTCAG-3'	
hResistin	Fwd	5'-TGCAGGATGAAAGCTCTCTGT-3'	-
	Rev	5'-GGGTCTTGCTAGACACCAACA-3'	

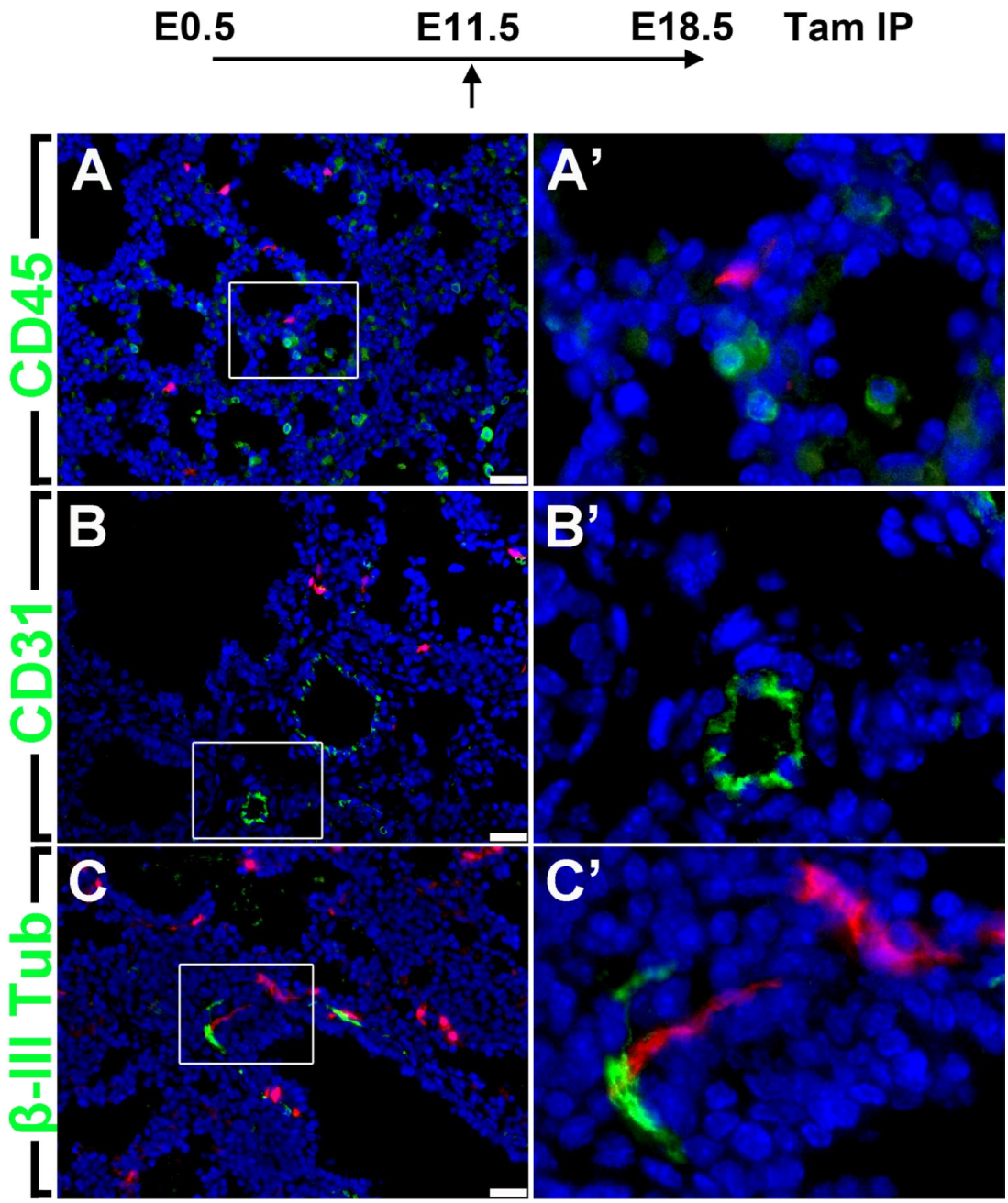

Figure S1. *Fgf10*-expressing cells from E11.5 do not stain for hematopoietic, endothelial or neuronal markers at E18.5.

Immunofluorescence staining for CD45 (**A**), CD31 (**B**) and β-III Tubulin (**C**) on E18.5 *Fgf10*$^{iCre/+}$; *Tomato*$^{flox/+}$ lungs. High magnification images for the areas in the boxes are shown in (**A'**), (**B'**) and (**C'**) respectively. Scale bar: 25 μm.

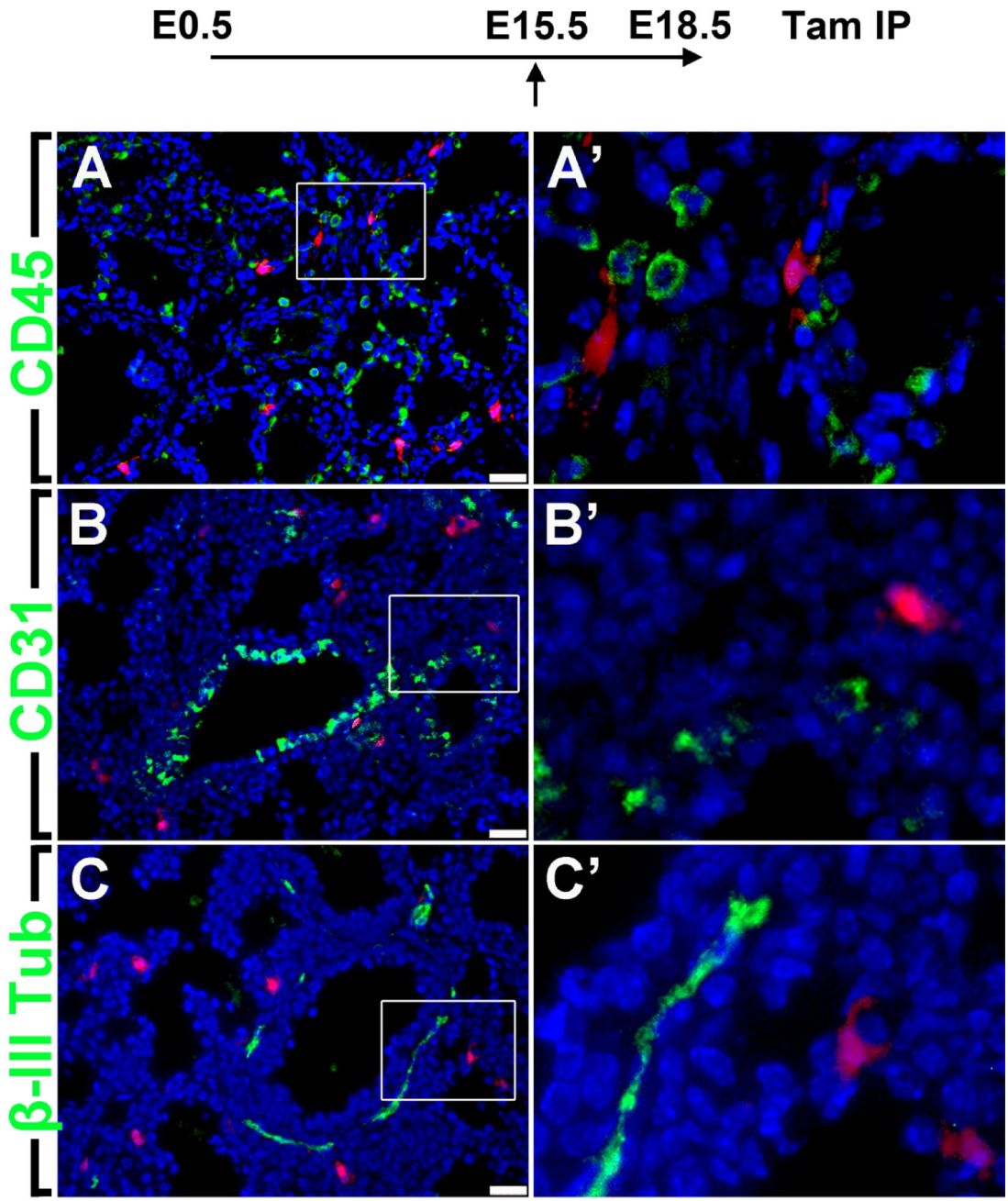

Figure S2. *Fgf10*-expressing cells from E15.5 do not stain for hematopoietic, endothelial or neuronal markers at E18.5.

Immunofluorescence staining for CD45 (**A**), CD31 (**B**) and β-III Tubulin (**C**) on E18.5 *Fgf10*$^{iCre/+}$; *Tomato*$^{flox/+}$ lungs. High magnification images for the areas in the boxes are shown in (**A'**), (**B'**) and (**C'**) respectively. Scale bar: 25 µm.

10. Acknowledgements

Finally, I would like to take this chance to thank all the people who helped me through and made the completion of my PhD possible.

First of all, I would like to express my deep gratitude to Prof. Dr. Saverio Bellusci for giving me the chance and trusting me to be among his earliest students in his newly established lab in Giessen. His enthusiasm and passion for his work have certainly inspired me and made me feel excited about every single experiment I performed throughout my doctoral studies. I want to thank him for giving me the freedom and providing me with all the resources as well as mentorship that I needed.

Secondly, I would like to thank Heike and Kerstin for the friendly atmosphere as well as their administrative help and making sure that contracts are signed on time and legal documents are translated! I would also like to thank Bre who was there all the way from day one, through good and bad times. Thank you, Bre, for being a trustful friend and colleague and I wish you all the best in your future career! I would also like to acknowledge my fellow graduate students in the Bellusci lab, Alena, Cho, Amit and Salma, and I wish them good luck in completing their studies.

Many thanks also to our collaborators, Prof. Dr. Virender Rehan and Dr. Denise Al Alam, for providing some of the data and samples (as acknowledged in the corresponding figure legends). I also acknowledge Dr. Susanne Herold and Jennifer Quantius for their help with FACS measurements, Dr. Ingrid Henneke for her help with bleomycin treatments, and Dr. Melanie Königshoff for providing cDNA from bleomycin-treated mice. I would also like to thank Prof. Dr. Werner Seeger, Prof. Dr. Norbert Weissmann, Prof. Dr. Andreas Günther, Dr. Robert Voswinckel, Dr. Guillermo Barreto, Dr. Mohammad Hajihosseini, Dr. Gianni Carraro and Dr. Stijn De Langhe for their advice and constructive criticism. I would also like to acknowledge Dr. Rory Morty, the director of the MBML program, and Prof. Dr. Eveline Baumgart-Vogt and Dr. Lorna Lück, the organizers of the GGL

program. I also thank lab technicians Matthew, Jana, Judith and Jacques for their friendship and technical support. I also acknowledge Dr. Daniel Zahner and animal caretakers Christian Eng, Viktoria Gutjahr, Sabrina Schick and Martin Stellwagen for their indispensable help.

I would also like to thank my close friends for the good times that we spent together. Thanos, thanks for being there in times of need and I wish you all the best. I would also like to thank Anja and Hamza for being good friends and for their support. I also acknowledge Mohammad and Anna for their love and support.

I would also like to express my thanks and gratitude to the person who believed in me the most and offered me unconditional support. Vicky, thank you for standing by me throughout my journey and for every moment we spent together. This work would not have been possible without your presence and support.

I would also like to acknowledge the Petri's for being my second family and for making me feel welcome and at home. Ella and Theo, thanks a lot for your support and love. Many thanks also to Janina and Waldi as well as the Gerth's, Valentina and Sven, for their friendship and support.

Finally, I would like to express my deep love and gratitude to my parents in Lebanon, Soheil and Marie, for their support and patience. I owe them everything that I am and will ever be. I would also like to thank my brothers, Michel (and his wife Rita), Nabil and Wassim for their support and for being there when I needed their guidance. Thank you bros for everything. You are the best!

Lastly, I would like to thank the people who reviewed this dissertation: Matthew, Vicky, Michel and Janina.

Der Lebenslauf wurde aus der elektronischen Version der Arbeit entfernt.

The curriculum vitae was removed from the electronic version of the paper.